**Mesoscale imaging, inactivation, and collaboration in a standardized visual decision-making task**

*A dissertation presented by*

Christopher Stephen Krasniak

*to the*

Cold Spring Harbor Laboratory School of Biological Sciences

*in partial fulfillment of the requirements for the degree of*

Doctor of Philosophy

*in*

Biological Sciences

*at*

Cold Spring Harbor Laboratory

*on*

April 5, 2022

*This page is unintentionally left blank*

# Abstract

Typical neuroscience experiments in the field of decision-making have focused on recording in one or a few brain areas while animals perform a task created by and only used in their own lab with their own custom hardware and software. This makes combining information from these studies to address big questions, such as how information across the whole brain produces a decision, impossible. Big questions such as this are better addressed by collaborations that can enforce standardized methods across their members and can therefore pool their efforts and resources. One such collaboration, the IBL, is focusing on how the mouse brain solves a basic perceptual decision-making task. Towards this goal, in collaboration with the IBL, I have created a standardized visual decision-making task that allows comparison of experiments both between labs and between experimental modalities. I have recorded thousands of neurons across the brain in contribution to a brainwide map of single cell spiking activity during decision-making. These recordings are in contribution to three main scientific goals, a brainwide map of activity related to decision-making, methods for standardized and reproducible electrophysiology recordings, and an electrophysiological atlas of the mouse brain. In my own experiments performed alongside those of the IBL, I used an unbiased inhibition scan across the dorsal cortex to determine the causal cortical areas for performing the IBL task. This revealed that visual cortex inactivation impairs accumulation of contralateral visual information, and secondary motor cortex inactivation biases the starting point of the decision process away from the contralateral side. I additionally performed calcium imaging of the whole mouse dorsal cortex as an independent source of neural recording from the IBL brainwide map. These recordings indicate that task information is broadcast widely across the cortical network, but the strongest information is localized in the expected nodes: initially after stimulus onset in V1, then progressively in M2. These recordings additionally revealed two cortical representations of stimulus or choice expectation: a selective prestimulus suppression, and post stimulus excitation for the expected stimulus-driven areas in V1 and M2, and a potential embodied expectation that is reflected in the

paw and torso somatosensory areas. Finally I have shown proof-of-principle experiments that one can simultaneously optogenetically manipulate targeted cortical areas, while monitoring the neural activity across the whole dorsal cortex with widefield calcium imaging. Though this experiment still has a few flaws such as the visual detection of red light, it could lead to many discoveries about the basic function of cortical networks.

# Acknowledgements

As I hope to convey in this thesis, any scientific work is never the product of one person alone, but always the collaborative effort of a community. As such there are many contributions, both direct and indirect that I must acknowledge as critical for this work. It first starts with my parents, who gave me the freedom, means, and encouragement to pursue something as ambitious as this work. Arriving at CSHL was of course a critical part of my intellectual journey, and I must thank the School of Biological Sciences and those who keep it running for first accepting me to come be a part of this community, and exposing me to all different scientific thought. The school also gives its students nearly full freedom in choosing the lab they want to join, which allowed me to join the lab that I thought did the most interesting work and whose members had the most interesting perspectives.

The first year or two of my time in the Zador lab and the Marks building were formative of my scientific development, and I want to particularly acknowledge Fred Marbach, Fede Carnevale, Barry Burbach, and Akihiro Funamizu for teaching me much of what I know about systems neuroscience. Being in the Zador lab of course led me to interact with Tony from time-to-time, which was always enlightening. If nothing else, Tony taught me to "tell them what you'll tell them, tell them, and tell them what you told them," and that if I really wanted to be successful in his lab then I shouldn't follow his advice on experiments. On top of these more tangible teachings, under Tony I have really changed how I think to now be much more quantitative, and to follow ideas a bit further down the road to find their most interesting implications. I am also indebted to Alex Pouget who, besides convincing me I need to go to ski in Switzerland, really brought great excitement, insight, and direction to our exploration of the widefield imaging data.

On a more hands-on level, there were many people who made this work possible, or at least shaved years off the time it would've taken me to do it myself. Hemanth Mohan helped me make my inhibition scanning setup, the first rig I built that wasn't already fully planned out, and also gave me code

# Table of Content

# List of Table and Figures

# List of abbreviations

**DDM**          Drift Diffusion Model

**IBL**            International Brain Laboratory

**M2**             Secondary motor cortex

**RT**              Reaction time

**SDT**            Signal Detection Theory

**SOWI**        Scanning Optogenetics with Widefield Imaging

**S1**              Primary somatosensory cortex

**V1**              Primary Motor cortex

# General Introduction

**1      Standardized research and the role of mesoscale collaboration in neuroscience**

Decision-making research in the field of neuroscience has traditionally been carried out by individual labs. Each developed their own behavioral task, and focused neural recordings on a select set of brain areas from which they are experienced in recording. Increasingly there has been a realization that behavior arises from the interactions of not only neurons within an area but across many brain areas, and many labs have adjusted accordingly by beginning to interrogate whole circuits of interconnected areas, a hallmark of systems neuroscience. However, brains are large and complex, and not even in the small brain of the lab mouse *Mus musculus,* could a single researcher record neural activity at the scale required to form a brain-wide model of how single-neuron activity combines across the brain to give rise to decision-making behavior. A whole-brain approach to a question such as this requires the collaboration of groups of researchers with different areas of expertise, and who can combine efforts to make substantial steps forward in understanding how the brain works.

One relatively recent trend in this decade has been the initiation of several major mega-projects aimed at making larger leaps forward towards understanding the brain, such as the BRAIN initiative in the US, the Human Brain Project in the EU, and the Brain/MINDS project in Japan. Some however, have questioned the utility or effectiveness of these large-scale collaborations (Frégnac and Laurent, 2014; Hunter, 2015; Mainen et al., 2016; Poo, 2014), and furthermore the only one of these projects that focused on answering a single scientific question, the Human Brain Project, has been widely considered a failure (Theil, 2015). One proposed solution, has been collaboration on the meso-scale, operating between the extremes of a large consortium, and the typical neuroscientific lab (Abbott et al., 2017; Mainen et al., 2016). This led to the creation of the International Brain Laboratory (IBL), a collaboration of over 20 labs working towards understanding a single visual decision-making task in mice. This project is too large for any single lab, and so requires the coordinated effort of researchers working on the same clear objectives. The first of these objectives are to create a standard, reproducible behavioral task that will be shared

across the collaboration, and to record single neuron activity across the whole brains of mice performing this task.

A collaboration such as this requires that different experimenters in different locations can perform the same experiments, and share the data they generate. The key to combining data across different research groups performing the same experiment in different labs is reproducibility. This requires performing the same experiments, with the same apparatus, and obtaining comparable results across several independent groups. This reproduction of results is often difficult, especially when dealing with biological systems (Errington et al., 2021; Li et al., 2021), which are inherently noisy and complicated. Reproduction can be so difficult that the field of neuroscience, like many other fields, has been described as having a 'reproducibility crisis' (Baker, 2016; Botvinik-Nezer et al., 2020; Button et al., 2013), where researchers report an inability to reproduce results published by other labs, or even from their own previous experiments. This seems to be of especially large concern for mouse behavior (Kafkafi et al., 2018) where differences as unexpected as the sex of the experimenter can change the results of an assay (Sorge et al., 2014).

One important source of the lack of reproducibility across labs is likely the poor documentation of methods and results. In an attempt to reproduce the findings in cancer biology primary research papers, a team found that 0/193 experiments had sufficiently detailed procedures to repeat experiments (Errington et al., 2021). Even after experiments are completed, when one is working with extremely large datasets, preprocessing and analyses increase in complexity and therefore the number of options for different parameters and processing steps increases dramatically. This features prominently in neuroscience research, and will only be increasingly true as the number of simultaneously recorded single spikes is still growing exponentially (Steinmetz et al., 2018). It has been shown that specific choices of how to preprocess can dramatically alter the conclusions a research group draws from the data (Li et al., 2021), and because of this, different groups can draw completely different conclusions from the same dataset (Botvinik-Nezer et al., 2020).

Collaboration across labs can solve both of these problems of ensuring reproducible results and pursuing large questions. To answer the large question of how activity across the mouse brain contributes to solving a visual decision-making task, the IBL required at least 10 different scientists performing the same experiment in different labs. This necessitates the reproduction of results, and towards this goal, we have thoroughly standardized our procedures, hardware, and software (The International Brain Laboratory, 2020a, 2020a; The International Brain Laboratory et al., 2020; The International Brain Laboratory, 2021; The International Brain Laboratory et al., 2021). As half of the collaboration is theoretical and computational neuroscientists, and we hope to combine information from different neural recording modalities, the creation of a standard data architecture and code base has been, and will continue to be, an essential element of effective collaboration, and is the only way to collate results to fulfill the IBL's purpose. Though there have been growing pains throughout the process, the collaboration has generally been a success, by completing one of its first objectives of creating a standard behavior (The International Brain Laboratory et al., 2021), nearing completion of its second main research product, securing additional funding to diversify its operations, and learning to more effectively collaborate along the way (Wool, 2020). Hopefully these successes will continue, and if our goals are reached, the results of the IBL will be far more impactful than any one of its member labs could produce.

## 2        The cortical basis of perceptual decision-making

At the core of the IBL's scientific goals is determining the neural basis of a perceptual decision-making task in mice. The study of perceptual decision-making has the basic goal to determine the neural basis of a learned transformation of sensory information to motor output, something that is constantly happening in behaving animals. Intervening steps in this process are the sensory detection of stimuli, their combination with prior expectations to form a percept, the decision of which choice in a learned context to make, and the motor execution of this choice. This field of study builds on a history of psychophysics (Fechner, 1860) for its behavioral components, signal detection theory (SDT, Shannon,

1948) and drift-diffusion models (DDM, Ratcliff, 1978) in its theoretic backbone, and applies modern neuroscientific tools to pursue the underlying neural basis.

Signal detection theory mainly is thought of in the perception of stimuli. Consider a two-alternative forced choice task, similar to the one used in this thesis, where a subject must determine if they see stimulus 1 or stimulus 2. SDT frames this problem probabilistically by characterizing each stimulus as a gaussian distribution with some mean and standard deviation. This indicates that there is not a perfect representation of the stimuli, but rather there are noisy representations of them. On each presentation of a given stimulus, the perception of this stimulus is drawn from its distribution, so if the distribution for the two stimuli are non-overlapping, then there will be no errors in perception. However as the stimuli become noisier or more similar to each other, their distributions will have more overlap, making it more likely that one stimulus will be mistaken for the other. In addition to this, it is clear that perception is not only influenced by the current sensory evidence, but also by prior experience [citation needed]. Bayes' Theorem provides us with an optimal way to combine this prior information with the likelihood of the current information to give the posterior distribution, from which the percept is drawn [citation needed]. Using this framework, one can generate predictions of the probability that each choice will be made given the stimuli and previous history, and this probabilistic representation directly results in a psychometric curve when averaged across many trials.

Decision-making is a process that evolves through time, yet SDT only describes perception in a static way. Drift-diffusion models bring time and decisions into this framework. The DDM framework similarly represents the stimuli as noisy gaussian distributions, but instead of representing the perception as a single comparison of two distributions, it posits that the subject is continually sampling from these two distributions during decision-making. As samples are taken from these noisy, overlapping distributions, the evidence is gradually accumulated for the more probable stimulus. The DDM framework also provides a stopping time for the decision, where once this accumulation of evidence crosses some threshold, a decision is reported in favor of whichever threshold has been crossed. This allows for explanation of different types and shapes of reaction time distributions [citation needed].

14

The study of the neural basis of perceptual decision-making was first pursued in primates, using the visual random-dot motion task that first connected a psychophysical behavioral task with neural recordings during task performance (Newsome et al., 1989). This body of work has described that single neurons in visual cortex area MT have activity well-suited for psychophysical detection of stimuli according to signal detection theory, and that noisy, correlated activity of populations of neurons in the visual cortex can be used to predict the animal's behavior. This demonstrated an example of the neural basis of perception, but to make a decision, theories of bounded evidence accumulation showed that this information needs to be integrated over time, and signal detection theory indicated that the difference between the neural activity for the different decision options needed to be calculated. It was later shown that the information for the different decisions was sent to a more frontal cortical area, LIP, where the difference of the evidence for different options is integrated over time, as predicted by the DDM framework, and maintained until a decision is made (Shadlen and Kiani, 2013). These findings were able to use neural recordings to find strong and convincing correlations between the theoretical processes underlying decision-making and neural activity in the cortex.

However, the key issues with these insights are that the findings are largely correlational, and they are also restricted in their scope, as the techniques at the time were limited to recording small populations of neurons from single cortical areas. Another large advancement in the field of decision-making came from a different body of work once it was established that rats could perform evidence accumulation and perceptual decision-making in much the same way as primates, and in accordance with decision-making theory (Brunton et al., 2013). Also important is that mice, with their large and ever-growing arsenal of genetic tools, are just as amenable to perceptual decision-making as rats (Jaramillo and Zador, 2014). With the addition of rodents to the study of perceptual decision making, and all of the genetic and biological tools they possess, the study of decision-making has broadened and deepened drastically (Najafi and Churchland, 2018). It now has expanded to include the roles of different cell-types in the production of decisions (Najafi et al., 2020), how perturbations of different nodes in the decision-making process underlie different features of the process (Guo et al., 2014; Li et al., 2016), and most recently the

representation of decision processes across the whole dorsal cortex (Makino et al., 2017; Musall et al., 2019; Zatka-Haas et al., 2021).

This extensive research into the neural processes underlying decision-making leaves us with some strong expectations, and some open questions of the role of different cortical areas in the process. We expect that activity in the visual cortex will be correlated to the visual stimulus (Wekselblatt et al., 2016; Zatka-Haas et al., 2021), that activity in the anterior lateral motor cortex will correlate more closely with the decision that the mouse makes (Guo et al., 2014; Inagaki et al., 2019; Li et al., 2016), and that correlates of the presence of an action will be distributed across the cortex (Musall et al., 2019; Zatka-Haas et al., 2021). We further know that decisions are not made based solely on the current sensory evidence, but prior information about the probability of different stimuli also influences the decision process (Dayan et al., 1995; Doya et al., 2006). However open questions include what the representation of this prior information will look like and in which areas it will reside, to what extent is the task information localized to individual cortical areas versus widely distributed, and if different decision processes can be affected by manipulating activity in different cortical areas.

## 3      Large-scale, data-driven research

Computers and computation have become an invaluable tool for scientists of all fields. Not only have the improvements in computational power drastically influenced how science is done by allowing much larger simulations, and much more computationally intensive models and analyses, but there have been a host of other improvements in hardware and software supporting and using this newfound computational ability. In software, strong correlational techniques have not only been increasingly expanded and improved upon, but many have been made easily accessible by free, open-source software implemented in the easy-to-use and versatile language Python (Developers, 2022; Paszke et al., 2019; Virtanen et al., 2020). In supporting the advances in computational power, there have also been improvements in the speed of reading and writing data, as well as the increased availability of data storage. These changes in the ease of recording, accessing, and analyzing data has led to an increase in

data-driven research as opposed to the standard scientific method that has been productive for scientists since its establishment in the scientific revolution over four centuries ago.

The standard scientific method consisting of forming hypotheses, designing controlled experiments to test those hypotheses, and revising the hypotheses based on the results of those experiments, has been extremely fruitful. This scientific method that was brought into practice in the late 1500's and is taught as doctrine in primary and secondary schools today, has given rise to most major scientific findings until the late 1900's. This method is not only promoted in primary schools, but nearly all scientific publications, funding agencies, and even the instructions for writing this thesis promote framing your results as a question asked, data collected, and then updating the questions asked. In practice, though often applicable, this scientific method is not always how scientists do science (Elliott et al., 2016). In some fields of science, experiments are simply not possible such as in astronomy, and paleontology, or were not feasible until recently, such as the study of evolution. These fields, in the absence of available experiments, are based on combinations of data (observations), and they have been operating successfully for centuries (Müller-Wille and Charmantier, 2012). However with the rise of the computer, these non-experimental and non standard scientific methods have been integrated into scientific fields more traditionally based in the standard method such as biology, causing some friction (Angier, 1990; Mazzocchi, 2015).

The newly arising approach to science leveraging the recent improvements in computational tools mainly differs from the standard scientific method for its lack of specific hypotheses, and experiments testing them. In this model, researchers collect a large amount of data (usually using a new technique that has made such data collection possible), then perform analyses on these data. A high-profile example of such research is the Human Genome Project (HGP), which was initially criticized for its lack of hypotheses (Angier, 1990), but has since been seen as an invaluable resource to the scientific community and which catapulted biology into the computational age (Gibbs, 2020). Though the promises of the HGP were many, the goals were simple, to sequence the entire human genome, and use this sequence to determine the genetic basis of diseases. Such large scale data collection and analysis are often criticized as

'fishing-expeditions' (Lazer et al., 2014) or indiscriminately performing statistical tests to find significant correlations in the absence of specific hypotheses, which are plagued by nonsense correlations.

In reality, it's true that data is nothing without hypotheses, but hypotheses and theories are also nothing without theories. This highlights a model of scientific inquiry that is more iterative than the traditional linear scientific method (Kell and Oliver, 2004). As the standard method dictates, theories must be tested and revised based on the available data, therefore creating a circle (Elliott, 2012) out of the often linearly depicted method. In this light, data-driven or non-hypothesis driven science can be simply seen as entering the scientific process at a different location than at hypothesis formation. Even if a single scientific study never fully closes the loop between hypothesis, experiment, and data, it is still a part of the scientific process, and that loop can be closed by future work in the field. Therefore much of data-driven, correlational, or non-hypothesis driven research can be seen as methods for creating hypotheses that can later be tested. For example, no FDA-approved drugs have been created directly out of the field of genomics, yet the correlations found in genomics can be used to find targets that can be experimentally tested (Emilien et al., 2000). Similarly, neural recordings only produce correlational data, yet they can be used to generate hypotheses of the computations or behaviors that those neurons produce, which can later be tested with experimental manipulations. In fact, since the introduction of optogenetics to neuroscience research, a common story line in high profile neuroscience papers has been to first describe a phenomenon with neural recordings, then to design perturbation experiments to disrupt the described phenomenon, then to place this within some hypothetical framework.

Within neuroscience in particular, the advancements in abilities to record data have lagged behind the computational ability to record neural activity. Only a few decades ago, neuroscientists were limited to recording the activity of a handful of neurons at once, while today we can record thousands. This rapid progression of tool development has only allowed the field of systems neuroscience to engage in such large scale data-driven research in the past 10 years. Though the correlational tools of neural recordings have been used for over a century, the ability to record activity across networks and even the whole cortex

has only been available very recently. Therefore, the use of such tools is just beginning to be fully exploited to find correlates of behavior and computation across large neural circuits.

Using such large-scale, non-hypothesis driven methods are the focus of much of this thesis. Though within each experiment there were a set of expectations that were set, many of the questions addressed were only asked after the data was collected. Even the main perturbational experiment I show in this thesis manipulates activity in each cortical area I had access to in an unbiased, data-driven manner. I performed a large set of analyses on these data, that some may describe as a fishing expedition. However, they were all performed with the most conservative statistical methods available so as to limit the influence of false correlations. The hope is that the results reported here can be seen as a small step in the larger scientific discussion on the functioning of neural circuits in perceptual decision-making. These results will inform both the explicit and implicit models that the field uses to think about decision-making, and will be tested and compared to other results from within the standardized IBL framework.

## 4      Summary of contributions to the field

In contribution to understanding the neural basis for perceptual decision-making, this thesis will present my progress towards four goals: 1) create a standardized visual perceptual decision-making task in mice, 2) contribute single cell recordings across the whole mouse brain in this task, 3) causally manipulate ROIs across the whole mouse dorsal cortex in this task to determine the roles of different cortical areas in different decision processes and 4) describe the neural correlates of behavioral variables in this decision-making task across the whole dorsal cortex.

*A standardized visual decision-making task in mice*

To study the process of perceptual decision-making across the whole brain, it was first necessary for the IBL to establish a standardized, reproducible visual decision-making task that could be deployed across the member labs. It was critical that this task provided psychophysical performance and manipulated the prior expectation of the stimulus, so as to be able to study all of the decision-making

processes outlined above. This task is presented in Chapter 1, where we as the IBL demonstrate that behavior across labs is indistinguishable from each other, and that the mice in our task demonstrate the standard decision-making behaviors as seen in psychophysics and that they integrate past evidence into their decisions. Critically, I also show that, using the same task with a different experimental paradigm, I can reproduce the behavior, and with the IBL data infrastructure I can trivially compare results from different experiments to those of the IBL as a whole.

*Single cell recordings across the mouse brain*

As a contribution to the IBL's first main production of neural recordings, I performed over 100 acute recordings with Neuropixels probes, recording thousands of neurons. Though my contribution to this work was completed over a year ago, the data collection and analyses for this project are still ongoing by other IBL members. In chapter 2, I present an overview of my contributions to this herculean project, indicating my penetrations are distributed across the brain, but that accurate targeting was a challenge. The main results for this dataset have yet to be published, but will include reporting on how reproducible such recordings are, the distribution of neural representation of decision variables across the brain, and an atlas describing the electrophysiological properties of different brain areas.

*Causal manipulations to determine area contributions to decision variables*

One key technology that has recently arisen in neuroscience is optogenetics, allowing spatially precise, relatively non-invasive causal manipulations of neural activity. I leverage this technique in Chapters 3, 4, and 7, to inhibit areas across the dorsal cortex to determine the contribution of different cortical areas to decision-making. I confirm previous findings that key nodes are the primary visual cortex and secondary motor cortex, and I extend these results to show that inhibitions of visual cortex only cause perceptual errors, whereas inhibition of motor cortex causes impulsive-like decisions, as well as perceptual errors. However, these findings are complicated by the fact that chronic removal of visual cortex does not affect behavior. I furthermore demonstrate a method to perform localized optogenetic perturbations and map their global cortical effects.

*Describing the neural correlates of decision-making across the cortex*

Through whole dorsal cortex widefield imaging, I was able to find neural correlates of decision-making across the cortex. My findings agree with previous research, as well as the causal manipulation experiments I have performed, showing that the areas most heavily involved are primary visual cortex and secondary motor cortex. I extend these results, showing that task information is distributed across the dorsal cortical surface, widely broadcast to nearly all areas. I furthermore provide a novel description of the neural correlates of a bayesian stimulus prior, as well as what appears to be an embodied form of choice expectation.

# Results

## 1        A standard, reproducible decision-making task for head fixed mice

<u>Contribution Note:</u> The following chapter is mainly a report on work done by a large collaboration of over 30 people, all members of the IBL. I was a member of the Behavior Working Group responsible for producing this work, as well as performing pilot tasks before the presented task was chosen. As such I was a part of many group decisions and discussions about the task creation and associated protocols. Additionally I collected tens of thousands of trials of behavioral data that was used in this paper (Lab 3 in the figures of this chapter), and in pilot tasks that preceded the final task and training procedure described herein. The figures in this section are largely regenerated using code and data from (The International Brain Laboratory et al., 2021), mainly written by other IBL members. The following text is my own, but it leans heavily on the aforementioned paper and the conclusions and data are a shared product of the IBL. The main addition to the data in this chapter is that I have added mice that are used in the following chapters of this dissertation but were not used by the IBL as a whole, and modified the analysis code to include them as an additional 'Laboratory' in each figure.

### 1.1 Introduction

Decision-making research in the field of neuroscience has traditionally been carried out by individual labs. Each works on their own behavioral task, and focuses neural recordings on their pet brain area. Increasingly it is clear that behavior arises from the interactions of neurons across circuits and brain areas, and as the tools have become available to perform research at these levels, many labs have adjusted to interrogate circuits of interconnected areas. However, recording activity across the whole brain is a daunting task. Not even in the relatively small brain of a lab mouse could a single researcher record neural activity at the scale required to form a brain-wide model of how single-neuron activity combines across the brain to give rise to decision-making behavior. This is the goal of the IBL (Abbott et al., 2017), a collaboration of over 20 labs working towards recording individual neurons from across the entire brain during a standard decision-making task, and using this data to generate models and analyses of the neural basis of decision-making. With ten different researchers contributing to these neural recordings, the first step was to create a standard decision-making behavior that could be reproduced in 10 labs across the U.S. and Europe.

The key to combining data across different research groups performing the same experiment in different labs is reproducibility. This requires performing the same experiments, with the same apparatus, and obtaining comparable results across several independent groups, a non-trivial task. This seems to be of especially large concern for mouse behavior (Kafkafi et al., 2018) where differences as unexpected as

the sex of the experimenter can change the results of an assay (Sorge et al., 2014). Because

reproducibility is a core requirement for the IBL to succeed, special care was taken to standardize as

much about the experiment as possible, starting with the inbred strain of mice that was used, through

surgical protocols and housing requirements, and all of the hardware and software for training and

recording the decision-making behavior. Everything that was known to vary but could not be standardized

due to differences in institutional requirements or availability of certain reagents or equipment in different

countries, was saved as meta-data.

Using this emphasis on standardization, the IBL as a whole was able to produce a standardized

decision-making behavior that was reproducible across 7 labs, including our own. The only significant

differences found between the labs was the learning rate with which the mice acquired the task; but once

the task was acquired, there were no differences in performance between the labs (The International Brain

Laboratory et al., 2021). There is of course a high variability across individual mice, but this will exist

within a lab as well as across labs. Because the variability between mice was larger than the variability

between laboratories, we can claim that the behavior is reproducible, and the results comparable, across

labs.

An additional benefit of having a standard reproducible behavior is that once this is established,

not only are the results comparable across labs performing the same experiment with that task, but when

different neural recording modalities or manipulations are introduced for animals performing this task, the

results of these new experiments are directly comparable to the existing data. Here I will show that not

only is there reproducible behavior across labs in this visual decision-making task, but additionally the

behavior for all mice used in this thesis (excluding sessions with optogenetic neural manipulation) is

indistinguishable from that collected for the IBL's brain wide electrophysiology map project.

**1.2 Materials and methods**

*Mice*

Both male and female mice were used for these experiments, with ages from 3-7 months old. All

were C57BL6/J inbred mice obtained from Jackson Laboratory or Charles River. They were co-housed

with the exception of when a mouse was required to be single-housed for health reasons, usually an aggressive male mouse attacking its cage mates. Mice were housed differently depending on the local institution regulations and practices, but all cages had minimum enrichment of nesting material and a mouse house. All were kept in rooms with a 12-hr light-dark cycle, and were fed food with 5-6% fat content, and 18-20% protein.

*Surgeries*

A detailed protocol for the headbar implantation surgery used in these experiments is available through Figshare (The International Brain Laboratory, 2020a). Briefly, mice were anesthetized with isoflurane and head fixed in a sterotax with earbars. The hair above the scalp was then removed, a majority of the scalp and the periosteum over the skull were removed. Bregma and lambda were marked and the head was positioned as near to a 0 degree angle between these two landmarks as possible in all directions. The headbar was then cemented to the skull in one of three predefined positions, and the edges of the scalp were glued and cemented to the skull to avoid retraction. Then the remaining open skull was sealed with a clear UV-curing glue and the animal was allowed three days to one week to recover before water deprivation began.

*Behavioral training apparatus*

A detailed parts list and installation instructions for the IBL behavioral training setup used for training in all sections of this document can be found on Figshare (The International Brain Laboratory, 2021). The basic design of the rig is an adaptation of one previously developed for a related task (Burgess et al., 2017). All labs used the exact same hardware with the exception of different power adaptors for European and American labs. Each rig primarily consisted of an LCD screen (LP097Q, LG), positioned in front of a custom 3d printed mouse holder. The mice were head fixed with the attached head plate such that they rested on the mouse holder with their forepaws resting on a steering wheel (86652, LEGO). Rewards of 10% sucrose water were delivered through a silicone tube, and the sucrose water flow was controlled with a normally-closed pinch valve (225P011-21, NResearch). The structure of the rig components was created with Thorlabs parts inside of an acoustical cabinet (9U acoustic wall cabinet 600

x 600, Orion). Screen frame updating was measured with a photodiode (BPod Frame2TTL, Sanworks) placed in front of a small square on the screen that flipped from black to white each time the screen was updated. Wheel position was recorded using a rotary encoder (05.2400.1122.1024, Kubler) coupled to the wheel with a custom 3d printed piece, and attached to a Bpod rotary Encoder Module (Sanworks). A video of the mouse was recorded and displayed during training with a USB camera (CM3-U3-13Y3M, Point Grey). Task sounds were played on a speaker (HPD-40N16PET00-32, Peerless by Tymphany), and sounds during the behavior were recorded with an ultrasonic microphone (Ultramic UM200K, Dodotronic). All task data and event generation was coordinated by a Bpod State Machine (Sanworks). The task code was written in Python 3.8 and visual stimulus generation and video capture was coordinated with Bonsai and the BonVision package (Lopes et al., 2021, 2015).

*Behavioral training*

A detailed protocol on animal training and handling can be found on Figshare (The International Brain Laboratory, 2020b). Following the recovery period after headbar implantation, mice were water restricted. Mice were usually to 1ml of water per day (variable across institutions), and often on weekends mice were given 2% citric acid water ad libitum (Urai et al., 2021). Mice were handled for 10 minutes during water administration for at least two days prior to head fixation to reduce the stress response to handling; mice were never picked up by the tail before a behavioral session. Following this restriction, mice were habituated to the rig by having increasing lengths of head fixation for 3 consecutive days (15, 30, and 60min), while a gabor stimulus was passively viewed by the mouse. The stimulus appeared randomly at either 35 visual degrees left of center, 35 degrees right, or in the center of the screen. When the stimulus was in the center of the screen, it was paired with a 3ul delivery of 10% sucrose water. After these three habituation days, the behavioral training commenced.

On each trial, the mouse must keep the wheel stationary for 200-500ms to initiate a trial. This is followed by the onset of the stimulus at either -35 degrees (left) or +35 degrees (right) on the screen, which is also paired with a pure-tone go-cue. The contrast of the stimulus was randomly drawn from a set of contrasts that varied with training progression (initially starting with 100% and 50%, eventually

progressing to a final set of 100, 25, 12.5, 6.25, and 0% contrast as performance increases). After the onset of the stimulus, the mouse has 60s to respond. A response is triggered by moving the steering wheel which is coupled to the stimulus azimuth. After the stimulus is moved 35 degrees from its starting location, a response is recorded and the stimulus position is frozen (for most of these sessions there was a known bug that for very fast wheel movements, the stimulus was erroneously frozen at positions other than 0 or 70). If the stimulus is moved to the center of the screen, a correct response is triggered and the mouse receives a 10% sucrose water reward (from 3-1.5ul per trial, depending on training progression), and the stimulus is frozen in position for 500ms. If the stimulus is moved off the screen, an error is triggered and a 500ms white noise burst is played and there is a 2s timeout delay until the next trial can be triggered. Early in training, animals frequently become very biased, repeating a choice with a very high probability. To counteract this we use a debiasing algorithm that chooses the stimulus side inversely proportional to the choices that the mouse has recently made, such that the more a mouse reports a right stimulus, the more often a left stimulus will appear, so that the reward rate of strongly biased behavior is decreased. This debiasing is only used in early stages of training before biased blocks are introduced. Throughout training, the animals are monitored with a livestream from the USB camera to ensure the mouse is able to perform the task (possible errors include the lick spout moving to be out of reach of the mouse or the mouse escaping head fixation).

Mice were trained on this 'basic' visual decision making task, until they reached a set criterion of performance for three consecutive days based on the fitted parameters of a psychometric curve to behavior after all contrasts were introduced. After these criteria were met, the animal progressed to the 'full' version of the task. In this full version, the trial structure remained the same as the basic task for the first 90 trials of each session except that the debiasing algorithm was no longer used. Following that, the stimulus side was no longer drawn with equal probability for each side, but was instead drawn from a biased set of .8 on one side and .2 on the other. The side of the biased block was strictly alternating and lasted for 20-100 trials, with an average of 50 trials per block.

*Psychometric curves*

Psychometric curves were fitted using a maximum likelihood estimation procedure according to an error function parameterized as follows:

$$P \; = \; \gamma \; + \; (1 \; - \; \gamma \; - \; \lambda)erf(\frac{c-\mu)}{\sigma} + 1) \, / \, 2$$

Where *P* is the probability of choosing a left stimulus, *c* is the stimulus contrast, and the following psychometric parameters are fitted: $\gamma$ the lapse rate for left stimuli, $\lambda$ the lapse rate for right stimuli, $\mu$ the response bias, and $\sigma$ the contrast detection threshold.

*Thesis mice*

All of the above materials and methods apply to all of the data in the following chapter for the mice attributed to Labs 1-7. The mice reported as "Thesis mice," however, have a few deviations from the above methods. Thesis mice refers to all mice used in experiments I conducted independently from the IBL used in chapters 3-7 in this thesis. The first difference is the genotype of these mice, some include VGAT-ChR2 mice (stock number 014548, Jackson Laboratory), which were created in a C57B6/J background and maintained by out-breeding to the C57BL6/J line, so are likely very similar genetically to the majority of the mice used in the IBL experiments. Another main genotype in the thesis mice group is a cross between a TRE-GCaMP6s mouse (Wekselblatt et al., 2016)(Jax stock number 024742), and a CAMK2-tTA driver line (Mayford et al., 1996) (Jax stock number 007004) used in chapters 4 and 5. These mice were a gift from the Churchland lab. The GCaMP6s mice were generated in a C57BL6/J x DBA F1 hybrid, and the CAMK2-tTa mice were generated in a C57BL6/J background, so though there is more difference between these mice and the IBL mice, they are still majority C57BL6/J background. The final mouse genotype in the "Thesis mice" were a triple transgenic of the TRE-GCaMP62, CAMK2-tTA, and VGAT-cre mice (strain 016962, Jackson Labs) were created in a joint C57BL6/J; FVB background (Vong et al., 2011)**.** Therefore these mice are also not entirely in a C57BL6/J background (as evidenced by their Agouti phenotype).
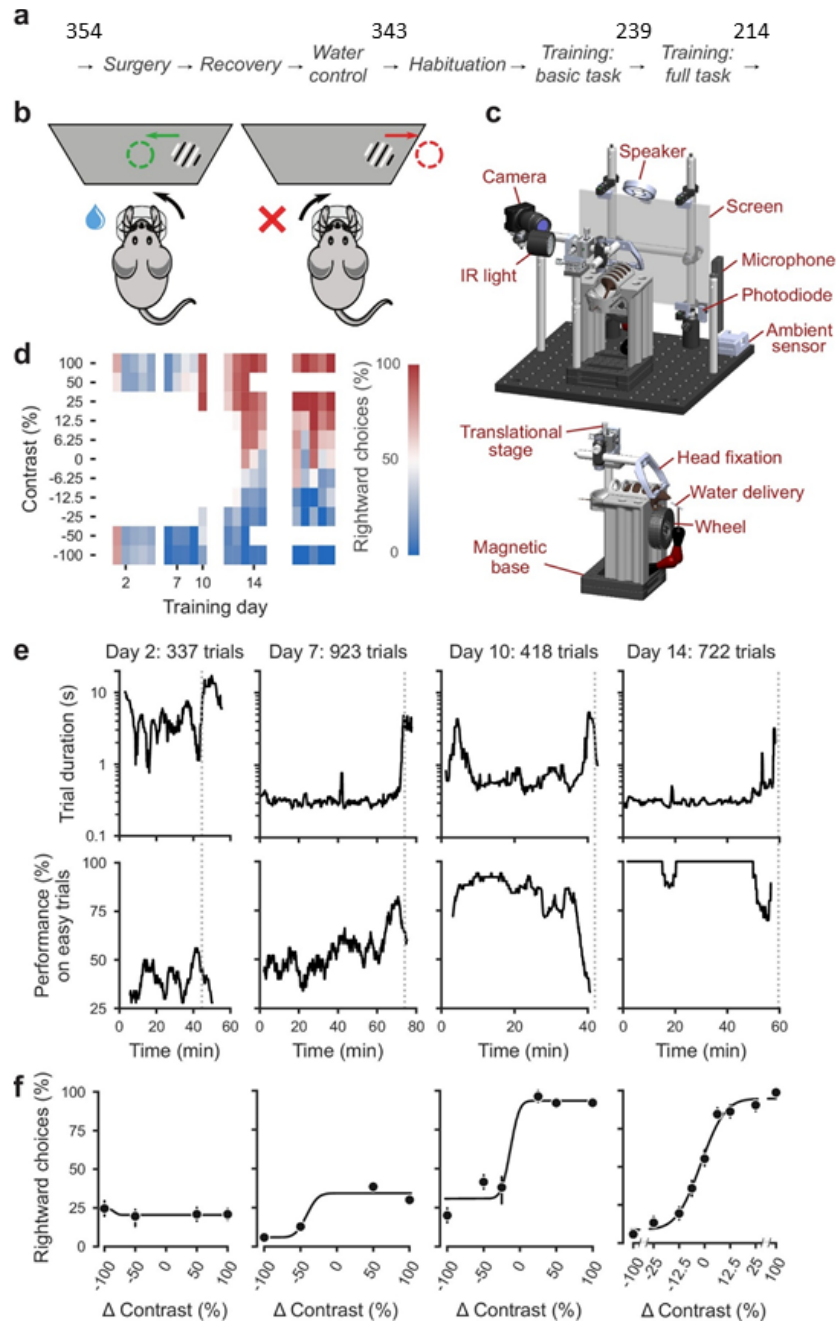
The thesis mice also differ from the general IBL mice in their training procedure as there was no habituation period during training. Water restriction and handling were done as described above, and following this mice began immediately performing the task upon the first head-fixation. This was done to reduce training time (removes three days where the animal is not training), and in general I believe it to be more humane as the reward rate given during the task performance even on the first few days is often greater than that used during the IBL habituation. Training was the same after this, excepting that after the basic task was acquired, the response window was shortened to either 2 seconds (for inhibition scanning mice) or 10s (for widefield imaging mice), and the ITI was increased by 1 second for widefield imaging mice to allow the calcium signal ample time to return to baseline.

Thesis mice were filtered on the IBL database by selecting mice that belonged to project code "zador_les," see forked version of github repository "Paper behavior" (https://github.com/cskrasniak/paper-behavior/tree/CSK_thesis) for details. These were compared to mice from the IBL project "ibl_neuropixel_brainwide_01" for each lab location.

**1.3 A reproducible decision-making task for head-fixed mice**

To create a standardized and reproducible decision-making behavior, we followed two main paths: standardization of materials and methods described above, and the automated gradual shaping of behavior through a standard training pipeline. Mice were first implanted with a headbar for head-fixation. At the time of writing, 354 IBL mice have undergone the headbar implantation surgery, and 11 of these mice have been unable to progress in training due to surgical complications (Figure 1.1a). Therefore, 343 mice have been handled by the experimenter, water restricted, and habituated to head fixation. Following this, mice began training on the basic task. The goal of this training was for the mouse to learn the motor response of moving the wheel to the left for stimuli appearing on the right, and vice versa for stimuli on the right, with the stimulus location yolked to the movement of the wheel until a response is triggered (Figure 1.1b). During the first 400 trials of training the gain between the wheel movement and the stimulus movement was much higher than for the rest of training, so that triggering a response was very

easy. This was done to simply encourage mice to move the wheel and get more reward despite not yet having learned the task. During the early stages of this training, only very high contrast stimuli were shown, and the volume of reward was kept high. The volume of reward was not tied specifically to the animal's accuracy, but rather to how many trials the mouse completed. Each training session in which a mouse completed 400 or more trials, the reward volume was decreased by 0.1ul. The contrast set that was shown to the mice was tied to the animal's performance over the last 200 trials. Such that a new contrast is only added when the performance on the existing contrasts was above 80% correct (Figure 1.1d). This is valid for the addition of the 25% and 12.5% contrasts, the more challenging 6.25% and 0% contrasts are added based on simple trial counts after the addition of all previous contrasts. A final automated aspect of the task was the detection of when a mouse should end the training session. There were several criteria that triggered a warning to remove the mouse from training. Early in training the most common reason for session completion was reaching 45 minutes of training without having completed 400 trials (Figure 1.1e, day 2). Later in training, the most common session end trigger was an increase in reaction time (Figure 1.1e, days 7 and 14), followed by a dramatic decrease in performance (Figure 1.1e, day 10). This gradual changing of task parameters was done to mimic the gradual 'shaping' of animal behavior that is traditionally done in most systems neuroscience labs; however it was done based on automated criteria in an attempt to decrease variability in how mice learned to perform the task.
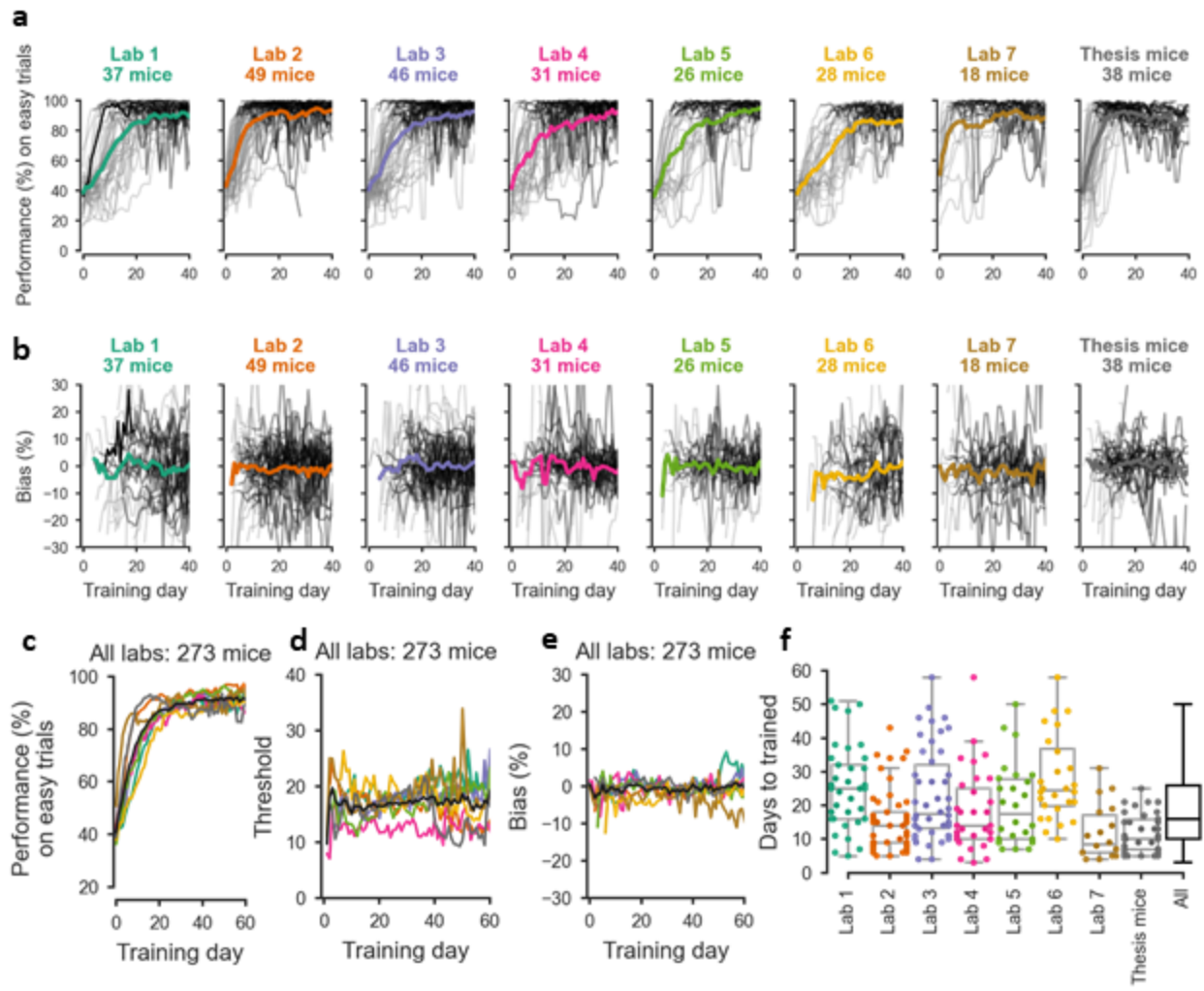
**Figure 1.1.** Animal training on the basic IBL task. (a) The standard training pipeline with the numbers of mice that have made it to each part of the pipeline as of January 1, 2022, excluding mice still in training that could yet progress in the pipeline. (b) Schematic of the task goal, arrows indicate the movement of the stimulus and wheel, the animal triggers a correct response (green) by moving the stimulus to the center of the screen and is rewarded with a drop of sugar water. (c) Three-dimensional schematic of the basic IBL training rig and its components. (d) Training progression of one example mouse, colors indicate the percent rightward choice made at each contrast level. Initially only easy contrasts are available, but once the mouse learns the stimulus side association more contrasts are introduced. (e,f) Performance on example days for the same mouse in (d). (e) Trial duration and performance on high contrast trials across training days, dotted lines indicate when the mouse triggered the session end criterion. (f) Psychometric curves across training, originally the mouse started off highly biased as is typical, and gradually progressed to have strong psychometric performance until it was considered trained (day 14).

30

Mice were considered trained on this basic task when they met certain criteria of strong

performance based on fitted psychometric curves across three days of training, and had a sufficiently fast

reaction time on 0% contrast trials (see methods). The acquisition of this basic task is the largest source of

dropout of mice in the pipeline, with about 30% (104/343) of mice failing to learn this simple

stimulus-motor pairing, or being unable to continue training for other experimental, practical, or health

concerns (Figure 1.1a). Following training on this basic task, animals were introduced to the biased

blocks in which the stimulus side probability alternated from .8 on left to .8 on the right side in blocks of

about 50 trials. Training continued as normal for these sessions, except that there was no longer any

anti-biasing algorithm as we now encouraged animals to bias their behavior, albeit in blocks. Mice were

considered fully trained when they reached a significant amount of bias between the percent chosen left at

the zero contrast trials between the left and right blocks. Most animals that learned the basic association

were able to maintain strong psychometric performance while showing this biasing of behavior (214/239

mice, Figure 1.1a).


**1.4 Training progression is highly variable across mice, and different among labs**

Despite standardizing as much as possible about the mice and their training, there still existed a

large difference between the learning rates of individual mice. This can first be seen in the high rate at

which mice never learned the task (Figure 1a). However, even excluding these mice, there was enormous

variability in the rate at which individual animals learned the task (Figure 1.2a). There were some

similarities in how mice progressed through training, such as that in all labs mice began training strongly

biased to one side or the other (Figure 1.2b), which can also be seen in that mice consistently performed

below chance on easy trials early in training due to the bias correction increasing the presence of the

non-preferred stimuli (Figure 1.2a). In addition to the variability between individual animals, there was

also variability between different labs in how quickly they were able to train mice on average (Figure

1.2f). The lab with the fastest training rates was able to train mice in less than half the time as the slowest

lab. Interestingly, the mice trained for this thesis exhibited faster learning rates than the average IBL mice. The only notable difference in training protocol for these mice relative to the IBL mice is that they did not participate in the habituation period of training.
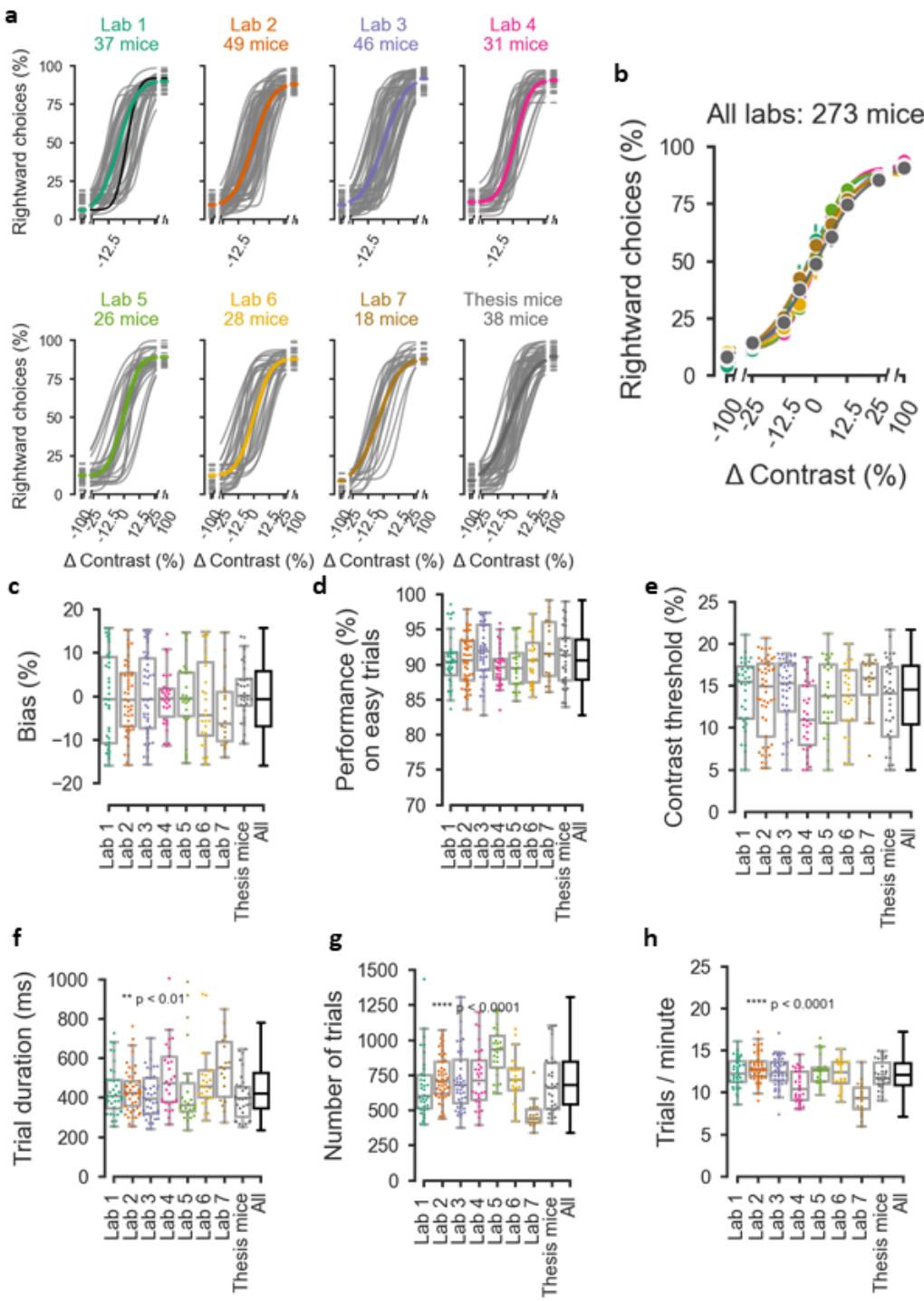
**Figure 1.2.** Training rates are variable across individual animals and days. (a) Performance on easy contrasts for each mouse (gray traces) within each lab (colored traces are lab average) across the first 40 days of training. (b) Psychometric bias of individual mice (gray traces) and for the lab on average (colored traces) across labs. (c) Overlay of lab averages from (a) to compare performance on easy contrasts across training days. (d) Average psychometric threshold across days of training for each lab. (e) Average psychometric bias across training days for each lab. (f) Days of training required to reach the first 'trained' criterion for each lab (colored dots) for each lab.

**1.5 Behavior of Thesis Mice is indistinguishable from all other IBL mice**
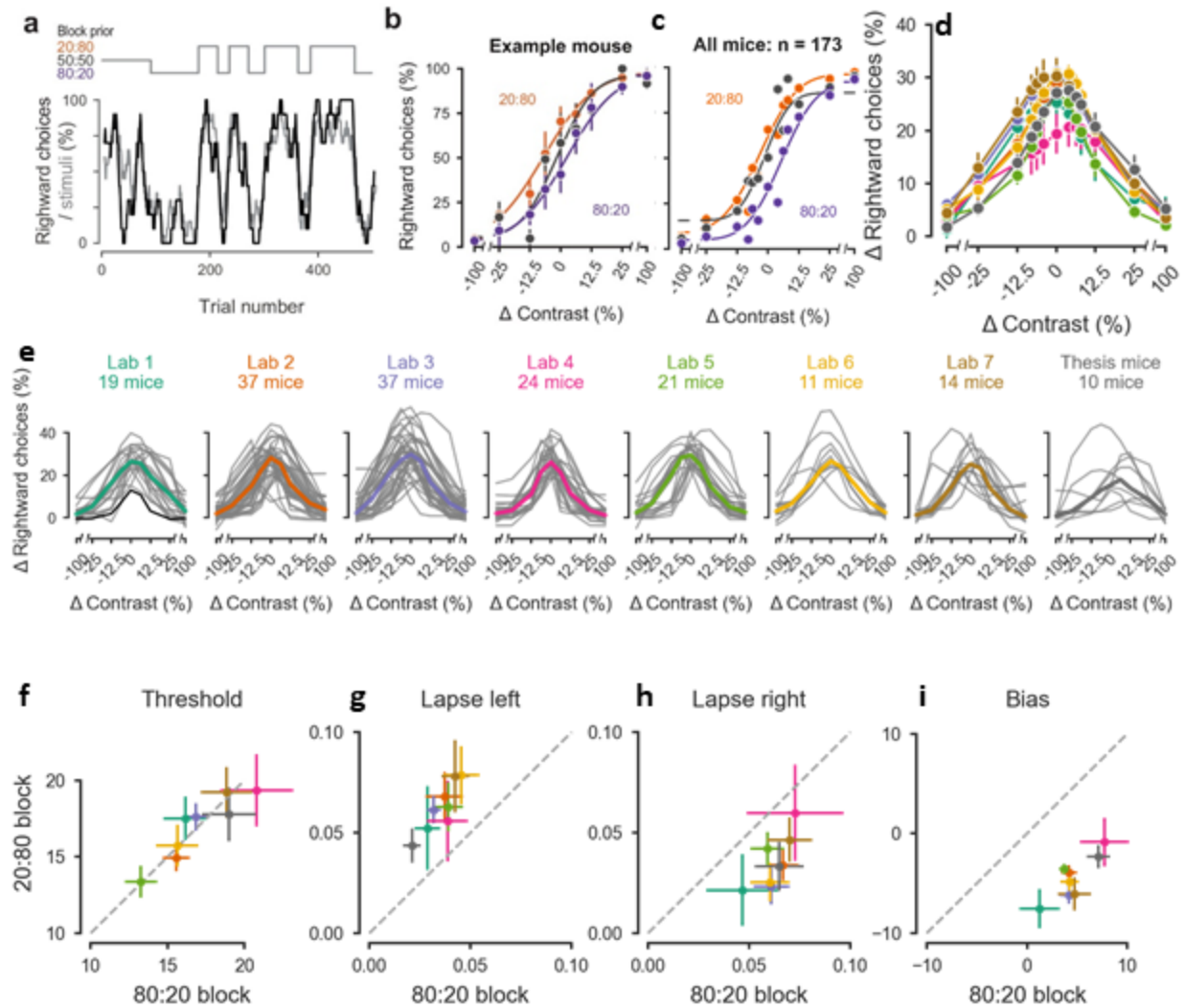
Although there may be significant variability in the rate of training of mice, experiments were only performed with mice that had reached terminal performance, so the relevant point to compare mouse performance is after they have acquired the task. I first visualized the psychometric performance of mice on individual sessions to get an idea of the variability on single sessions. Within labs, there was a large variability in the performance of mice on individual sessions following reaching the 'trained' criterion on the basic task (Figure 1.3a). However when averaging across sessions within a lab, the psychometric performance of different labs, including the Thesis Mice, was indistinguishable (Figure 1.3b-e, lapse p = 0.262, threshold p = 0.125, bias p = 0.638, Kruskall-Wallis H-test for independent samples).  Though the psychometric behavior did not significantly differ between labs, there were significant differences between the labs for trial duration, number of trials per session, and trials per minute (Figure 1.3 f-h). This seemed to mostly be driven by long reaction times in Lab 7 and to some extent Lab 5 for reaction time measures, and a large number of trials in Lab 5 and very few trials per session in Lab 7. Interestingly, despite dramatically decreasing the length of the response window and slightly increasing the ITI for the Thesis mice, the median trial duration, number of trials completed, and trials per minute did not significantly differ from the rest of the IBL mice.

Though it is reassuring that the psychometric performance of mice on the basic version of the task is the same across labs and in the Thesis Mice, all recordings in the IBL (Chapter 2) and during widefield imaging (Chapters 5 and 6), were performed on the biased version of the IBL task, or the 'full task.' In this version of the task, instead of having a static 50% prior of which side the stimulus will appear on a given trial, the stimulus prior alternates between 80% left and 80% right (Figure 1.4a). Mice learn to use this prior and their psychometric performance therefore shifts based on this prior (Figure 1.4b,c). When stimuli are more likely to appear on the right side, rightward responses are more likely (20:80/orange in Figure 1.4b & c). The extent of this bias shift can be visualized by subtracting the two psychometric curves for the two biased blocks, which reveals that, as expected, the bias is present for all stimuli, but increases for more difficult stimuli. This can additionally be seen by comparing the psychometric

parameters for the two different blocks. The detection threshold is unchanged between the two blocks, indicating that the mouse's visual abilities do not change between the different blocks (Figure 1.4f). However the lapse on the easiest left contrasts is significantly higher for right blocks than left blocks (Figure 1.4g), lapse on the right side is significantly higher for left than right blocks (Figure 1.4h), and the psychometric bias is significantly shifted right for right blocks, and left for left blocks (Figure 1.4i). However none of the differences between the labs for any of these parameters for either block were significantly different from each other (Table 1).

**Figure 1.3.** Psychometric behavior between labs and Thesis Mice is indistinguishable. (a) Psychometric curves for two sample sessions for each mouse in each lab just before reaching the 'trained' criterion on the basic version of the task. (b) Overlay of psychometric curves fitted to all data from individual labs and Thesis Mice. (c-e) Psychometric parameters for each lab (individual boxes) and each mouse (individual dots) from the sessions included in considering a mouse 'trained.' (f-h) box and whiskers over mice and individual dots mean over sessions as in c-e, (f) trial duration from stimulus onset to response trigger, (g) number of trials per session, and (h) trials completed per minute across labs.

**Figure 1.4.** Behavior is biased by the biased blocks similarly across labs. (a) An example session indicating the block prior probability on top, showing that stimuli and rightward choices in a 10 trial rolling mean track the stimulus probability. (b) One session from an example mouse demonstrating the bias in the psychometric curve between blocks. Orange traces are for blocks in which right stimuli are more likely, (20:80) and purple traces are for blocks in which left stimuli are more likely (20:80). (c) same as b, except for all 173 mice that were trained on the biased blocks. (d) The difference between the right block and left block psychometric curves for each lab overlaid. (e) Psychometric bias curves as in d, with mouse averages in colors and individual sessions in gray. Black line in Lab 1 is for the example mouse in b. (f-g) scatter plots of the mean psychometric parameter for the right block (20:80) versus the left block (80:20). Each dot is the mean +/- standard deviation across mice within each lab.

| Block tested | Variable tested | Test type | Test stat value | p-value |
|---|---|---|---|---|
| Left | Threshold | Kruskal-Wallis | 14.09 | 0.099 |
| Right | Threshold | Kruskal-Wallis | 16.23 | 0.094 |
| Left | Left lapse | Kruskal-Wallis | 12.11 | 0.155 |
| Right | Left lapse | Kruskal-Wallis | 7.29 | 0.456 |
| Left | Right lapse | Kruskal-Wallis | 4.70 | 0.696 |
| Right | Right lapse | Kruskal-Wallis | 15.04 | 0.094 |
| Left | Bias | Kruskal-Wallis | 9.63 | 0.280 |
| Right | Bias | Kruskal-Wallis | 16.05 | 0.094 |
| Block compare | Threshold | Wilcoxon SR | 7064 | 0.566 |
| Block compare | Left lapse | Wilcoxon SR | 1967 | 0 |
| Block compare | Right lapse | Wilcoxon SR | 2013 | 0 |
| Block compare | Bias | Wilcoxon SR | 2 | 0 |

**Table 1.1**. Statistical tests for psychometric parameters displayed in Figure 1.4 f-i. "Block tested" column indicates whether the test is for the psychometric parameters from a curve for the left or the right block of stimulus prior, testing the null hypothesis that the parameters for the mice in each lab come from a single distribution. "Block compare" in this same column tests the null hypothesis that the left and the right blocks have the same parameter value. "Variable tested" column indicates which psychometric parameter the test is for. Test type indicates if a Kruskall-Wallis H-test (non-parametric ANOVA) or a Wilcoxon signed-rank test (non-parametric paired t-test) was used. The "Test stat value" column shows the value for the test statistic of the comparison used, and p-value shows the associated p-value.

**1.6 Discussion**

In this chapter, the IBL and I demonstrated that both the simple psychometric task used as the starting point of the IBL task, and the full IBL task, can yield reproducible results across labs. Here I extended the conclusions of (The International Brain Laboratory et al., 2021), that this decision-making behavior is also reproducible when performed by transgenic mice, with moderate changes to task timing, and even while performing a potentially visually disruptive experiment, widefield-whole dorsal cortex imaging.

One area in which we could not decrease inter-lab variability, and also the source of the largest inter-mouse variability, was the rate of training. One source of variability that could explain why the Thesis mice were among the fastest training mice is that they never experienced the 'Habituation' stage of training where they are head-fixed in the rig and receiving rewards but not performing the task. It is possible that this habituation phase, when mice passively receive rewards at well below the reward rate of trained mice, leads mice to be less-likely to actively explore the task and therefore decreases learning rates. However, this could be simply due to some other variability source as the Thesis mice were no faster at training than those in Lab 7. There are many unmeasured sources of variability that could easily contribute to this variability in learning rate, including differences in social dominance, early life stress, maternal care, or just random biological noise (Pancaldi, 2014). However, at this point, these differences in learning rates are only an inconvenience in that some labs are much slower at training mice than others. For the experiments these mice were trained for, the rate at which the mouse learns is irrelevant to their ultimate performance. When the IBL begins to interrogate learning mechanisms however, this between lab variability could become an issue.

One surprise that came out of these experiments was the high number of mice (104/343) that completely failed to learn even the basic psychometric task. It is possible that this is a symptom of the automated training pipeline, that only allows mice to progress through training and never to go backwards to an earlier training stage. In fact two papers using fully automated training procedures where animals perform voluntary self head-fixation in the home cage report similarly high rates of animal dropout

(Murphy et al., 2020; Poddar et al., 2013), though this rate is likely to vary greatly depending on the task difficulty. It seems that this failure rate is larger than what is typically seen in training on a similar task where the experimenter tailored the training progression to the individual mice (Burgess et al., 2017), and in a direct comparison of manual versus fully automated training on a whisker deflection detection task, there was a slightly lower failure rate for manual than home-cage automated training (Hao et al., 2021). However, it is unsurprising that attempts to increase throughput while decreasing the effort and skill required to train animals would increase the failure rate. Even with this slightly increased failure rate from automation, the trade-off seems likely to be worthwhile, given the dramatic increase in the ratio of number of animals trained to effort required of experimenters.

One large assumption in this work is that the type of standardization and automation that were introduced in these experiments led to the reproducibility seen across labs. However, we have no negative control for such a claim. A head-to-head comparison of training without standardization to training with standardization is difficult to make could be interesting to see if the standardized elements of the IBL training procedure constrain the behavior in any meaningful way, or if the task inherently constrains the behavior. We may begin accumulating evidence towards this through variability in the training procedures that individual experimenters may choose to use for training mice not destined for IBL experiments, as is the case with the Thesis Mice in these experiments.

One of the most important conclusions to draw from this chapter is that even with several changes introduced to the tasks, training procedure, and genotype of the mice included in the Thesis Mice when compared to the standard IBL mouse, they still exhibited behavior indistinguishable from each other. This is critical, as it indicates that any conclusions that are made with experiments on the Thesis Mice are generalizable to the IBL mice as a whole. This is the first addition of a new experimental modality to the IBL task so far, though more are planned in upcoming work, including more wide field imaging, mesoscale two-photon imaging, and fiber photometry. The aggregation of the results across many different experiments using different modalities is the best way to continuously build our scientific knowledge of how the brain solves a decision-making task. This requires that the behavior is unchanged

between these different experiments, and so this finding is a promising step in that direction. Therefore this result should be seen as a resounding victory for the approach of the IBL and how large-scale collaborations can serve scientific advances.

## 2 Electrophysiological recordings towards a brainwide map of neural activity

Contribution Note: The following chapter is mainly a report on work done by a large collaboration of over 30 people, all members of the IBL. I was a member of the Ephys Working Group responsible for designing the experiments, testing the hardware and software, and collecting the data that will be used in three upcoming papers for which I have not done any analyses. My main contributions to this phase of the IBL were testing of hardware and software and collection of data.

## 2.1 Introduction

Having successfully established that we could generate reproducible decision-making behavior across different laboratories, the IBL next shifted its focus towards the main research output that it was first founded to produce. This is a set of single-cell resolution neural recordings from across the entire brain of mice performing a decision-making task. These recordings have been performed with multiplexed extracellular recordings with Neuropixels probes (Jun et al., 2017) with several goals in mind. The first, as was done with the recording of behavioral data, was to show that these large-scale electrophysiological recordings were reproducible.

Some key impediments to reproducibility are poor documentation of methods (Errington et al., 2021), and differences in preprocessing of data (Botvinik-Nezer et al., 2020). The IBL was forced to tackle some of these issues of reproducibility head-on simply by the way the collaboration was conceived. Given that the same experiment must be conducted by at least 10 different experimenters each in separate labs, standardized experimental setup and protocols needed to be generated to allow the original collection of data. This solves the problem of ineffective dissemination of procedures and equipment seen in reproduction efforts by the Reproducibility Project: Cancer Biology (Errington et al., 2021). An important step towards the reproducibility of preprocessing and analysis taken by the IBL has been its data infrastructure (The International Brain Laboratory et al., 2020) which includes features such as the versioning of preprocessing steps, and saving the scripts used to analyze the data as metadata, allowing for easy comparisons between the same data after using different preprocessing such as spike-sorting algorithms. Combining these two strategies with stringent quality control on session, probe, and single unit levels (de Vries et al., 2020; Siegle et al., 2021) will hopefully lead to highly reproducible and therefore generalizable results.

In addition to generating a highly reproducible dataset with all the required information to follow the same standards, the IBL's electrophysiological recordings had the scientific goals of creating a brainwide map of decision-making related activity of single neurons, and creating an electrophysiological atlas of the whole mouse brain. The brain wide activity map intends to explore which areas of the brain represent different variables in the decision-making process, and how the brain combines information to produce a motor report of the decision. The electrophysiological atlas will follow from this same set of recordings, as we have recorded across the whole brain in an unbiased manner. This will be an extremely useful dataset for establishing the different electrophysiological features of different regions across the mouse brain, many of which may never before have been recorded.

Here I report my contribution to this dataset, showing my penetrations across the entire brain. I only show the penetrations on a two dimensional map, but each of these penetrations record along the length of the probe varying across the whole depth of the cortex. I also report one large source of variability in these recordings, the accurate targeting of desired coordinates, and how my accuracy improved over time. In the end however, the targeting accuracy remains a small roadbump toward our brainwide map as we can accurately locate electrode positions post-hoc.

**2.2 Materials and methods**

*Mice, surgeries, and behavioral training*

All mouse purchasing, handling, and training were done as described in the methods for Chapter 1.

*Electrophysiological recording*

Note: for a more detailed description of recording procedures please see the *IBL protocol for electrophysiology recording with Neuropixels probes* (Steinmetz et al., n.d.). For a detailed description of how to build an IBL electrophysiology rig including a parts list, see the *IBL electrophysiological (Ephys Neuropixels) rig setup instructions: Hardware and software v1.0* (Meijer et al., 2021). These are internal documents of the IBL but will be made available upon request, and will be published with the upcoming IBL reproducible electrophysiology paper (manuscript in progress).

Before recordings began, mice were first habituated to the new environment (the electrophysiology rig instead of the behavioral training rig) for three days, with 5, 10, then 15 minutes of

delay between head fixation and the onset of the task. The idea here was to habituate the mice to the delay introduced by needing to place the recording probes in the desired location before the onset of the task. After these three days of habituation were complete, assuming behavioral performance did not decrease below threshold, a craniotomy was performed in the morning according to the IBL craniotomy surgery protocol (Chapuis, n.d.). Briefly, the animal was anesthetized with isoflurane and head-fixed using the implanted head-plate. The UV glue sealant over the top of the skull was then removed and the location of the desired craniotomies were marked relative to bregma, or if bregma was not visible, lambda was used as the landmark. Craniotomies were then made with either a dental drill, or a biopsy punch (1, 2, and 3mm diameters were used). If a 2 or 3mm biopsy punch was used, a plastic "honeycomb" implant was glued in the craniotomy with superglue. This honeycomb implant is a small plastic disk with a series of holes on it layed out in a honeycomb-like hexagonal grid. This stabilizes the cortex for larger craniotomies while still providing access for probes into 7 (for 2mm) or 19 (for 3mm) different holes in the honeycomb. Every attempt was made to maintain the integrity of the dura mater when making craniotomies and the surface of the brain when exposed was kept moist with ACSF at all times except when gluing the honeycomb into the craniotomy. After the craniotomy was complete, the entire exposed skull was covered with kwikast silicone, taking special care that the craniotomy was first filled to the brain surface, then flooding the whole dorsal skull. Following the first craniotomy, all animals were individually housed so other mice could not remove the protective silicone layer. Mice were given a minimum of 4 hours of recovery time following this brief (~30min) surgery before a recording was performed. Recordings were performed once per day for 1 to 7 days in an existing craniotomy before a new craniotomy was made for more recordings. A maximum of 6 craniotomies were made per mouse, in a maximum of 3 surgical days.

Before the recording, the intended penetrations and several back-up sites were planned given the available craniotomies and the IBL recording plan map. The mouse was then head-fixed, the silicone removed, and the well on the skull flooded with ACSF. The back of two neuropixels 1.0 probes were coated with CM-DI-I (V22888, Invitrogen). The bulk of the ACSF was then removed with a foam spear

44

tip, with only enough remaining to keep the brain surface moist (this was done to limit the loss of the Di-I off of the probe). The probes were then, one at a time, maneuvered to whichever landmark was to be used for that mouse (bregma or lambda) with a micromanipulator (Dual micromanipulator system for Neuropixel recordings, Sensapex) and the position zeroed. The probes were then moved to the desired targets. I then attempted to penetrate the surface of the brain at the target location with the probe, but often the surface of the brain was too firm or the probe was obstructed by the dura, bone, or a blood vessel. In the event of obstruction, I made slight adjustments within ~150um radius of the intended location attempting to insert the probe, but if that failed I then continued to one of the back-up locations. This process was done for two probes in all experiments except for in the event that one or both probes were not able to be inserted in any existing craniotomy. Once a probe broke through the surface of the brain, it was slowly inserted using speed setting 2 on the micromanipulator (~10um/s) until it reached the desired depth. The probe was then left to settle for 15 minutes to relieve any pressure created around the probe and to minimize drift of the brain relative to the probe in the recording. After this 15 minute period, the electrophysiological recording was started, then the video recording, followed by the start of the behavioral task.

Recordings were performed with a standard IBL electrophysiology for neuropixels rig (Meijer et al., 2021). Spike GLX software (http://billkarsh.github.io/SpikeGLX/) was used to control the data acquisition; electrophysiological data was recorded with an IMEC PXIe controller in a NI PXIe-1071 chassis, and synchronization signals for the other data streams (task/behavior and video) were recorded with an NI BNC breakout box (BNC-2110). These recordings were performed at 30kHz temporal resolution.

*Post processing of electrophysiological recordings*

After each recording session the data was put through the IBL automated data pipeline and uploaded to the database. A more detailed report of the preprocessing and data pipeline along with the associated code is available in (The International Brain Laboratory et al., 2020). In general, the data was transferred to a local server that ran the automated pipeline to detect new sessions, run a custom lossless

compression of the recording, perform spike sorting with kilosort2 (Pachitariu et al., 2020), then extract the relevant data sets and upload them with the raw data to a centralized IBL database. There was no manual curation of spike sorted data, and all extracted data is versioned, so sessions may be rerun using new spike-sorting algorithms as they become available.

*Histology and probe location assignment*

For a detailed account of the probe localization and alignment, see (Liu et al., 2021). After all experiments were completed within one mouse (when no more penetrations were available or due to other experimental barriers), the mice were sacrificed. They underwent transcardial perfusion with 4% paraformaldehyde, 24hrs of post-fixation in 4% PFA at room temperature, then were shipped in insulated boxes in 10% sucrose solution to the IBL imaging core at the Sainsbury Welcomme Centre in London, UK. There they underwent serial-section 2 photon microscopy using a green channel for autofluorescence, and a magenta channel to locate the CM-DI-I used to mark the probe penetration. The brains were then aligned to the Allen CCF with an Elastix-based registration method (Lester and Arridge, 1999). The probe trajectories were then manually traced using lasagna (https://github.com/SainsburyWellcomeCentre/lasagna) and uploaded to the IBL database. Following tracing, the probe location along the track was determined.

This probe localization along the track is required, because there is some limited diffusion of the dye in the brain and the tip is not always well marked and so the bottom terminus of the dye may be unreliable. Therefore we considered the track of the probe to be true, but the brain area assignment along the probe track was left open to scaling and shifting. This was done by using a python GUI (https://github.com/int-brain-lab/iblapps/tree/master/atlaselectrophysiology) developed by Mayo Faulkner in the IBL to allow the alignment of electrophysiological features seen in the recording (spike widths, spike amplitudes, LFP power in different bands, spike rates, etc.) to the anatomy from the probe tracing. This was done independently by the experimenter who performed the recording, as well as at least one other experimenter. If the alignments of the different experimenters were significantly different, it was resolved with a third alignment from a third experimenter.

**2.3 Electrode penetrations across the whole brain**
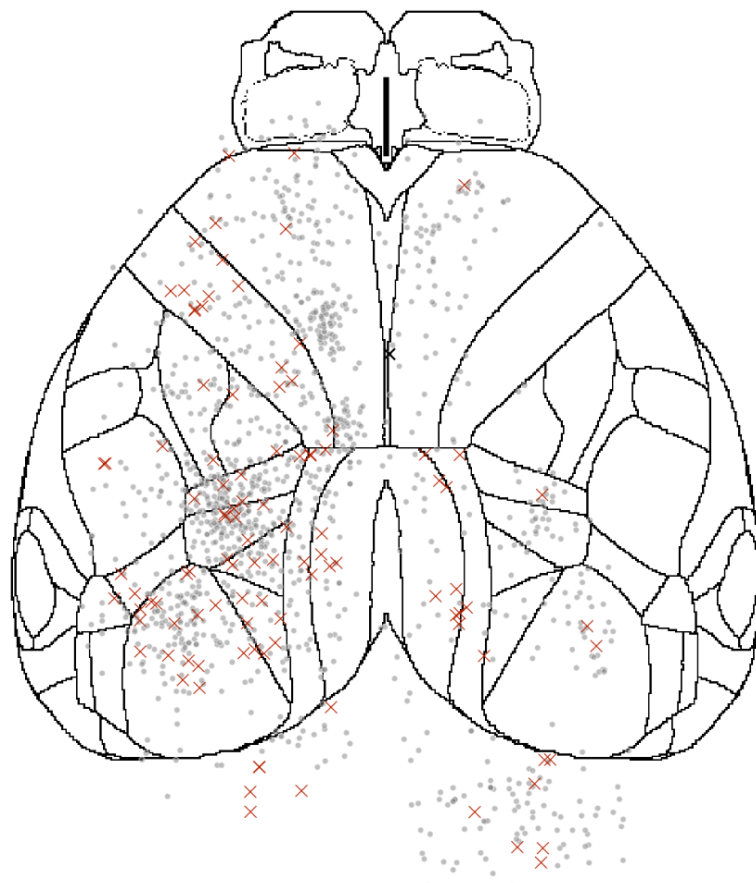
  Though the recordings I performed, and the recordings of all the IBL labs, created a vast trove of exciting single-unit electrophysiological data from across the whole brain, I was not able to perform any significant analysis on the spike data itself. I was not a member of the Neural Analysis Working Group, and doing the experiments themselves was enough of a time commitment that I could not also spend significant time on the analysis of the neural data. With that, here I will only describe the experiments themselves, my contribution to the overall IBL goal, and some issues in the experimental process.

  The IBL recording plan includes three main types of penetrations, each towards three different scientific goals. The first are brain wide map penetrations, which are recordings performed across the entirety of the brain, attempting to tile the entire brain except the most caudal parts of brainstem and the olfactory bulbs. These penetrations were planned at different angles and depths, such that the entire volume of one hemisphere of the brain would have recordings with the maximum distance of 500um between any two electrodes. An additional constraint is that each of these recordings are to be repeated, so that there is at least one duplicate from a different experimenter for each recording site. A second set of recordings are the bilateral recordings, in which probes were placed in one of three pairs of bilateral sites, so that we could record from the same location in both hemispheres simultaneously. This will allow us to validate the assumption that the mouse brain is nearly completely symmetrical across the midline for activity related to this task, which is important as the brain wide map penetrations are only performed in a single hemisphere. The final set of penetrations are in a single repeated site, where it was planned that each mouse that was recorded from would have a recording in this location (anterior visual cortex/ posterior parietal cortex, through visual thalamus, and into the striatum). This set of recordings has the goal of measuring the variability in our recording protocols and the variability in neural activity across subjects and amongst labs.

  Towards these goals, for what was termed the first-pass map, 583 penetrations were planned, excluding those in the repeated site. These were to be divided amongst 9 labs leaving 65 required penetrations per lab (excluding the repeated site). I was the second experimenter to complete all of the

required penetrations (before quality control), taking 105 penetrations to complete the required 65 penetrations. The additional insertions included 11 where there was some recording failure that made the data unusable (usually excessive electrical noise in the recording), 10 that were not in any planned recording site, 8 in the repeated site, and 11 where the recording was the third penetration out of the two required at a given location. These penetrations across the whole brain as can be seen in Figure 2.1 (red Xs) in relation to all other IBL penetrations (gray circles). They are spaced across the entire dorsal cortex, with a majority on the left hemisphere. Those penetrations near the midline on the right hemisphere are actually deep medial penetrations that are angled such that they cross the midline and record from medial areas on the left hemisphere. The more lateral penetrations on the right hemisphere that start on the cortical surface were intended bilateral sites. The IBL plan included recording in the right hemisphere of the brainstem and cerebellum so that neural responses are related to the same side of the body as in the left hemisphere of the cerebrum, and those penetrations can be seen caudal to the cortex in Figure 5.

Of the 105 penetrations that were recorded, 104 were able to be spike-sorted. From these 104 spike sorted insertions I recorded 14822 total unique well-isolated units, with a mean of $142 \pm 82$ sd good units per recording from 188 unique brain regions. Surprisingly few of these insertions were discarded by the first level of quality control with 100 passing insertion-level quality control measures, leaving me with 14033 neurons from 175 brain areas recorded in 52 different sessions as contribution to the IBL brainwide activity map.

**Figure 2.1.** Location of my IBL brainwide map penetrations compared to all IBL penetrations, projected onto a dorsal map of the mouse cortex. My penetrations are marked in red x's on the dorsal surface of the cortex with all IBL penetrations marked with gray dots. Penetrations marked below the map are targeted to the cerebellum and hindbrain. Penetrations marked to the left of the cortical map are angled such that they enter the brain below the visible dorsal cortex.
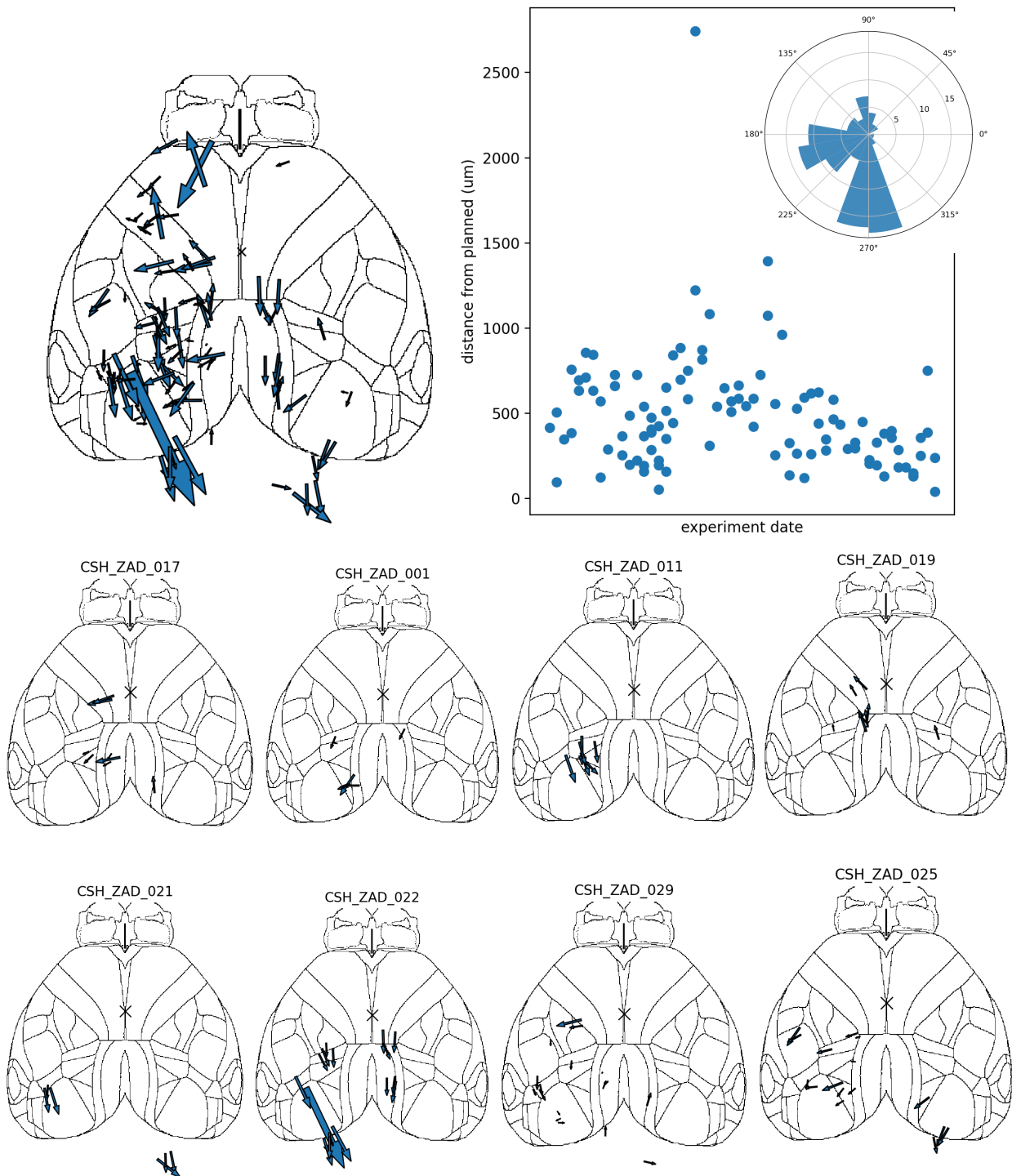
**2.4 Error in probe insertion targeting**

One large difficulty in these experiments is the precision with which you can target in the brain using coordinates relative to skull landmarks. Most sources claim the most accurate one can be in targeting relative to skull landmarks is within 300um of the intended target (Rangarajan et al., 2016). Though my targeting on average was less accurate than this (Figure 2.2b), near the end of experiments, I eventually reached this 300um mean distance from the target; but it took ~80 experiments for me to be able to reach this terminal accuracy.

Being surprised about my lack of accuracy, I set out to determine if there were any systematic targeting errors in my experiments. I first visualized this by viewing the vector between my intended target and the actual site of penetration as recovered by histology (Figure 2.2a), I then made a histogram of the angles of these vectors, to determine if there were any consistent errors across all of my experiments. I found that most of my errors in targeting led me to have a more lateral and more posterior penetration than intended. One potential source for this error could be an improper scaling between the reference atlas that was used to plan the penetration coordinates (an MRI atlas based on in-situ tissue), and the reference atlas used to annotate the final locations of the probes (allen CCF, based on ex-vivo fixed tissue). If this were the case, we would expect either a majority of the error to be in the 180-270 degree range if there was under-scaling (planned coordinates closer to bregma than intended), or in the 0-90 degree range if three were over-scaling (planned coordinates further from bregma than intended). This would be the case as a vast majority of penetrations are behind bregma and on the left hemisphere, so if the typical penetration was further from bregma than intended, it would be further left and down, but if it were closer than intended it would be further right and up. From the summary of angles (Figure 2.2b, inset), it seems possible that the atlas used for planning was under-scaled relative to the atlas used for histology. To investigate if this were the case, or if there were some other systematic targeting issue, I then plotted the penetration error in individual mice that had 5 or more penetrations.

When assessing the targeting error relative to the surface of cortex, if there were in fact an under-scaling error as described above, for each animal the arrows would be radiating out from bregma,

with larger targeting errors further from bregma. However if there were a simple shift of the experimental bregma from the true bregma, then in each animal the arrows would be roughly the same size and direction, no matter their location on the cortex. A majority of the mice seem to more closely exhibit the pattern expected by an error in labeling or in the accuracy of the experimental bregma (Figure 2.2c), a majority of the errors within a mouse seem to be in the same direction and have the same magnitude, irrespective of their distance from bregma.

**Figure 2.2.** Insertion targeting errors in my experiments. (a) The vector from intended target to histology-recovered location of penetration for all of my recordings, larger arrows are for larger errors. (b) Targeting error magnitude as a function of increasing time, (inset) histogram of angle of targeting errors. (c) Eight mice and the vector from intended to actual penetration for all recordings performed in that mouse, arrows as in (a).

**2.5 Discussion**

I have contributed heavily to the IBL's dataset of brainwide electrophysiology, recording across the entire brain according to the IBL recording plan. This dataset will prove invaluable to the field as a resource for reference as well as for computational modeling. As the second researcher of ten to finish their prescribed recordings, I faced some impediments, as well as had some advantages. One difficulty in being an early adopter was that the full data pipeline was not complete before I began performing my recordings. Therefore I did not receive feedback that, for example, for some of my sessions one of the infrared lights was broken, and the resulting behavioral videos were too dim. This will likely lead to a higher failure rate of my recordings once the full set of quality control is implemented. Another area where being an early adopter may have increased error is that for many of my recordings, the histology pipeline was not operational, either because the imaging core was not yet functional, or because I performed many of my recordings during the first year of the COVID-19 pandemic when the imaging core was not staffed, leaving me with no feedback on my targeting accuracy.

This lack of feedback was likely one source of error in the accuracy of targeting, and likely affected other researchers to some extent as well. Another of the many compounding sources of targeting error was the level of experience I had going into these experiments. My inexperience undoubtedly was a large contributor to this variation, and contributes in the start by the surgical procedures, both headbar placement as well as craniotomies, as well as in the final placement of the probes relative to skull landmarks. Originally I had believed that after a couple of iterations I would be an expert, and I felt like an expert after about a quarter of the recordings were complete. But as was seen in my targeting accuracy over time, this expert level came much later than I had expected, after about 75% of my recordings were done. This will likely not only be a problem for me, as though all the other experimenters in the IBL are post-docs, many of them were coming from experimental backgrounds outside of in-vivo rodent work, and so had no related experimental experience either. One potential impediment to becoming an expert electrophysiologist in these conditions is that instead of only targeting one or a few areas repeatedly as is classically done, IBL researchers are not repeating penetrations in the same location. Therefore learning

53

the idiosyncrasies of performing craniotomies and stable recordings in a certain area will take much longer or not be done at all.

Unfortunately, the errors in targeting that I present here are only scratching the surface of what the true errors are, as I am only showing errors in 2D targeting. Very small angles off of the intended angle in any direction, especially for deep penetrations, can lead to large errors in three dimensional targeting, and so the true error is likely to be much larger. Importantly though, the experimental design of the IBL makes errors in targeting more of an inconvenience than a fatal flaw. In the classic neuroscience experiments, one is trying to target individual brain areas, and if they are small nuclei located deep in the brain, often up to 50% of mice will be excluded from the study from missing the target nucleus (Rangarajan et al., 2016; Vale-Martínez et al., 1999), and more often these mis-targeted insertions are simply not reported. In the case of the IBL, our goal is to record from one whole hemisphere, tiling the brain with recording electrodes. The set of penetrations that were planned were guidelines to maximize coverage with the fewest recordings, but in reality the recordings will not be true to this plan, and despite all of the planned penetrations being performed, there will still be gaps of areas that are left unrecorded. We knew this from the start, and thus planned a two-pronged approach where we would follow the map for the first phase, then fill in gaps and more difficult recordings in phase 2. Hopefully, as researchers gain more experience, their targeting will be optimized and filling in the remaining gaps will be efficient.

This plan requires that we are able to accurately reconstruct the location of our electrodes post-hoc. Recent work by the IBL and others in the Svoboda lab has shown that using DI-I probe labeling, 3D brain registration, and electrophysiological features from the recording, we can accurately localize electrode position. By using ground truth experiments through optogenetic stimulation exciting passing fiber tracts with only select electrodes active on neuropixels probes, they showed alignment error to be on average 74um (Liu et al., 2021). As this size is smaller than any nucleus in the mouse brain, this is sufficiently accurate targeting for the IBL's scientific goals.

Targeting issues aside, the dataset that I have collected with the IBL will be historic and invaluable to the field, it will provide more recordings from more brain areas than have ever been

collected, all with a rich set of video and behavioral data. This will hopefully be used in hundreds of papers from researchers both within and outside of the IBL. The most important contribution of the IBL in collecting this dataset however, may be the associated set of protocols, documentation, and data infrastructure supporting the processing and storing of the multiple data streams recorded in these experiments. This will hopefully increase the standardization of protocols across the field of systems neuroscience, create a baseline for quality control, and provide an invaluable resource for labs using these techniques.

**3      Dorsal cortex inhibition scan reveals visual and motor areas are required for task performance**

Contribution note: The work in the following chapter was conceived of, planned, and analyzed by myself and Tony Zador. I performed all of the experiments and built required hardware and wrote required software for these experiments.

**3.1 Introduction**

Much of neuroscience research, especially that using primate and human models, is based largely on correlational research. Even when causal manipulations are used they are typically done in a targeted manner, where a single target is chosen and manipulated to determine its role in a neural process. Though these targeted approaches provide invaluable insight into the neural underpinnings of behavior, exploratory unbiased methods can often yield surprising or unexpected results that can alter our understanding or raise new questions (Guo et al., 2014). With this in mind, I set out to perform a whole dorsal cortex inactivation scan to determine the causal cortical areas involved in the IBL decision-making task.

Dorsal cortical inhibitions in a related task showed effects of inhibition in V1 and M2 (Zatka-Haas et al., 2021). However, the task used by Zatka-Haas et al. differed from the IBL task in several ways. The largest differences were that the Zatka-Haas et al. animals had to make a two-part decision, first if they should respond or withhold response, then if they should respond, which side they should choose. The second is that the Zatka-Haas et al. mice were required to compare contrasts of stimuli on two different sides, and decide which stimulus had the higher contrast to make its response. Finally, their task also included a delay period before a decision could be reported, whereas the IBL task is a true reaction time task, allowing the mice to respond whenever they reach a decision.

In the task used by Zatka-Haas et al. (Burgess et al., 2017), it is clear that the animals are required to compare the visual stimuli on either side of the screen to make a correct decision. However, in the IBL task, it is unclear if animals are comparing the stimuli on either side, or if they are solving two separate detection tasks for each side of the screen independently. By performing unilateral inhibitions, we can explore the likelihood of these two strategies. If unilateral inhibition only causes an effect for contralateral

stimuli but not ipsilateral, this will indicate that the hemispheres are working independently to solve the detection of stimuli in each of their respective visual fields. If unilateral inhibition instead affects decisions for both contrasts, it would suggest that the two hemispheres are comparing their activity to solve the task.

A similar set of inactivation scan experiments have been performed in several behavioral tasks in mice (Allen et al., 2017; Guo et al., 2014; Pinto et al., 2019; Zatka-Haas et al., 2021), but none of these were reaction time tasks. Each of these tasks had a required delay between sensory stimulus and decision time, which involves short term memory (Erlich et al., 2011; Inagaki et al., 2019; Shenoy et al., 2013) and therefore lie in a very different task space along the speed-accuracy tradeoff continuum (Heitz, 2014). By looking at the distribution of reaction times in this task for different inhibition locations, it may be possible to disentangle their contributions to the decision process (Ratcliff and McKoon, 2008; Ratcliff and Tuerlinckx, 2002). A popular model used in decision-making research, the Drift Diffusion Model (DDM, Ratcliff, 1978), makes specific predictions about how changing different variables in the decision process differentially affects reaction times. For instance, if the reaction times for one choice are increased, but the reaction times for the other choice are unaffected, this indicates an increase in the drift rate for the slowed choice. However, if the decision were biased in some manner, such as by making one choice more likely than the other, this would result in shorter reaction times for one option, but longer reaction times for the other, due to a shift in the starting point of the drift process (Ratcliff and Tuerlinckx, 2002).

Here I will show that unilateral inactivation of motor or visual cortex causes an ipsilateral choice bias. These inactivations bias behavior for contrasts on both sides of the screen, indicating the cortex is comparing information for each stimulus between the two hemispheres. Furthermore, different effects of inhibiting motor cortex and visual cortex on reaction time seem to indicate different roles in the decision-making process. Inhibitions of visual cortex cause a decreased rate of accumulation for contralateral stimuli, and inhibitions of motor cortex cause a shift in the starting point of the diffusion process away from contralateral choices. This finding indicates that the role of visual cortex in this task is

limited to the accumulation of evidence, whereas motor cortex activity more directly influences what choice is made.

## 3.2 Materials and methods

*Mice*

Mice used in these experiments were male VGAT-ChR2 transgenic mice (stock number 014548, Jackson Laboratory; (Zhao et al., 2011)), crossed with emx-tta mice (JAX). The emx-tta was intended for another experiment not reported here, and its presence seemed to introduce a neuroanatomical abnormality in the mice used here. There was irregular cortical vascularization in these mice, which appeared both anatomically and functionally, to result in an anterior shift in the position of visual cortex in these mice. Therefore when mapped to the allen CCF, it seems as if the main effects are mostly in somatosensory cortex as opposed to visual cortex.

*Surgery*

When the mice were aged 3 months, they were implanted with a headplate and a clear skull cap. This procedure was mainly based on the IBL headplate implantation protocol (The International Brain Laboratory, 2020a), and so shares the same aseptic procedures as well as surgical equipment and consumables except where noted. In brief, anesthetization was induced with 3% isoflurane in oxygen, and maintained with 1.5% isoflurane, the head was stabilized in a kopf stereotactic setup, and the fur on the scalp was removed with epilation cream (Nair). Next the scalp was coated with 5% lidocaine gel and intraperitoneal meloxicam was injected (5mg/kg). Following the removal of the lidocaine cream, the scalp was cleaned with alternating application of betadine and ethanol, then a majority of the dorsal scalp was removed using the following rough boundaries: anterior to between the eyes, laterally to the beginning of the cheek muscles, and caudally to the beginning of the neck muscles. The skull was then wetted, the periosteum removed, the lateral tendons connecting the neck muscles to the skull were released from the skull with forceps, and the muscle on the surface of the temporal skull plate between the eye and ear was separated from the skull with a scalpel. Any blood was washed away and the skull was dried, then the

skin was retracted as far as it could allow and glued to the skull with vetbond. Dentin activator (Parcell) was then applied across the skull, then the headplate was glued in place with metabond, keeping as much of the dorsal cortex clear as possible, applying metabond mostly to the olfactory and occipital skull plates, and filling in the remaining lateral gaps from the release of the cheek muscles. The metabond was then covered with black dental cement to provide better light isolation and to ensure the skin did not retract from the implantation. Superglue (Zap-a-Gap) was then applied in two consecutive layers over the bare skull, first only on the middle not touching the headplate to prevent a meniscus from surface tension at the edges, then after this dried, to the remain bare skull around the edge, connecting it to the headplate/metabond.

*Mouse training*

Mice were trained in an IBL training rig (The International Brain Laboratory, 2021) using the standard IBL protocol (see Chapter 1 and (The International Brain Laboratory, 2020b) with a few exceptions. The first exception is that instead of the IBL protocol for habituation, mice were first habituated to the experimenter once water restriction began (1 week following surgery), by the mice receiving their daily water from a blunt 1ml syringe while they were held in the experimenter's gloved hand. Following this there was no period for habituation to the rig, the mice began performing the IBL task (The International Brain Laboratory et al., 2021) from the first time they were headfixed. Following this, training progressed according to the IBL protocol, learning first the association between stimulus side and wheel movement, then having more difficult contrasts added in. The only changes to the IBL task was a shortening of the response window from 60s to 2s, and that the biased blocks were never introduced, so that there was always a 50% stimulus prior. These last changes were only made after the animals reached the trained criterion.

*Optogenetic inhibition*

Optogenetic inhibition was performed by shining light from a 473nm wavelength DPSS laser (Shanghai Laser & Optics Century Ltd.) to a location on the dorsal cortex of the mouse. The laser beam was collected into a 50nm core optical fiber patch cable (Thorlabs), collimated with a thorlabs fiber

collimator mounted on a kinematic mount (Thorlabs KC1-S) that allowed small adjustments of the beam position to allow for zeroing on bregma. The beam was then directed onto the mirrors of an x-y galvanometer (Thorlabs GVSM002-US) which allows the laser beam to be redirected programmatically in two dimensions, allowing fast scanning of the laser across the cortex. From the galvanometer mirrors, the beam is then directed through a blue band-pass filter (Thorlabs, FB470-10), and reflected on a short-pass dichroic mirror into the objective lens (Nikon 135mm). The objective focuses the beam onto the surface of the brain with a diameter of 400um. There is another of the same objective lenses inverted and mounted above the dichroic mirror which allows us to visualize the location of the laser beam with a camera (FLIR), so that the laser may be centered on bregma before each experiment. This inverted lens system is nearly identical to the one used in Chapter 5.

The laser position was controlled with custom software written in MATLAB 2019b, using the Data Acquisition Toolbox to control output voltages from an NI DAQ (USB-6011). One DAQ was used to control the two mirrors of the galvos, and a second was used to control the laser stimulation as there are only two analog outputs per unit. The code to run this experiment can be found on my Github page https://github.com/cskrasniak/lesion_project/tree/master/GalvoScanning. At the onset of each trial, a location for inhibition was randomly chosen from a set of coordinates with the only requirement being that no two coordinates could be chosen twice in a row, and the two control coordinates off of the dorsal cortex were chosen at twice the frequency of the other coordinates. The software generated a 40hz sine wave whose max power was 3.2 mW/mm², which began 100ms prior to the onset of the stimulus, and ended 100ms after the end of the response period with a linear downward ramp for the last 100ms. This yields a total time of 2.2s per trial in which the laser is on. These parameters for this laser and these mice have previously been shown to exhibit consistent inhibition down to the deeper cortical layers while minimizing the spread of inhibition to ~1mm diameter and resulting in relatively little rebound activation (Guo et al., 2014).

Before experiments began, the laser diameter at the cortical surface was measured by reducing the laser power near its minimum, and directly shining the laser onto a CCD sensor of a camera

(CM3-U3-13Y3M-CS, Point Grey; with lens and IR filter removed) placed at the intended location of the cortical surface. With a known pixel size of the sensor, the beam diameter is then easily measured. Additionally, the galvanometer input voltages were calibrated before experiments by placing a micro ruler (TDI MRM200H) along each axis in turn, directing the beam to the edge of the axis with the kinematic mount. Then voltage is applied to the mirror for that axis to determine the amount of voltage required for 1mm of translation of the beam. This is repeated for the second axis, and these ratios are saved and used to convert between voltage and the coordinates on the cortical surface in mm relative to bregma.

*Statistical analysis*

To determine the statistical significance of the inhibition effects on choice biasing for individual inhibition coordinates, a Chi-squared test was used, as implemented in Scipy (Virtanen et al., 2020). The test was conducted between the choices for all the trials (omitting no-go trials) where the laser was directed at a given location, versus the choices for all the trials where it was directed at either of the two control spots. The p-value of the two control spots was determined by comparing the trials from one control spot to the other. A p-value was calculated with this test, usually by comparing the choice made on all trials of all contrasts for each laser coordinate, unless specified that a specific contrast set was used. Additionally, the reaction time was compared for each spot in a similar manner, instead using a Wilcoxon ranked-sums test also from Scipy. A Bonferroni correction for multiple comparisons was applied to each p-value by multiplying the raw p-value by 62, the total number of inhibition spots.

To determine the statistical significance of alterations in the psychometric parameters of motor and visual cortex inactivations, a psychometric curve (see Chapter 1 methods) was fitted to each session for the control spots, the left inactivation and the right inactivation for a given set of coordinates (4 visual or 4 motor cortex coordinates). An ANOVA was then performed using each session as a sample between the three conditions of left, right, and control for each of the four psychometric parameters (lapse left, lapse right, bias, and threshold).
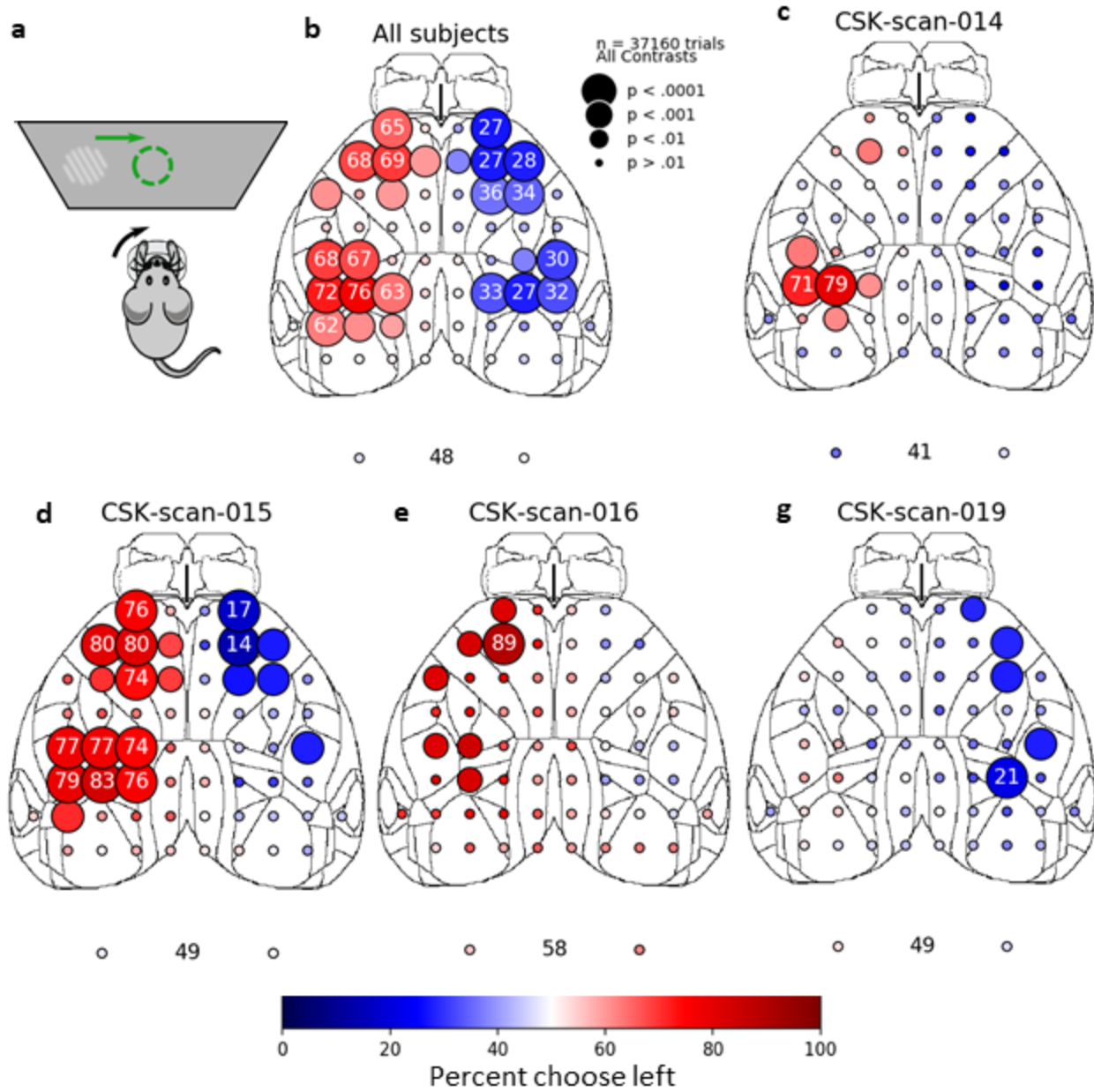
### 3.3 Visual and secondary motor cortex are required for the IBL task

To determine which cortical areas were required for the IBL task, I performed a dorsal cortical inhibition scan on VGAT-ChR2 mice implanted with a clear-skull cap preparation (Guo et al., 2014). Mice were trained to perform the IBL task according to IBL standards, and after animals reached the trained criterion (The International Brain Laboratory, 2020b), I began to perform the cortical inhibition scan while animals performed the basic version of the IBL task (no biased blocks). Sixty-two coordinates were used for inhibition, 31 on each hemisphere layed out in a 1mm by 1mm grid with two control spots that were off the cortical surface, on the animal's head-plate. The inhibition lasted for 2.2s, from 0.1s before stimulus onset to 0.1s after the end of the response period (response period was shortened from the 60s in the normal IBL task implementation to 2s so as to limit length of laser inhibition, this did increase the percent of no-go trials from normal IBL mice, though no-go trials still made up less than 5% of responses). Given that there are 558 conditions (9 contrasts* 62 inhibition coordinates), and about 800 trials per session, all analyses were performed by either concatenating sessions within animals, or pooling all sessions for all animals.

To determine if this inhibition significantly biased animal behavior, I calculated the percent of leftward choices made by the animals for each inhibition coordinate. If an area had no effect on biasing animal choices, the percent of leftward choices should be near 50%, which is true for the two control coordinates (Figure 3.1b). However, if inhibition at a given coordinate does cause a significant bias, the percent of leftward choices would be biased above or below 50%. When the anterior visual cortex or motor cortex on the left side is inhibited, there is an increase in leftward choices by the mice, indicating a bias away from the contralateral choice, with the mirrored effect seen on the right hemisphere (Figure 3.1b). When comparing the percent chosen left for each inhibition coordinate to that of the two control coordinates, we see that coordinates in motor and anterior visual cortex are significantly different from the control spots.

Though these effects seem consistent and easily interpreted when combining the effects of inhibition across mice, the results are actually quite idiosyncratic when viewed for each mouse separately
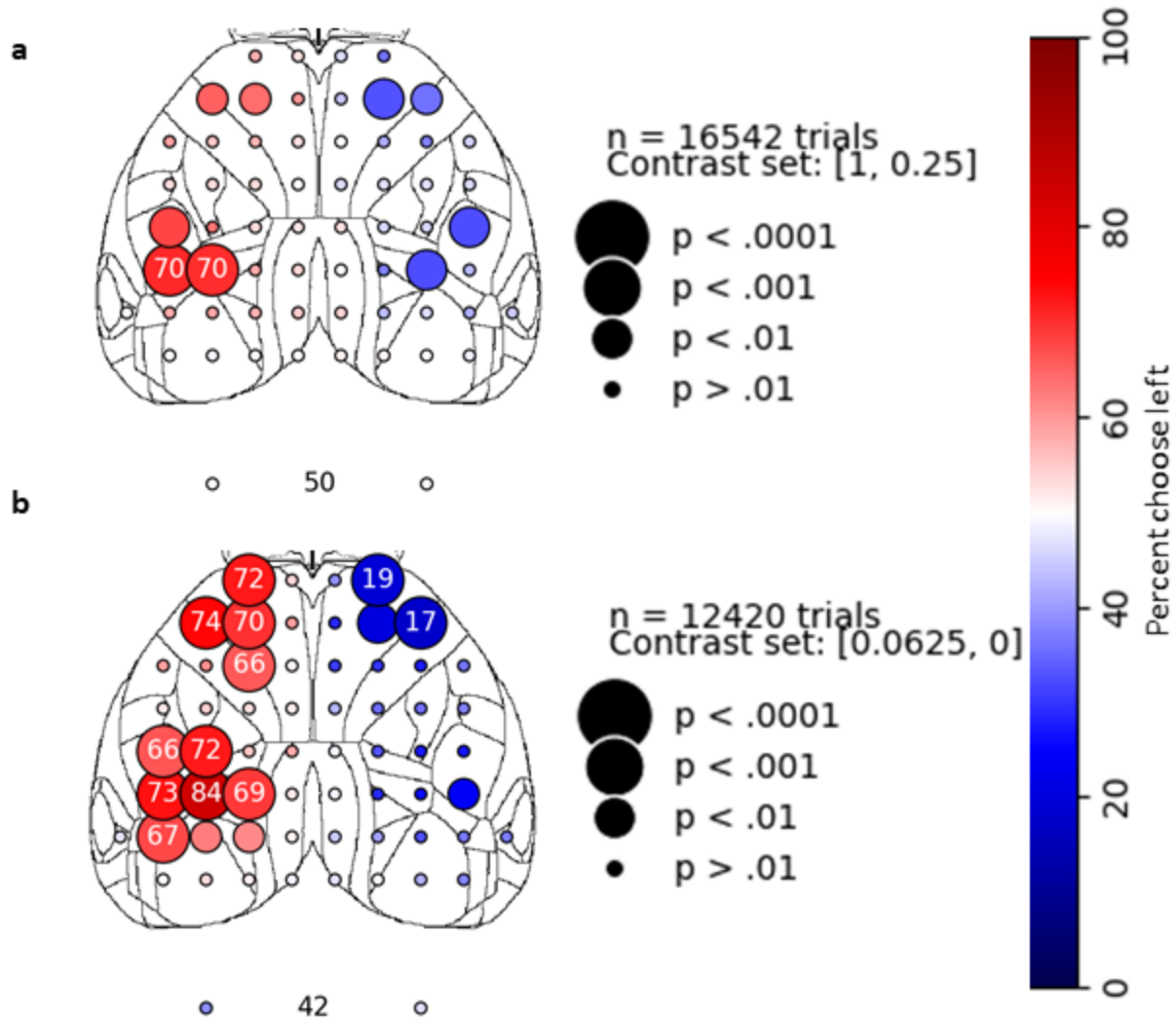
(Figure 3.1c-f). For some mice only visual inhibitions caused a significant bias, for others both visual and motor areas, some had unilateral effects and some bilateral, in nearly every combination of those factors. One reason for these differences could be statistical, as two mice (mouse 14 and 16, Figure 3.1c, e), showed a high baseline bias, with nearly 60% of choices on control trials being made to one side. However, this does not explain the asymmetry in the other two mice. The reason for these idiosyncrasies remains somewhat mysterious. In particular, we found no significant correlations between different behavioral strategies and inhibition effects.

**Figure 3.1.** Inhibition scan reveals motor and visual cortex are required for performing the IBL task. (a) Depiction showing that "choose left" is the mouse indicating that the stimulus is on the left side of the screen. (b) Inhibition effects pooling trials across 5 VGAT-ChR2 mice. Each dot indicates an inhibition target, the size of the dot indicates its Bonferroni-corrected p-value from a Wilcoxon signed-rank test comparing the choices made for trials from when that site was inhibited to the trials when the laser was on the control spots. The color and the number inside the dot indicates the percent chosen left for that inhibition target as indicated by the colorbar at the bottom. The two dots below the cortical map are the two control inhibition targets where the laser was on, but which were off the cortical surface on the headplate of the mouse. The number between those dots is the mean percent choose left for those inhibition control trials, indicating the animal's bias. (c-g) Inhibition maps as in (b) but for individual mice.

64

**3.4 Effects of cortical inhibition of visual or motor cortex are stronger on low contrast trials**
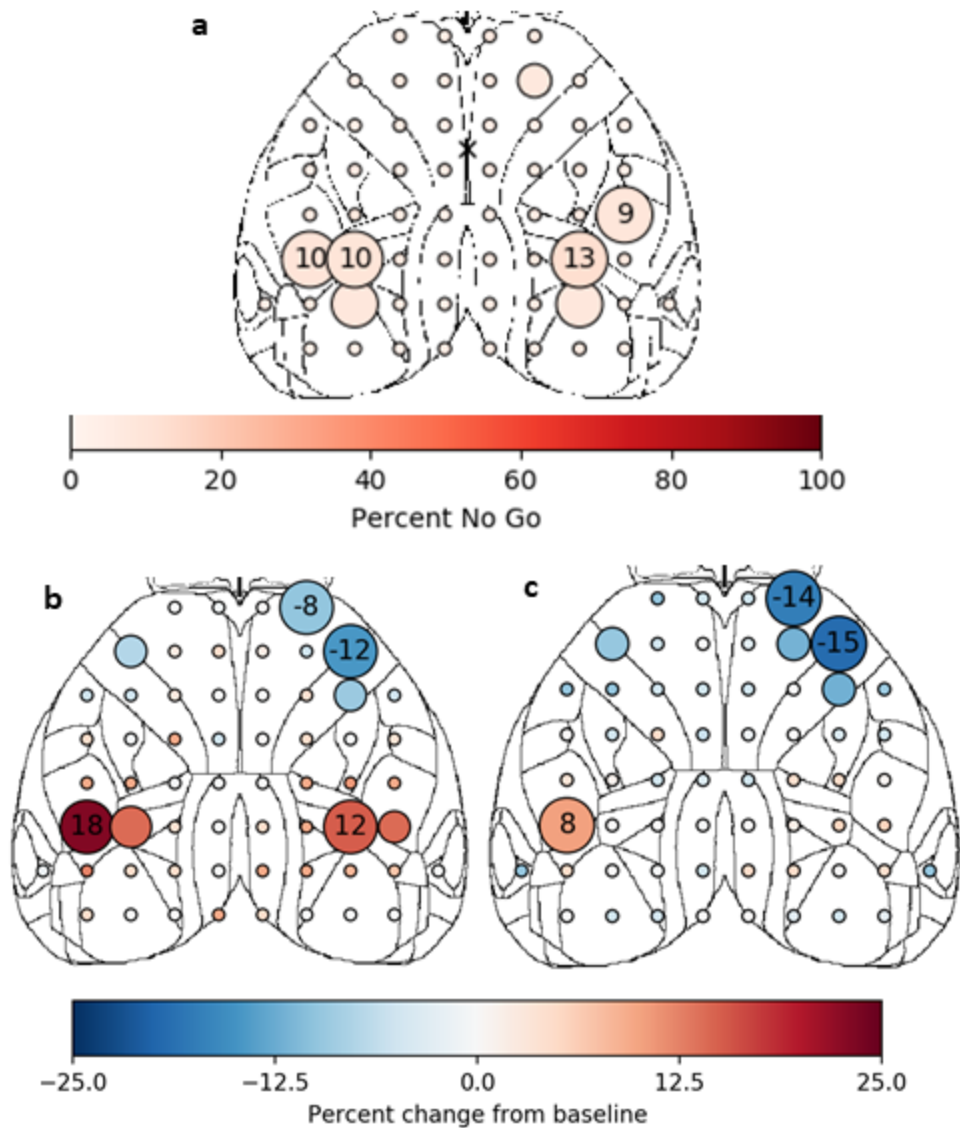
Above, I only show the effects of this inhibition on the combination of trials of all contrasts. To see if the size of the effect of inhibition varied as a function of the stimulus intensity, I performed the same analysis as above, but for separating out only the strongest contrasts (1 and 0.25) and the weakest contrasts (0.0625 and 0). This reveals that there is a more restricted set of spots that are significantly biased by the inhibition than in the lower contrast trials, and there is relatively less biasing of the behavior on higher contrasts (Figure 3.2a). In comparison, inhibition of the lower contrast stimuli (Figure 3.2b) showed more individual coordinates significantly biased by the inhibition, and generally stronger effects in spots that were already significantly biased. This indicates that behavior is still biased even when there is unambiguous visual evidence; however neighboring inhibition coordinates to the most impactful coordinates are also able to bias decisions when there is less visual information. Additionally, inhibition of visual areas on the right hemisphere does strongly bias choice behavior, but due to a high baseline bias in the same direction in these mice, only one of these spots shows statistically significant biased behavior (Figure 3.2b).

**Figure 3.2.** Weaker stimuli show stronger biasing of behavior from inhibition. (a) Inhibition effects of only the high contrast stimuli (100 and 25%) pooled trials for 5 animals. (b) Inhibition effects of only the two weakest contrast stimuli (6.25 and 0%) pooled trials for 5 animals. Both plots as described in Figure 3.1.

**3.5 Inhibition of visual cortex increases reaction time, motor cortex decreases reaction time**

It is clear that inhibition of visual and motor cortex significantly bias the choices that animals make. I next investigated if the time it takes to make a choice was altered by inhibition of any cortical area, and if this differed at all from the areas that bias behavior. To do this I plotted a similar inhibition map as in the previous two sections, but now instead of comparing the percent of left choices, I instead plotted the response time of the mouse from stimulus onset until the triggering of a response. Interestingly, it seems inhibition of visual areas increases reaction time, whereas inhibition of motor areas decreases reaction time (Figure 3.3b). This change in reaction time could be largely due to a change in the percent of no-go trials where the mouse failed to respond, in which case a reaction time of 2s is recorded. It seems there is a significant increase in no-go trials for visual inhibition locations, but not for motor areas (Figure 3.3a). When excluding no-go trials, there still is an increase in reaction times for visual inhibition coordinates, but this is only a significant increase for one such coordinate (Figure 3.3c). Even after excluding no-go trials, the motor effect remains, showing there is a decrease in reaction times for anterior lateral motor cortex inhibition.
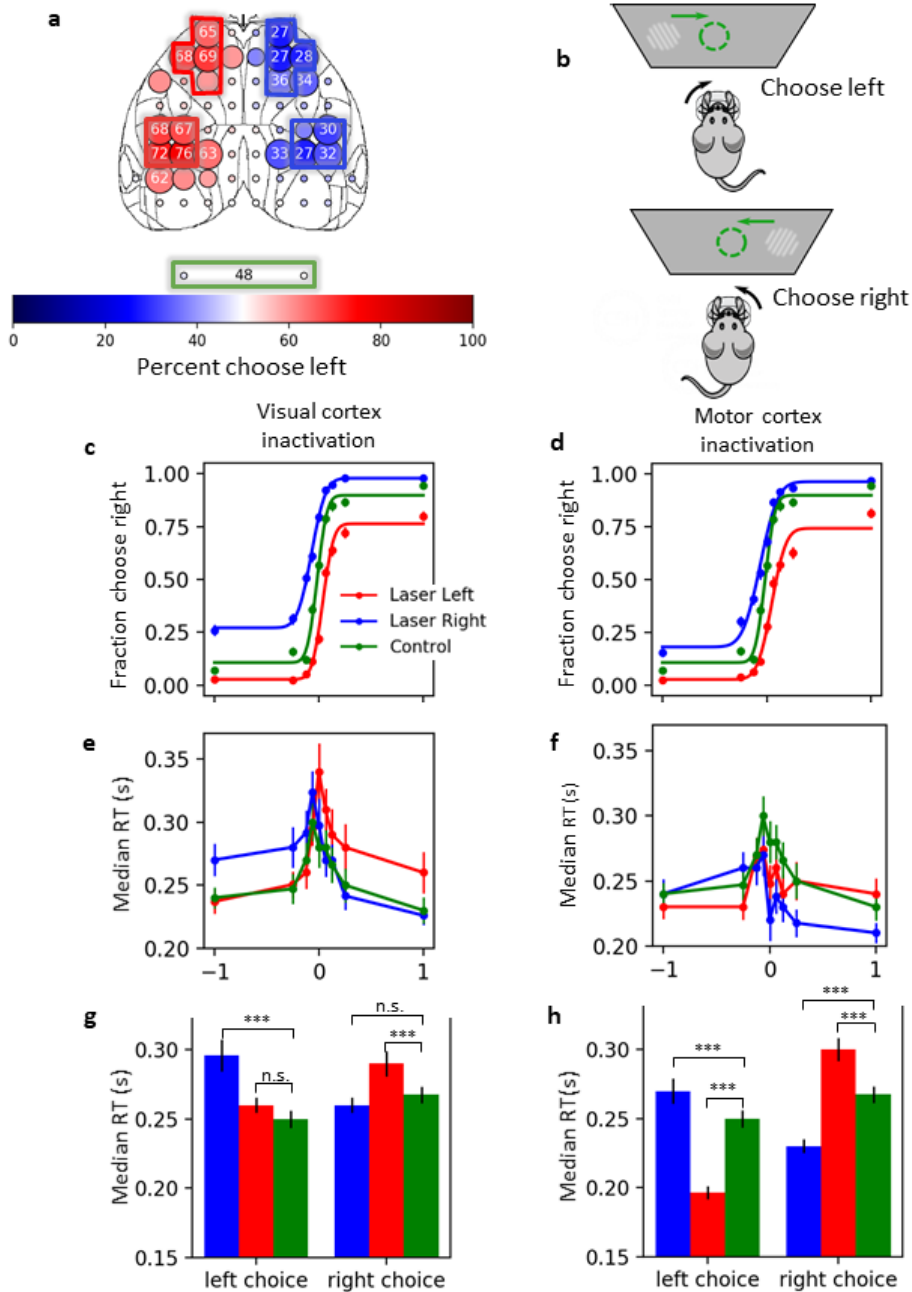
**Figure 3.3.** Inhibition of visual cortex increases reaction time, while inhibition of motor cortex decreases reaction time. (a) Inhibition map as in Figure 3.1, but now with a comparison of the number of no-go trials of inhibited spots to control spots for all stimuli across 5 mice. (b) Inhibition map comparing the reaction times when different spots were inhibited. Colorbar and numbers indicate the percent change in median reaction time from the median reaction time of the two control laser locations. (c) Same as (b) but after no-go trials are excluded.

**3.6 Inhibition of visual and motor cortex alters psychometric and chronometric curves**

Having seen that visual and motor cortex consistently showed the largest effect of inhibitions, I then sought to determine if there were any specific behavioral effects this inhibition had when looking across the entire psychometric and chronometric curves. To increase the statistical power for these comparisons, I chose the four inhibition coordinates for each of the left and right motor and visual cortex that had the strongest effect of inhibition and pooled the behavior from inhibitions of those four coordinates (Figure 3.4a). To see the behavioral effects of inhibition of visual cortex, I first took the behavior from the visual inhibition coordinates on the right and left hemisphere for each session and fit a psychometric curve to each, and compared them to a psychometric curve fitted to the control trials (Figure 3.4c). I then extracted the four fitted psychometric parameters (lapse right, lapse left, bias, and sensitivity) for each curve, and ran a one way ANOVA among the left, right and control inhibitions to see if the laser location significantly altered the fitted psychometric parameters. For inhibition of the visual cortex, each of the bias, right lapse, and left lapse were significantly altered by the laser location ($p = 0.006$, $p = 0.011$, and $p = 0.028$ respectively). Though the slope was shallower for both the right and left inhibition conditions, this difference was not significant in the ANOVA ($p = .122$). When the same comparison was made for inhibitions targeted to the motor cortex, a mostly similar pattern was observed, with significant differences in the bias, right lapse, and left lapse ($p = 0.021$, $p = 0.004$, and $p = 0.024$ respectively), and no observable difference in the psychometric sensitivity ($p = 0.260$, Figure 3.4d).

In addition to the parameters of the psychometric curve, I additionally investigated if there were differences in the reaction times (RTs) for the inhibitions in visual or motor cortex. Using the same set of coordinates as before, I constructed chronometric curves for laser right and laser left in the visual cortex, and control coordinates. These chronometric curves show that inhibition of visual cortex unilaterally causes a contralateral increase in RTs (Figure 3.4e). There seemed no clear difference in reaction time across contrasts for inactivation of the motor cortex, though it appeared some modulation was present. To further investigate if there is a location-dependent change in RT, I instead compared the RTs for the different inhibition conditions broken down by the animal's choice. For visual cortex inhibitions, the

contralateral increase in RT is still consistent when broken down by choice instead of contrast, with right

visual inhibitions increasing the RT of left choices (Wilcoxon rank-sums, $U = 8.29$, $p = 9.40e\text{-}16$), and left

inhibitions increasing right choice RTs ($U = 4.49$, $p = 5.76e\text{-}5$, Figure 3.4). Ipsilateral inactivation of

visual cortex did not significantly alter RTs (left choice: $U = 2.04$, $p = 0.330$; right choice: $U = -1.97$, $p =$

$0.388$). When broken down by choice, the lateralized effect of motor cortex inhibition on reaction time

however becomes clear, with choices ipsilateral to the inactivation side significantly decreasing RTs (left

choice: $U = -9.52$, $p = 1.32e\text{-}20$; right choice: $U = -8.66$, $p = 3.68e\text{-}17$) and choices contralateral to the

inactivation side showing significantly increased RTs (left choice: $U = 5.50$, $p = 2.99e\text{-}7$; right choice: $U =$

$6.00$, $p = 1.60e\text{-}8$). In sum, choice behavior is similarly bilaterally altered by visual and motor cortex

inactivation, but reaction times are only unilaterally increased with visual cortex inhibition, and bilaterally

modulated by motor cortex inhibition.
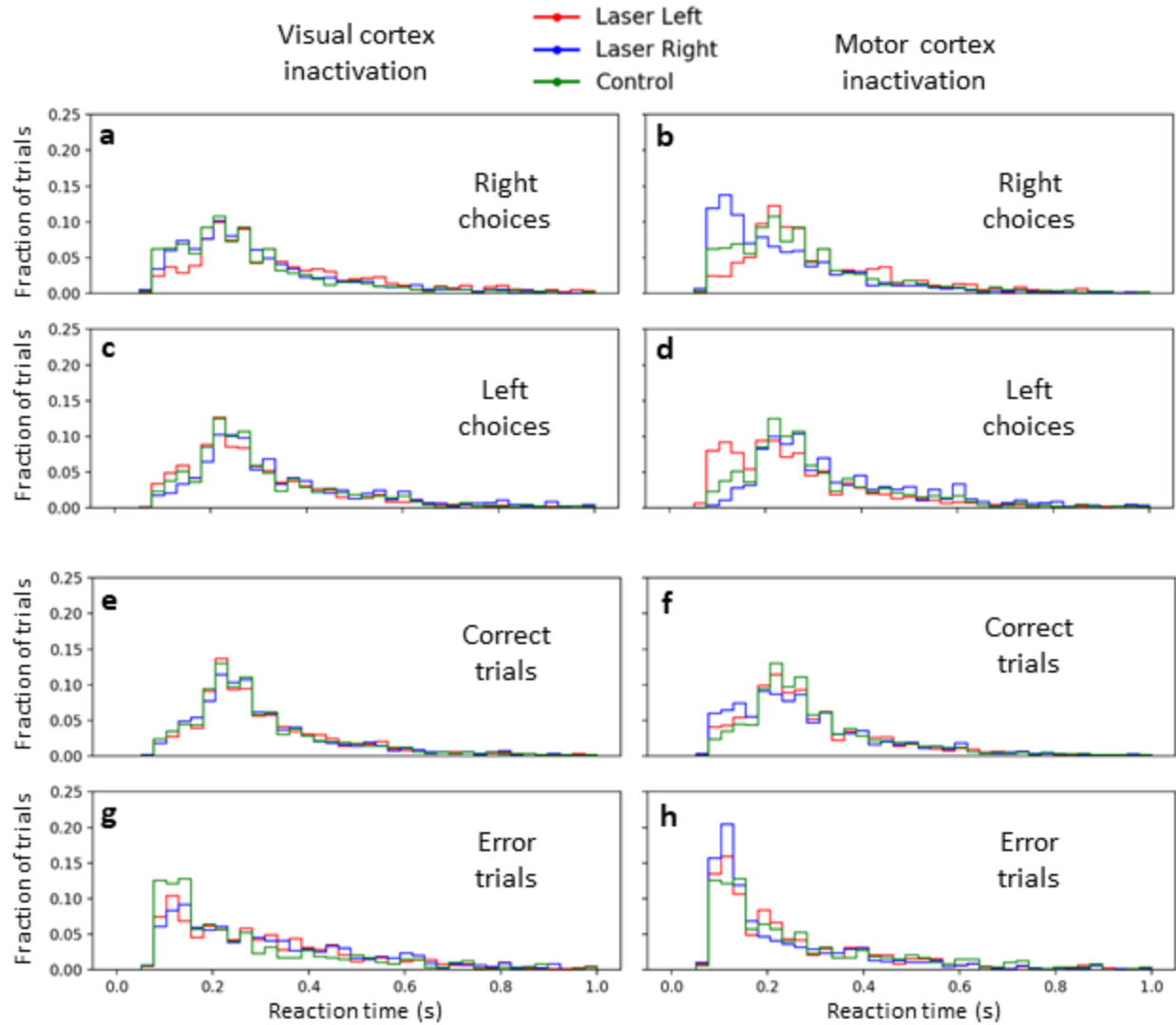
**Figure 3.4.** Effects of inhibition across all contrasts. (a) Review of inhibition effects shown in Figure 3.1, with boxes highlighting the inhibition coordinates pooled together in the left, right, and control conditions. Squares are for visual cortex, green rectangle for control, and tetris-like pieces for motor cortex. (b) Schematic showing what a left and right choice indicates for the mouse. (c) Psychometric curves for inhibition of left visual cortex, right visual cortex, or the control spots, data pooled across all sessions for 5 mice. Dots are mean fraction choose right ± standard deviation, lines are psychometric curves fitted to the pooled data. (d) Same as (c) but for motor cortex inactivation. (e) Effect of visual cortex inhibitions on the chronometric curve, same as in (c) but now for median reaction times as opposed to fraction choose right. (f) Same as (e) but for motor cortex inactivation. (g, h) Median reaction time for different inhibition locations broken down by choice type; *** indicates significance at the $p < 0.0001$ level, n.s. indicates not significant with an alpha of .05 for a Wilcoxon rank-sums test with a Bonferroni correction of 8 (four locations for each choice type).

**3.7 Motor inactivation causes impulsive errors, visual inactivation causes perceptual errors**

To further investigate the interesting finding that motor cortex inactivation causes bilateral changes in median reaction time whereas visual inactivation only causes a contralateral increase in median RT, I looked into differences across the whole distribution of RTs between the different inactivation conditions and different trial conditions. I first made the same comparison as before, looking at the visual cortex and how inactivation of right versus left hemisphere affected left and right choices. I find that the increase in median RTs with contralateral inhibition in visual cortex seen above is due to a decrease in all early RTs before 200ms, and an increase in the tail of the distribution (Figure 3.5a, c). When looking at motor cortex inactivation, bilateral changes in reaction times in opposite directions were noted, such that ipsilateral choices had faster RTs, but contralateral responses had slower RTs. Indeed we see this recapitulated across the whole distribution, with the increase in contralateral RTs looking similar to visual inhibitions, a decrease in the fastest RTs but an increase in the tail. Interestingly, the ipsilateral decrease in RT seems to appear not as an increase in the usual peak of RTs, but instead right near the leading edge for very fast RTs (Figure 3.5b, d).

The difference between inactivation of motor and visual cortex seems most clear when comparing their effects on correct and error trials. When inactivating visual cortex, if the response is still correct, there seems to be no clear change in the reaction time distribution; however the distribution of reaction times for error choices when either hemisphere is inactivated, is strongly shifted towards longer RTs. This manifests as a decrease in the very early responses, but an increase in the longer reaction times at the tail, indicating that these errors are due to increased difficulty in perceiving the stimulus (Figure 3.5e, g). In comparison, when inactivating motor cortex, on both correct and error trials, there seems to be an increase in the very short latency impulsive responses for inactivation of either hemisphere (Figure 3.5f, h). Taken together, this indicates that inhibition of visual cortex makes contralateral stimuli more difficult to detect, and increases perceptual errors. Whereas inhibition of motor cortex causes both an increase in perceptual errors for contralateral choices, and an increase in impulsive errors for ipsilateral choices.

**Figure 3.5.** Reaction time distributions for visual and motor cortex inactivations. Each plot shows the distribution of reaction times (from go cue onset to response triggered) for all trials for all mice, truncated at one second. The distributions are normalized such that the area for each distribution sums to 1. Green distributions are for control trials, red for left inhibition and blue for right inhibition. Left hand plots are for inhibition of the visual cortex and right hand plots are for inhibition of motor cortex.

**3.8 Discussion**

This dorsal cortex inhibition scan revealed alterations in the normal behavior in the IBL task when coordinates in visual and motor cortex were inactivated, showing that these areas causally influence the IBL behavior. When visual cortex was inhibited, we saw a biasing of choice behavior such that contralateral choices were less likely, and ipsilateral choices were more likely. This was true across all contrast levels, creating a vertical displacement in the psychometric curves. There was a stronger effect for weaker contrasts than strong contrasts, but this could have simply been due to a ceiling effect, since the high contrast trials were already near ceiling performance in the control trials. Inhibition of motor cortex had a nearly identical effect on choice behavior, causing a similar vertical shift in the psychometric curve making contralateral choices less likely and ipsilateral choices more likely. Though the effect on choice behavior seems to indicate no difference between motor and visual cortex inhibitions, the effect on reaction times seems to tell a different story. Inactivating visual cortex unilaterally increases reaction time for stimuli/choices on the contralateral side, whereas motor inactivation alters the reaction time of both contralateral and ipsilateral choices, causing many fast, impulsive-like RTs for ipsilateral choices, and increasing the RT of contralateral choices.

This difference seems to indicate a different role for the motor cortex and the visual cortex in the decision making process. Inhibition of visual cortex only causes increased RT for contralateral choices. Furthermore, the increase in RT seems to be contrast dependent, such that the largest increase in RT is for the strongest stimuli. This is consistent with a decrease in the rate of evidence accumulation in favor of stimuli on the contralateral side in the drift-diffusion model (Ratcliff and McKoon, 2008). Motor cortex inactivations however, cause both an increase in RT for contralateral choices, and a decrease in RT for ipsilateral choices, along with making ipsilateral choices more likely. When placed in the DDM framework, this would be most consistent with a shifting of the starting point for the diffusion process (Ratcliff and McKoon, 2008), as more time for evidence accumulation would be required for contralateral choices, yet very little or even no evidence is needed for ipsilateral choices. Importantly, looking at choice

behavior alone, it would appear these two areas are playing the same role in decision-making, yet more thoroughly exploring the reaction times indicates otherwise.

It is clear also that inhibition of visual cortex only has a unilateral effect, as it only increases reaction times for stimuli and choices on the contralateral hemisphere. This shows us that the difference between the evidence for each choice required by the DDM in a 2afc task (Gold and Shadlen, 2002; Shadlen and Kiani, 2013) is not calculated in the visual cortex. However, when inhibiting the motor cortex, choices on both hemispheres are affected, indicating that the motor cortex has access to, or itself calculates the difference between the evidence for either stimulus.

Several other studies have reported results from dorsal cortex inactivation scans such as reported here, and usually report effects on choice behavior in anterior motor and sensory cortex (Allen et al., 2017; Guo et al., 2014; Zatka-Haas et al., 2021), but also see (Pinto et al., 2019). The results presented here are novel in reporting the effects on reaction time, as all the previous tasks used had a delay period between sensory stimulus onset and decision time. As I have shown here, though the effects on choice behavior may lead you to believe these two separate areas play similar roles in the behavior, the reaction times indicate distinct differences. Other studies have relied on a separate experiment to try to disentangle the role of these areas, by inactivating for temporal subsets of the trial instead of the whole trial (Guo et al., 2014; Zatka-Haas et al., 2021). In both of these cases it is clear that activity in M2 is required later in the decision process than activity in the sensory cortex, a fact that agrees with the conclusion that M2 is driving decisions more than sensory perception. Part of the area inactivated in my experiment includes ALM, a critical node for motor preparation and short-term memory (Chen et al., 2017; Daie et al., 2021; Finkelstein et al., 2021; Gao et al., 2018; Guo et al., 2014; Inagaki et al., 2019; Li et al., 2015). ALM is known to have multi-state attractor dynamics that likely are critical for decision-making (Finkelstein et al., 2021; Inagaki et al., 2019). In the context of a delayed-match to sample task, these circuits lead to stable decision-making made robust due to interhemisphere and intrahemisphere recurrent connections (Li et al., 2016). However, these dynamics have not been studied in the context of a reaction time task as here. In a reaction time task, decisions are usually thought to be reported immediately after crossing a

decision threshold (Steverson et al., 2019), as opposed to a memory task where a decision is made and then maintained until response time (Li et al., 2016). In the results shown here, the unilateral inhibition of the motor cortex seems strong enough to frequently cause decision threshold crossing before the onset of any stimulus, causing extremely short latency responses.

Despite inactivation of visual cortex only causing a unilateral effect on reaction times, inhibition of both motor and visual cortex alters choices for all contrast levels, making contralateral choices less likely and ipsilateral choices more likely. This is especially interesting in the case of inhibiting visual cortex on high contrast ipsilateral trials, where the baseline accuracy is high and there is unambiguous sensory evidence well above the sensory threshold (Busse et al., 2011), but inhibiting ipsilateral visual or motor cortex still provides an increase in accuracy. This suggests that in solving this task, the information for each choice is compared to see which is stronger. By inhibiting the ipsilateral cortex, any noise that may be interpreted as favoring a stimulus on that side would be eliminated, and this would only provide behavioral improvement on high contrast trials if the activity is compared between the two hemispheres. which is not necessary for this task given that a stimulus need only be detected on one side of the screen or the other for accurate performance. However, it seems that the raw sensory information from visual cortex is not directly compared between hemispheres, as unilateral inactivation of visual cortex only leads to a contralateral increase in reaction time. Instead it seems more likely that the more processed representation of the stimulus that is present in frontal motor cortex may be compared between hemispheres as inhibitions here caused opposing reaction time effects on the two choices.

One aspect of these results that may seem noteworthy to those familiar with mouse neuroanatomy is that the inhibition coordinates that I am referring to as visual cortex are only in the very anterior portion of visual cortex and into the primary somatosensory cortex. This is most likely due to a strange malformation in the cortical surface of these mice that had abnormal vascularization in the cortex, which appears to have shifted the visual cortex more anterior than it is normally located. In mice from the same emx-tta line crossed to Gcamp6f, the whiskers and whisker pads are occasionally missing (Akihiro Funamizu, personal communication), which could plausibly lead to a loss of barrel cortex and an anterior

shift of visual cortex in its place. Given that task performance was strong and unaltered from other IBL

mice and that these same effects were mostly recapitulated with a more posterior shift in the visual areas

using another inhibition method (see Chapter 7), this abnormality should not alter the interpretation of

these results.

One surprising result from these experiments was the large variability from animal-to-animal as

to the set of areas of inhibition that affected the biasing behavior. This could partially be explained by the

high baseline bias of two of the animals. The rest of the animals were relatively unbiased however, and

still did not have choice biasing in all four areas of interest (left and right visual and motor cortex). It is

possible that different animals are using different strategies to solve the task, therefore each has a different

set of areas that inhibition would affect. An example of two different strategies would be to just monitor

the left side of the screen and report left when a stimulus is seen and right otherwise, versus monitoring

both sides of the screen and reporting whichever side the stimulus appears on. Despite looking though, I

was unable to find any behavioral correlates of potential different strategies between mice with different

inactivation patterns. It seems unlikely that the source would be some difference in the surgical prep, as

the preparations were visually inspected each day of the experiment to insure transparency across the

skull, and two experiments with the same surgical prep did not see much animal-to-animal variability in

the inactivation patterns (Nick Steinmetz and Karel Svoboda, personal communications). So the origin of

this large variability between individuals is still an open question. Because this is a relatively

high-throughput experiment, I believe with a large enough cohort of mice, one could more thoroughly

investigate if this variability is due to differences in strategy. Or in combination with simultaneous

widefield imaging, one could determine if there is a difference in the amount of inactivation present

depending on the target.

As mentioned earlier, a similar set of experiments has been performed in a similar task

(Zatka-Haas et al., 2021). The main differences from the IBL task and their task is that theirs is a two-part

decision as there is a no-go option, so mice first must decide to respond or not respond, then to respond

right or left if they decide to respond, mice need to compare the contrast of stimuli on two different

screens, and there is a delay period of several hundred milliseconds after stimulus onset in which no responses can be triggered. Despite these differences, we both found a very similar pattern of choice biasing due to inactivation, the main difference being that more of primary visual cortex was affected by their inactivation, likely because the stimulus in their task activated a much larger portion of the visual cortex. Zatka-Haas and Steinmetz et al. also saw through an inactivation time course that inhibiting the visual cortex had an earlier effect on performance than inhibiting motor cortex, consistent with a model that information first comes into the visual cortex and then is routed forward to the motor cortex. The results I present here extend these findings by observing the different effects on reaction time of inhibiting visual and motor cortex, showing further that the information present in the motor cortex is further in processing towards a decision given that unilateral inhibitions cause bilateral changes in reaction time, but unilateral visual inhibitions only cause unilateral changes in reaction time.

# 4       Chronic removal of V1 activity does not impair task performance

<u>Contribution note:</u> The work in the following chapter was conceived of, planned, and analyzed by myself and Tony Zador. I performed all of the experiments and built required hardware and wrote required software for these experiments.

## 4.1 Introduction

Having seen the behavioral effects of acute inactivation of visual cortex, I next wanted to test if V1 activity was required for performance of the task, or if only acute manipulations affected behavior. It is not always true that areas whose acute manipulation impairs behavior also alter behavior when chronically removed (Hong et al., 2018; Kawai et al., 2015; Newsome and Paré, 1988; Otchy et al., 2015). Given that I have shown that acute manipulations of neural activity can alter behavior, I next wanted to determine if the visual cortex was truly required for performance of the task, or if visual decision-making performance would be unaltered by the absence of visual cortex.

The visual cortex is known to be required for conscious visual perception in humans (Weiskrantz et al., 1974) and stroke or resection of primary visual cortex in all primates causes large, permanent deficits in many visual behaviors (Stoerig, 2006). Similarly it has been shown above and by others that acute optogenetic manipulation of visual cortex impairs mouse visual abilities (Glickfeld et al., 2013; Zatka-Haas et al., 2021), and that other primary sensory cortical areas in mice can be removed and not affect detection tasks (Hong et al., 2018). To my knowledge, it has never been investigated if chronic removal of V1 in mice has long term impacts on visual abilities.

Here I demonstrate that permanent aspiration of V1 in mice causes no deficit in the IBL basic stimulus detection task. I additionally show preliminary results indicating that chronic optogenetic inhibition on nearly every trial temporarily induces a behavioral deficit, but that deficit is overcome by training. This indicates that though V1 may play a role in the IBL visual decision-making task, it is not necessary for its performance.

## 4.2 Materials and methods

*Mice, headbar surgeries, and behavioral training*

All mouse handling, and training were done as described in the methods for chapter 1. The three cortical aspiration mice were C57B6\J mice, and their only difference from normal IBL procedure was that they had a bilateral aspiration of visual cortex (see below) at the time of the headbar implantation. The mouse used for the chronic bilateral V1 inhibition was a VGAT-ChR2 mouse. The same mouse had previously undergone the inhibition scan experiment in the last chapter. He had been trained fully on the task for multiple months prior to the experiment in this chapter, and had previously been exposed to various pilot inhibition experiments.

*Cortical aspiration surgery*

The bilateral visual cortex aspiration was performed during the IBL headplate implantation surgery. After the scalp had been removed, the skull cleaned, and the skin glued back, I made a large triangular craniotomy approximately over V1. As my main reference I used the large transverse sinus that sits at the posterior of the cortex as the bottom of my craniotomy, being sure not to hit this vein as that usually caused catastrophic bleeding. Before drilling I wetted some Gelfoam (Pfizer) with saline using pieces of various sizes, up to the size of the craniotomy. I then used a dental drill to drill an equilateral triangle with sides of ~3mm over each hemisphere of visual cortex. It is key to not drill fully through the bone on the back side of the triangle as this will usually puncture the transverse sinus. Once the two sides of the triangle were drilled through and the back side was drilled mostly through so as to create a sort of trap-door flap of bone, I grasped the bone chip from the anterior end with forceps, and peeled it off sideways, not vertically, again to avoid puncturing the transverse sinus. I then placed the bone chip in saline on ice. After this I aspirated the cortex using the mains vacuum hooked up to a small tube and a 200ul micropipette tip. I aspirated cortex until I could see the underlying white matter, being sure to suck up as much anterior and to either side of the craniotomy as I could, while not disrupting the transverse sinus. After this I applied the prepared gelfoam to the craniotomy and used surgical eye spears to dry the gelfoam until the active bleeding had stopped. I then replaced the bone chip, leaving the gelfoam inside

the skull, glued it back into place first with vetbond to seal the edges, then covered it with metabond. Leaving the Gelfoam inside the skull is key to keep the proper shape of cortex for later histology. After both hemispheres had been aspirated, I proceeded with the IBL headplate implantation surgery (see Chapter 1).

*Histological alignment of aspiration mice*
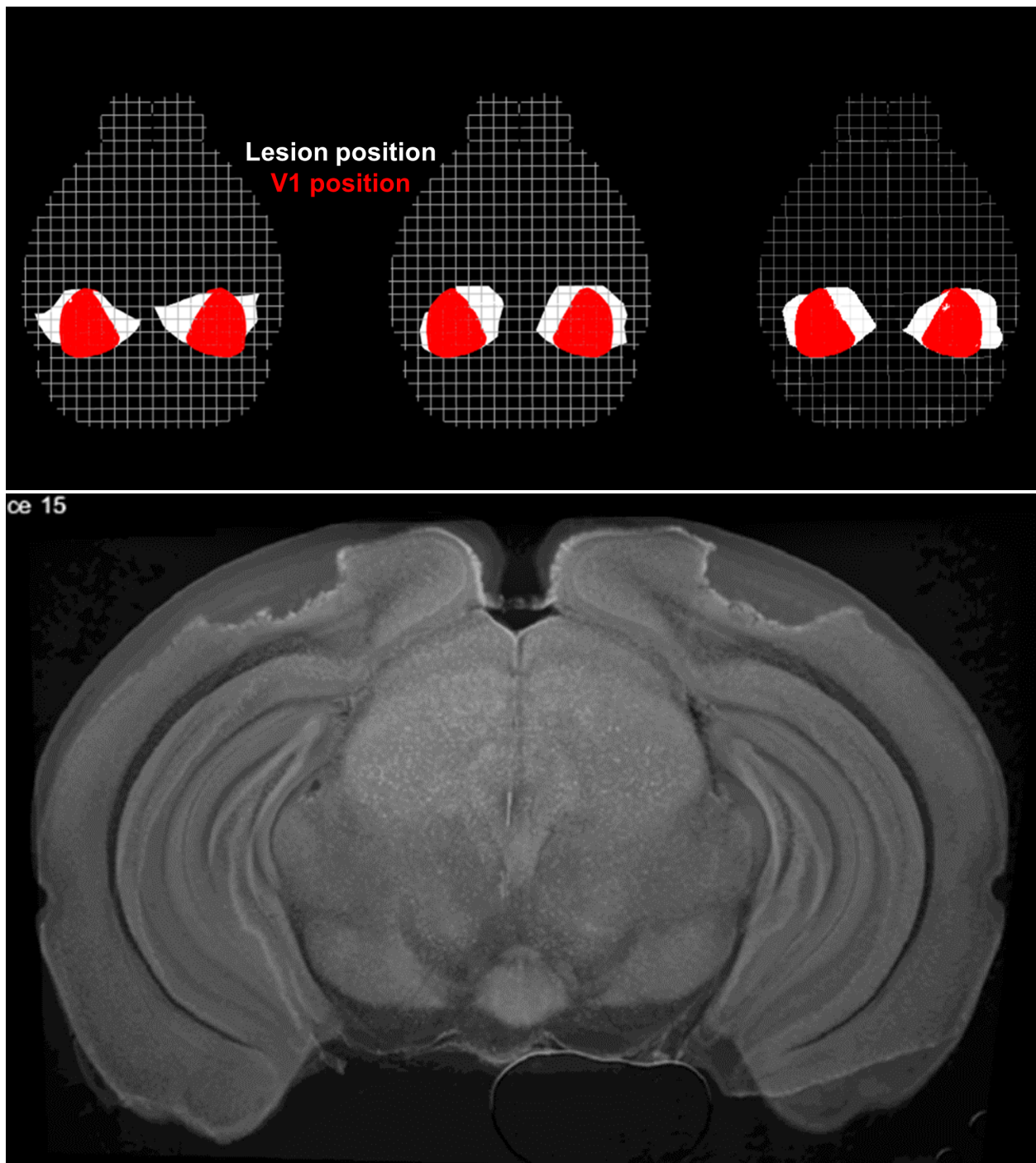
To visualize the extent of cortex aspirated in the surgery, and ensure that I had removed a majority of V1, I adapted a tool for the localization of electrode tracks from 2d histology (SHARP-track, to map the extent of my lesion (Shamash et al., 2018). After the experiments were complete, I perfused the mice with 4% PFA and removed and post-fixed their brains for 24 hours in 4% PFA at 4 degrees Celsius. I then sliced the region of interest in 100um thick slices, stained the slices with DAPI, and imaged each slice. The slices were then aligned to the CCF using SHARP-track. After aligned, I traced the points surrounding the edges of the aspirations on each slice using the probe tracing tool in SHARP-track. I then took these points and plotted the volume of the aspiration compared to the volume of the area assigned to V1 to confirm that a majority of V1 had been aspirated.

*Bilateral chronic optogenetic inhibition*
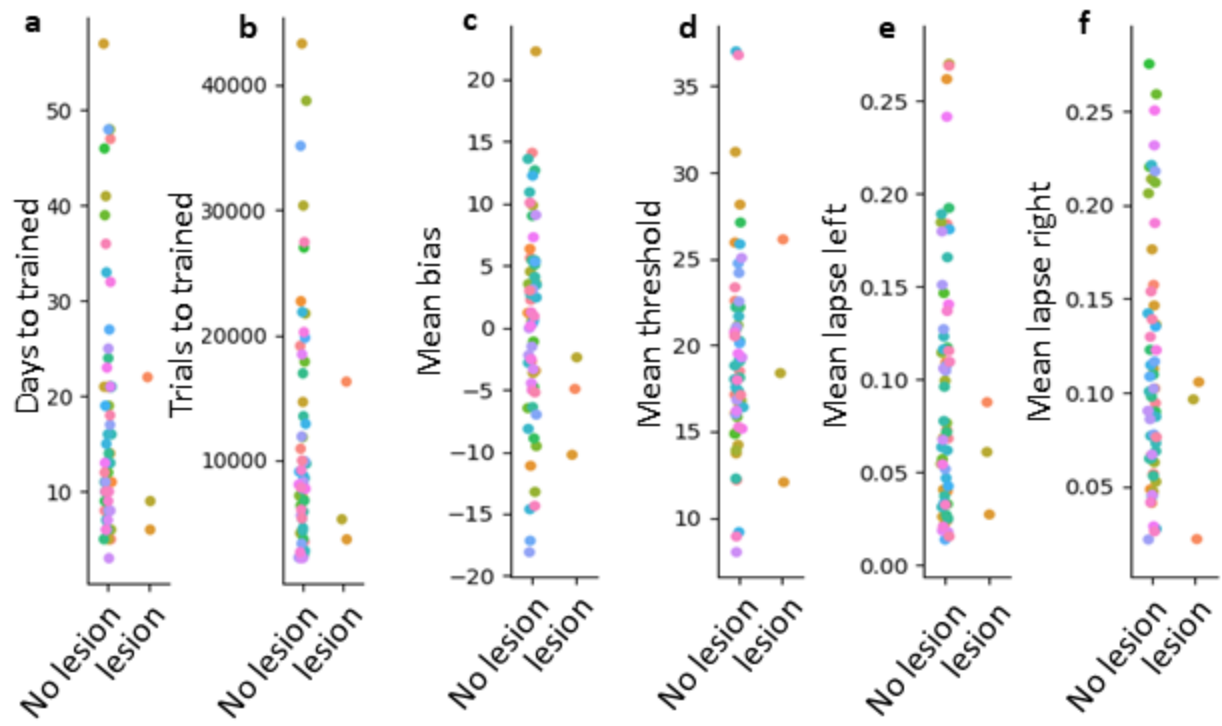
Chronic bilateral optogenetic inhibition was performed on mouse CSK-scan-015 seen in Chapter 3. It was performed in the same set-up with the same laser power as used in Chapter 3. The diameter of the beam in this case was increased to 800um to increase the coverage of V1 inhibition. Additionally the inhibition was performed bilaterally by alternating the laser position between the hemispheres of V1 inhibition. In this case, instead of a true 40Hz sine wave as was used for inhibition in Chapter 3, the wave was truncated so that the laser was off for the lower ¾ of the wave for each side. This eliminated any inhibition between the two hemispheres as the mirror alternated between the two positions, while still achieving 40Hz inhibition on each hemisphere of the visual cortex. The inhibition took place for the same duration, 2.2s starting 0.1s before and continuing 0.1s after the response period. The laser was not on between the response periods of the trials so as to limit overheating of the tissue, so it was not truly a chronic inhibition.

## 4.3 Bilateral aspiration of visual cortex does not impair training time or learned behavior

Having seen that acute inhibition of visual and motor cortex caused a significant bias in behavior, I next wanted to determine if chronically removing the visual cortex, the supposed gate of information for this task, permanently disrupted the behavior. To do this, I performed bilateral aspirations of primary visual cortex in three mice at the time of headbar implantation. Upon histological review of the extent of the lesions, I confirmed that nearly all of V1 was removed, along with much of the medial and lateral secondary visual areas (Figure 4.1). The receptive field for the stimuli used in this task is in the most lateral and anterior portion of V1, and this area was completely removed in all mice and hemispheres except the left hemisphere of the middle mouse. After these aspirations, I proceeded to train these mice in the standard IBL task. All three mice reached the trained criterion before the IBL cutoff of 'untrainable' at 40 days of training, and therefore were deemed to have no impairment in their ability to be trained on this task (Figure 4.2a, b). Furthermore, when comparing the fitted psychometric parameters of the sessions after the mice were trained, all three of these lesioned mice performed within the spread of normal behavior in the rest of the IBL non-lesioned mice for all four psychometric parameters (Figure 4.2c-f).
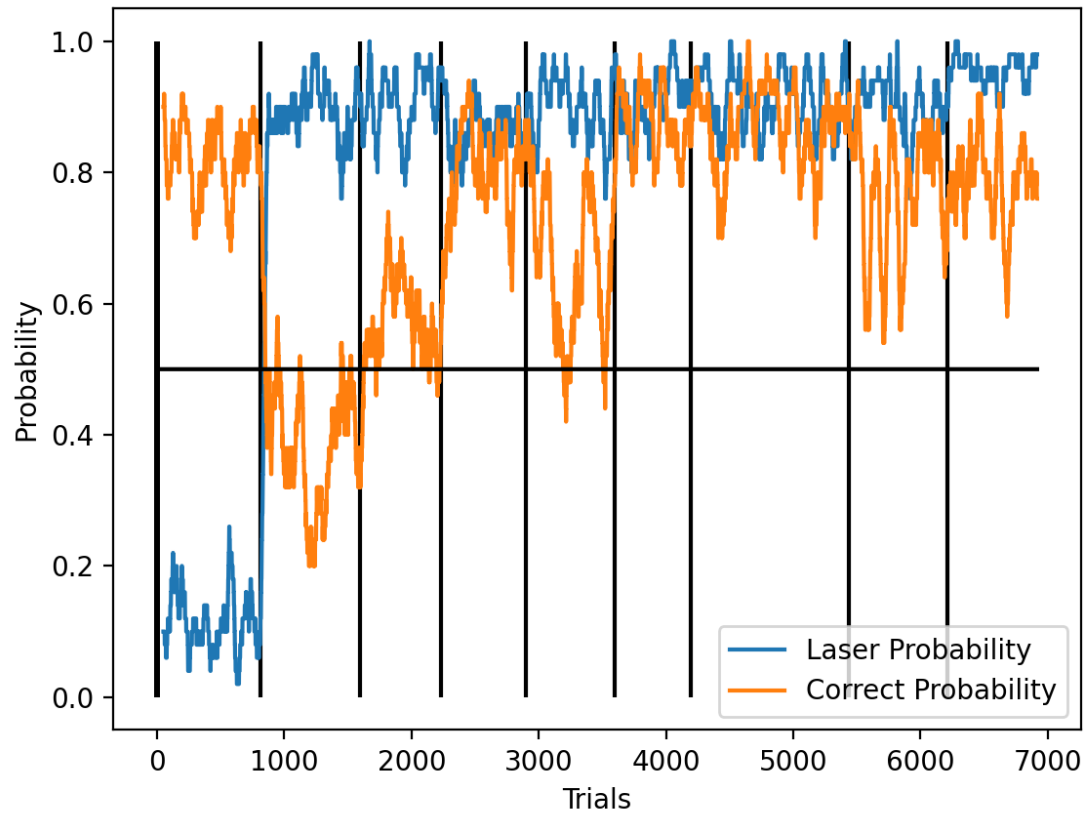
**Figure 4.1.** (top) Post-hoc histology of lesion locations (in white) and of the location of V1(red) following bilateral V1 lesions in three mice. Red is plotted on top of white, so the lesion position encompasses nearly all of V1, except the most caudal and lateral portion. (bottom) an example coronal slice of the post-lesion histology overlaid on the allen atlas to show approximate depth of the lesion.

**Figure 4.2.** Mouse training and performance are unaffected by bilateral visual cortex lesion. (a) Mouse training rate measured by number of days of training until reaching the IBL trained criterion for mice with bilateral visual cortex lesion and normal IBL mice without a lesion. Each color is for a different mouse. (b) Same comparison for trials to reaching the IBL trained criterion. (c-f) Comparison of fitted psychometric parameters from sessions after reaching the trained criterion for lesioned and intact mice.

**4.4 A mouse recovers from chronic bilateral inhibition of primary visual cortex**

Above I have shown that acute inhibition of visual cortex with optogenetics biased the behavior of mice. Shockingly though, permanent removal of the visual cortex through aspiration did not affect behavior. To try to determine if it is the inhibition with optogenetics in particular, the bilateral versus unilateral difference between the two experiments, or the chronic versus acute aspect that causes these different results, I performed chronic bilateral optogenetic inhibition of visual cortex in a trained mouse. Unfortunately I only have data from a single mouse on this experiment, so these results should be taken as preliminary. Using only the strongest stimuli, for a mouse that had already learned the task, I did several consecutive days of bilateral visual cortex inhibition. In session 0, I had the inhibition laser on for 10% of trials to achieve a baseline of the acute effects of bilateral inhibition (Figure 4.3, blue trace). In session 1, I increased the inhibition rate so that 90% of trials were inhibited to mimic a chronic inhibition such as an aspiration. On this day the behavior dropped below chance performance (bias correction was used so below chance performance indicates a bias to one side). Following each subsequent session of chronic inhibition, there was a jump in accuracy of the mouse, until on the third day of chronic inhibition, the mouse's accuracy returned to the baseline level. There was some day-to-day fluctuation in performance across the subsequent inhibition days, but as a whole the mouse retained the ability to perform the visual discrimination task with both hemispheres of V1 inhibited on 90% of trials.

**Figure 4.3.** Chronic bilateral inhibition in one mouse shows recovery of visual discrimination during inhibition. Blue trace indicates the probability that the laser will be on in a 10 trial rolling window, i.e. that there will be inhibition of the visual cortex, the first session had a inhibition probability of 0.1, and all sessions after had a 0.9 inhibition probability. Orange line indicates the probability that the mouse responded correctly in a 10 trial rolling window on the 100% and 50% contrast trials. Vertical black lines indicate the start of a new session.

**4.5 Discussion**

Here, I showed that despite the acute effects of inactivation of visual cortex on visual decision-making behavior demonstrated in Chapter 3, chronic inactivation seems to have much less or no effect. Bilateral visual cortex aspirations before training (and after, data not shown), seem to leave mice completely unimpaired in learning or performing the IBL visual decision-making task. Furthermore, in one mouse, consistent bilateral optogenetic inactivation of the visual cortex initially eliminated accurate behavioral performance, but ultimately that mouse was able to re-learn the task with just three sessions of training with chronic inhibition.

There are many caveats to this chronic optogenetic inhibition experiment, especially that it is only a pilot with a single mouse, and the results need to be replicated. Additionally there are potentially technical reasons for this result, for example it is possible that with such chronic inhibition, the ChR2 channel is somehow disrupted by such constant exposure to light. This reason seems unlikely though, since if this were true you would expect behavior to gradually improve within a session while the channel is being activated, but the main changes in performance seem to happen between sessions. This and several other concerns about if the activation is properly executed, could be solved by simultaneously measuring the neural activity while performing the inactivation. This could be done optically as in chapter 7, with simultaneous widefield imaging during chronic inactivation. This may be an extremely interesting experiment if the results presented here are true, as there would likely be changes over time that allow the animal to re-learn the task in the absence of visual cortical activity, which could be measured across the dorsal cortex. This would also allow comparisons of the cortical neural activity between chronic and acute inhibition, and to see how network activity differs between the two manipulations.

The observation of a complete lack of behavioral deficit following a bilateral aspiration of visual cortex in a visual task was very surprising. Although perhaps it should have been less surprising given recent reports of unaffected task performance with cortical aspirations in rodents (Hong et al., 2018; Kawai et al., 2015; Otchy et al., 2015). With removal of the motor cortex, there seemed to be an interaction with learning, where motor cortex was required to learn a motor task, but not to perform it

(Kawai et al., 2015). More analogous to the experiments in this chapter, removal of barrel cortex, the primary whisker somatosensory area, did not impair performance or learning of a simple whisker deflection detection task (Hong et al., 2018). These studies all report different effects of acute manipulations (both optogenetics and muscimol) from chronic removal of cortex. I demonstrate here concurring findings in the visual cortex. My findings also extend these results by demonstrating that optogenetic manipulations per se are not the source of the difference between acute and chronic activity removal, as repeated optogenetic inhibition failed to permanently impair behavior.

Why is it that acute inhibition impairs performance but chronic inhibition does not? There are two subtly different possibilities that best explain these results. The first is that there are two or more parallel, redundant pathways that are capable of producing the behavior; the cortical pathway may be the default, and so when acutely manipulated it affects behavior, but after permanent inhibition, the redundant pathway takes over (Hennig et al., 2018). This seems to be true in some cases with primate vision, loss of the visual cortex causes catastrophic loss of most visual functions (Weiskrantz et al., 1974), but some visual abilities can be restored with perceptual training (Das et al., 2014; Huxlin et al., 2009; Newsome and Paré, 1988; Sahraie et al., 2010, 2006). The main areas mediating this regain in visual behavior seem to be the superior colliculus and visual thalamic nuclei (Ajina et al., 2020; Isa and Yoshida, 2021; Kinoshita et al., 2019; Stoerig, 2006, p. 12). As the mouse visual system is much less fine-tuned than the primate system, with the visual abilities of mouse cortex more approaching those of primate superior colliculus (Busse et al., 2011; Glickfeld et al., 2013; Huberman and Niell, 2011) it is possible that the colliculus can perform this visually simple task independent of the cortex.

A related explanation, could be that the visual cortex and superior colliculus are not independent redundant pathways that can solve this task, but instead the superior colliculus itself performs the task, and behavior is only impacted when unnatural patterns of activity are present in visual cortex (Otchy et al., 2015; Wolff and Ölveczky, 2018). This idea is based on the fact that the brain is a highly interconnected network, and sudden, unnatural disruptions of activity in one area are bound to impact downstream areas. It is possible that, for example, superior colliculus normally solves this task, but

because it normally gets input from visual cortex, it is reliant on this input. Even if the input does not contain information, the input from visual cortex is required to have a normal activity pattern that leads to the correct pattern of activity in superior colliculus. Because this input is not informative, after a permanent lesion, the superior colliculus could regain its normal activity pattern through homeostatic maintenance of firing rates (Otchy et al., 2015; Wolff and Ölveczky, 2018). Which of these two possibilities are the true organization of the network function is still an open question, and performing this same set of experiments in superior colliculus may provide some answers as to which is true.

# 5        Wide field calcium imaging to decode task events

<u>Contribution note:</u> The work in the following chapter was conceived of, and planned by myself and Tony Zador. I performed all of the experiments and built required hardware for these experiments. Analysis was done in collaboration with Tony Zador and Alex Pouget.

## 5.1 Introduction

In the quest for creating a model of decision-making, the IBL is recording single neuron action potentials across the entire brain using neuropixels probes. However, one of the main limitations of the approach of the IBL is that the number of brain areas from which one can simultaneously record is still rather small, despite being much improved over previous electrophysiological techniques (Jun et al., 2017). Even from the 5-10 different brain structures that can be recorded simultaneously, only a handful of the millions of neurons in a given area can be recorded. Furthermore, though the IBL has designed their experiments so as to maximize reproducibility, often reproduction of results alone is not enough, and maximizing the fidelity of scientific findings instead requires triangulation, or verifying the findings with several different methods and approaches (Munafò and Davey Smith, 2018). As a complement to the single neuron recordings that make up the IBL brainwide map, I have performed wide field calcium imaging of the whole mouse dorsal cortex during performance of the IBL task.

In contrast to multiplexed single-unit electrophysiology, widefield imaging allows simultaneous monitoring of neural activity from across the entire surface of the mouse dorsal cortex (Wekselblatt et al., 2016). This comes at the cost of a lower temporal resolution, the loss of single cell resolution, and a limit to only accessing the dorsal layers of dorsal cortex as opposed to the whole brain. However, monitoring the activity of many brain regions at once, though still a relatively novel technique, has already led to many important insights that would not have been possible otherwise (Cardin et al., 2020; Musall et al., 2021, 2019; Ren and Komiyama, 2021; Shimaoka et al., 2019; Wekselblatt et al., 2016; Zatka-Haas et al., 2021). In addition, using optical imaging to record neural activity provides advantages such as the opportunity to easily combine it with optical manipulation of neural activity with optogenetics (see Chapter 7), as well as perform experiments chronically, for months using the same animal (Couto et al., 2021).

In this chapter I will focus mainly on using the neural activity recorded with wide field calcium imaging to decode task events. Neural decoding uses recorded neural activity to predict real-world or cognitive variables relevant to the animal, such as the identity of a stimulus, or a change in behavioral state. It is a statistical learning problem, in which you are trying to learn what stimulus or cognitive variable the neural activity predicts (deCharms and Zador, 2000). Given that it is a statistical learning task, there are many possible tools to perform it, ranging from state-of-the-art machine learning tools, to more foundational methods such as logistic regression. If the goal of the decoding is to perform as accurately as possible, assuming you have recorded enough data, the former is likely the best tool, as highly nonlinear models such as deep neural networks are well suited for finding patterns in neural signals (Glaser et al., 2020). However my goals are not just to obtain strong performance in decoding, but also to use the decoder to understand the computations that the brain may be using to solve the task. With this in mind, I chose to use logistic regression models to decode behavioral events from wide field calcium imaging data. These models allow us to predict behavioral variables such as the stimulus onset at or near the same accuracy of the mouse, but also yields linearly interpretable weights, in which we can see how the model combines the activity from different regions of the cortex, and across time, to make accurate predictions. This is a powerful correlative technique that constrains the large space of models the brain could be using to solve the task down to a model space conditioned on what information is actually present in the brain. This allows us to answer open questions in the field about how neural information is represented across the cortex.

One such open question is the routing problem (Olshausen et al., 1993), or how information that is represented in one area is sent to another at just the right time for coordinated activity across brain areas. It is well recognized that any full-scale model of the nervous system must include an explicit model of how information is routed between nodes (Graham, 2014). Many models that do explicitly include information routing use time-inefficient methods that require first sending a connection signal, returning an acceptance signal, then finally sending the desired information, a process that is far too slow for biological neural networks (Cassidy et al., 2013; Graham, 2014; Mišić et al., 2014). Instead, it has been

proposed that information is sent between areas in a more passive manner, following the rules of connectivity between areas, with a bias towards first sending information to highly connected nodes, that then have the capacity to send that information to many other brain areas (Avena-Koenigsberger et al., 2019). This provides a mechanism for information to quickly reach a desired target, but it does not address how information is made available in the areas required for task performance. It is possible that instead of information being sent only to the areas that require it for task completion, it is broadcast generally, and the areas that require that information are primed to make use of that signal.

Here, I show that the best model for predicting the stimulus or action from widefield data takes the time derivative, and compares activity between the two hemispheres of the visual and motor cortex. I show that cortical information representing these task variables is initially at a steady state, rapidly changes, and reaches a new steady state. I also show that all of the task information required for accurate decoding is located in two brain regions, V1 and M2, but this information is also available across the whole cortex, so that every cortical area has above chance decoding of these variables.

## 5.2 Materials and methods

*Mice*

Mice used in these experiments were six male mice obtained by breeding transgenic strains to obtain offspring heterozygous for each Camk2a-tTA (JAX strain 007004), and tetO-GCaMP6s (JAX strain 024742) such that they expressed GCaMP6s in most cortical excitatory neurons (Wekselblatt et al., 2016). All but one of the mice were co-housed and all had access to nesting material. They were kept in a 12-hr light-dark cycle and all experiments and procedures were performed in the light part of this cycle. All experiments and procedures were carried out with approval of the Cold Spring Harbor Laboratory Institutional Animal Care and Use Committee.

*Surgery*

Surgeries were performed as detailed in methods for Chapter 3.

*Mouse training*

Mice were trained in an IBL training rig (The International Brain Laboratory, 2021) using the standard IBL protocol (The International Brain Laboratory, 2020b) with a few exceptions. The first exception is that instead of the IBL protocol for habituation, mice were first habituated to the experimenter once water restriction began (1 week following surgery), by the mice receiving their daily water from a blunt 1ml syringe while they were held in the experimenter's gloved hand. Following this there was no period for habituation to the rig, the mice began performing the IBL task (The International Brain Laboratory et al., 2021) from the first time they were headfixed. Following this, training progressed according to the IBL protocol, learning first the association between stimulus side and wheel movement, then having more difficult contrasts added in. Once mice had fully acquired the stimulus discrimination, the biased blocks were introduced. The two modifications to the final task were an increase in the inter-trial-interval from .5s to 1.5s (to allow additional time for Gcamp6s signal to return to baseline, minimum total of 2.9 seconds between response and the next stimulus onset), and a shortening of the response window from 60s to 10s.

*Widefield imaging*

All widefield imaging hardware, software, and protocols were used as in (Couto et al., 2021). The widefield imaging scope was built inside an IBL electrophysiology rig (Steinmetz et al., n.d.), and used all the components of this rig to run the task. Imaging was performed with both blue (473nm) and violet (405nm) LEDs on strictly alternating frames coordinated by a teensy microcontroller (PJRC, TEENSY32). At the beginning of each imaging session, the clear skull cap was washed with ethanol, a black plastic light shield was placed isolating the imaging light to the skull, and LED intensity was adjusted such that each channel was within ~10% of the saturation point for that channel. Images were acquired every 33ms with a PCO Edge 5.5 camera (15hz per imaging channel) in rolling shutter mode with a 286MHz scan rate and 4 x 4 on-camera pixel binning. Image acquisition was performed using the labcams software package (Joao Couto, available through pip install labcams). Image preprocessing was performed after each imaging session using the wfield software package (Joao Couto, available through

pip install wfield). Standard widefield imaging preprocessing were used (Couto et al., 2021; Musall et al., 2021, 2019), which include automated motion correction by rigid body registration to the mean of all frames, hemodynamic correction by rescaling the fluorescence of the violet channel to match that of the blue channel and subtracting it away, denoising and compression by taking the singular value decomposition of the video and only keeping only the top 200 components, and a manual alignment to the allen reference atlas with four anatomical landmarks. Finally, Δf/f was calculated by subtracting off and dividing the fluorescence of each frame by the mean fluorescence across the whole session.

*Logistic Regression Decoding*

Decoding of task variables was performed using logistic regression as implemented in scikit-learn (Pedregosa et al., 2011). Before the decoding, to reduce the number of features, the imaging was downsampled 100-fold, by taking the mean of a 10 pixel by 10 pixel square of the true pixels. When I refer to pixels, I mean the downsampled version that all of the analyses were performed on. The input to the logistic regression was always event-aligned (stimulus onset or movement onset) df/f of shape $n_{trials}$ by $n_{pixels} * n_{frames}$, and was z-scored pixel-wise separately for train and test data, with all non-brain pixels set to 0. Additionally all trials where no response was made were always dropped from analysis. The models were trained to predict a binary outcome, for example stimulus side or block identity. In most instances, unless noted, an l2 penalty was used as regularization. An L2 regularized logistic regression regularizes the following cost function:

$$\min_{w,c} \frac{1}{2} w^T w + C \sum_{i=1}^{n} \log(\exp(-y_i(X_i^T w + c)) + 1)$$

Where $C$ is the strength of regularization, $w$ is the weights on the data matrix $X$, and $c$ is the bias term. Selection of the regularization term $C$ was performed with the *sklearn* the built-in function *LogisticRegressionCV* with values in the range of 0.02 to 5. This selection was done separately for each of 5 folds of an outer loop of cross-validation such that predictions were made for all trials, such that 5 separate models are trained per session. The "class-weight" argument was always set to "balanced," this

automatically adjusts weights of the decoder inversely proportional to the class frequencies, which allows the model to be trained with uneven class frequencies while maintaining a chance prediction level of 0.5 instead of the frequency of the most abundant class. Results from decoding are always reported from the fully cross-validated dataset following 5-fold cross validation. Weights from a single session of decoding were obtained by averaging the weights of all 5 decoders for that session. To limit noise from animal-to-animal and day-to-day variability, a separate model was trained for each recording session.

*Sparse decoding to find the most informative pixels*

To determine the location of the most informative pixels for decoding, I used a logistic regression decoder as detailed above, except using an L1 regularization as opposed to L2 therefore solving the follow optimization problem:

$$\min_{w,c} \|w\|_1 + C \sum_{i=1}^{n} \log(\exp(-y_i(X_i^T w + c)) + 1)$$

.

L1 regularization forces sparsity on weights, driving many weights to be 0, and only selecting the more informative features (Ng, 2004). To perform this decoding I trained a separate decoder for each session, and for a range of L1 regularization coefficients from the set [0.02, 0.05, 0.1, 0.25, 0.5, 1, 1.5, 2,5, 10]. For each decoder I then determined the number of non-zero coefficients, or the number of pixels that that decoder used, and which cortical areas those non-zero coefficients came from. To visualize the fraction of pixels that were chosen from each cortical area, for each session I took the first decoder that performed at or above the accuracy of an L2 decoder for that same session with the same 5-fold cross-validation splits, and located which cortical area the pixels were in. I then summed up all of the pixels in a given area from the selected decoder for each session, and normalized this by the total number of pixels used by all selected decoders to obtain the fraction of decoding pixels in an area.

*Statistical analyses*

To determine the statistical significance of the sign of the decoding weights, I performed a binomial test for each pixel. This is a standard test that compares the prevalence of the outcome of a sampling of a binary event to the prevalence expected by chance given the binomial distribution.
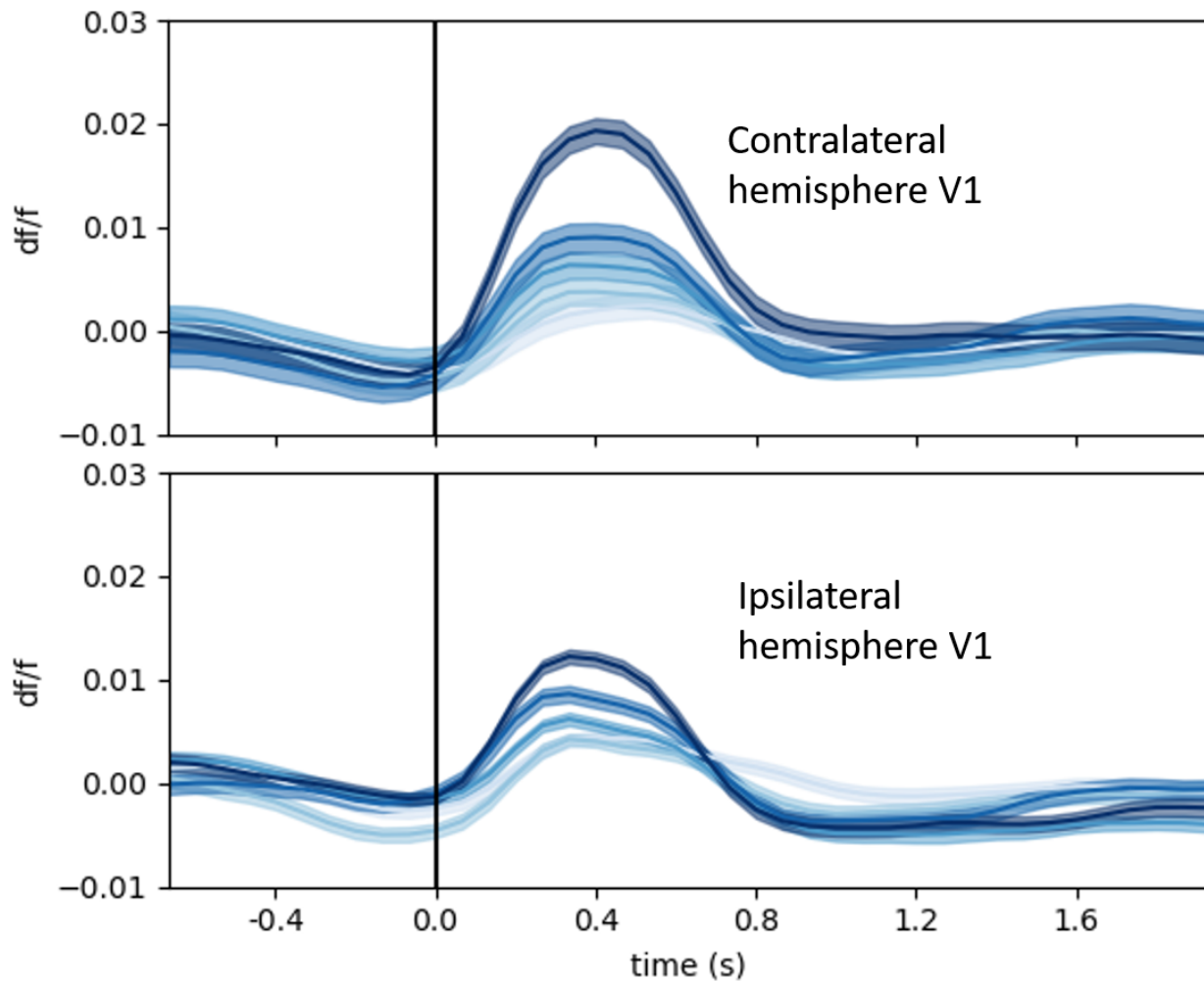
Specifically, I performed a logistic regression decoding of the stimulus identity for each imaging session. I took the weights of each of those 52 sessions for each pixel and binarized them such that they were either predicting left or right stimuli. I then performed a binomial test asking whether the weight on that pixel consistently predicted a left stimulus or a right stimulus, or if the sign of the weight on that pixel was no different than expected by chance. This was done by first binarizing the weights such that they were in the set $\{0, 1\}$, I then for each pixel calculated a p-value using the binomial test formula:

$$p(x) \ = \ \frac{n!}{(n-x)!x!} \bullet \left(\frac{1}{2}\right)^{n}$$

Where $n$ is the number of sessions, and $x$ is the number of sessions for which that pixel had the weight predicting the same stimulus. The bonferroni correction for multiple comparisons was then applied to this p-value, correcting for the total number of pixels on the cortical surface that the test was applied to (2664 pixels).

## 5.3 Contrast-dependent and lateralized visual activation in the IBL task

To ensure I was able to see reflections of real-world variables in neural activity, I first started by looking for one of the most fundamental signals of neuroscience, a stimulus-locked increase in neural activity in sensory cortex. I focused on a well-understood signal, the activation of primary visual cortex (V1) by lateralized stimuli. To see if there was higher activation of V1 for contralateral stimuli than ipsilateral stimuli, and if those responses were higher for stimuli of higher contrast, I created peri-stimulus time histograms for both hemispheres of V1 aligned to the onset of stimuli on the left side of the screen. From this, I predicted that there would be more activation in the right hemisphere for all contrasts, and that this activation would be contrast dependent, such that the stronger contrasts produced higher activation. Figure 5.1 shows this exactly, the strongest activation is for the strongest stimulus intensity and in the right hemisphere, with decreasing activation for decreasing contrast intensity. We also see an increase in activity in left hemisphere V1, but this is ipsilateral to the stimulus, and accordingly we see a smaller amount of activity at each contrast level than on the contralateral hemisphere.

**Figure 5.1** Activation of visual cortex is lateralized and contrast dependent. Plots showing contrasts appearing on the left side of the screen only. (top) Peri-stimulus time histogram for an example session for the right visual cortex time-locked to the onset of left visual stimuli of contrasts [1, 0.25, 0.125, 0.0625, 0], darker indicating the higher contrast value. (bottom) Same as top, but now for the left visual cortex for the same left stimuli. Lines are mean activity for one example session across all pixels within one hemisphere of V1, +/- standard error of the mean.
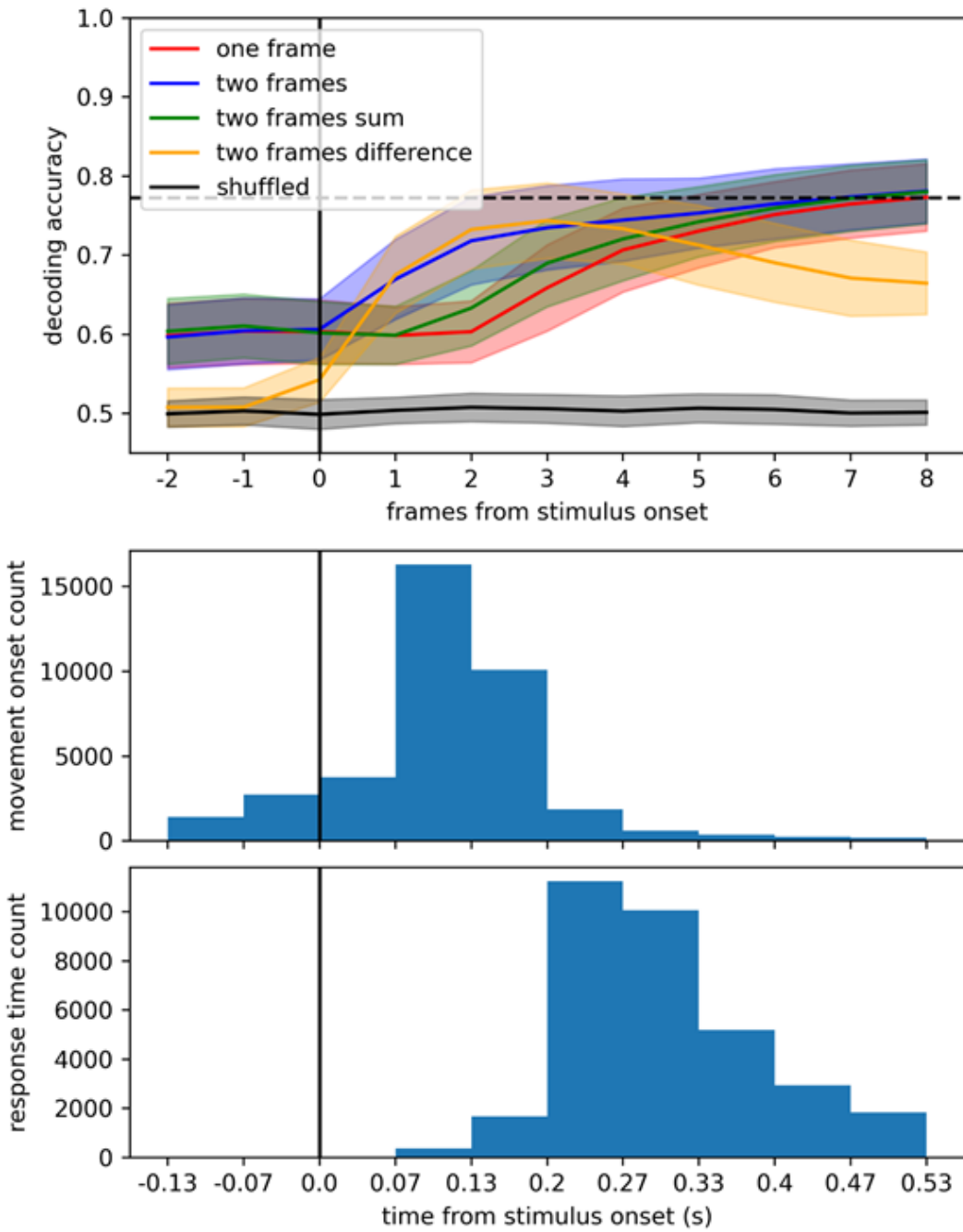
**5.4 Logistic regression to decode stimulus side from the whole dorsal cortex**

Given that there is differential activation of the contralateral cortex than of the ipsilateral cortex to visual stimuli presented in the IBL task, it is clear that there is information identifying the stimulus side available in the cortex. Given this, I should be able to decode the true stimulus side from the neural activity of the whole dorsal cortex. Because the key decision for the IBL task is to determine which side of the screen the stimulus is on, these decoders can be used to gain insight into how the activity in the mouse cortex can be used to solve the IBL task.

To decode the stimulus side from neural activity, I used a logistic regression model with an L2 regularization (see methods for exact fitting procedure), using the neural activity from the entire dorsal cortex to make the predictions. To differentiate between some of the neural computations that could be used to solve this task, I trained models with four different types of input: a single frame of stimulus aligned activity, the sum of two consecutive frames, the difference of two frames, and two frames of activity. Comparing these models gives us information about how the cortex might solve the task: if the single frame model performs best, that means the change in activity over time is not informative, i.e. that the information in the activity has reached a steady state. If the sum model is best, that indicates there is integration of information over time, if the difference model is best, that indicates that the time derivative of activity is most informative. Finally, the two frame model allows more complicated combinations of activity through time, allowing for different linear combinations of activity for different parts of the brain. The two-frame model is the most general of the four, but it also comes at the cost of fitting twice the number of parameters, as a weight must be learned for each pixel on both frames. Additionally, the other three models are subsets of the two frame model that it could in theory learn: the difference model is the two frame model enforcing the same weight of opposite signs on each pixel, the sum model is the same but enforcing the same sign on the weight of each pixel, and the single frame is the two frame model with all weights for the first frame set to 0. Therefore the two frame model should always be better than or equivalent to all of the other models, unless there is a failure to accurately fit all of the weights given the limited amount of data collected.

Figure 5.2a shows the performance of each of these models aligned to stimulus onset. For the three models containing information about multiple frames, the input to these models is for frame $t$, and frame $t$-$1$, such that they are aligned to the last frame that they have access to. Before stimulus onset, all models except the difference model have slightly above chance decoding, indicating that the information about the stimulus then is at a steady state, and subtracting the activity simply removes that information. Just following stimulus onset, there are two models that outperform the others, the two frame model and the difference model. As time progresses through the trial, the sum and one frame models begin to increase to that same level of accuracy, but the difference model drops off in performance. Taken together, this indicates that the most accurate signal to decode the stimulus just following its onset, is the change over time. However, a few hundred milliseconds after the stimulus onset, the derivative is no longer the best signal to use, indicating that the relevant activity has moved towards a more steady-state representation, similar to before stimulus onset. The two frame model consistently performs well as it can flexibly learn which neural computation should be used at different time points in the task. Interestingly though, before the stimulus onset and about 400ms after stimulus onset, there was no advantage of the two frame model over the single frame model, indicating that the stimulus information across cortex is in a steady state in those two periods, and is only changing in a small window around stimulus onset.

One important caveat to these results is that, given the lack of a delay between stimulus onset and decision time and the relatively slow sampling rate used in this imaging, it is difficult to disentangle the signals of action and visual response. Figure 5.2b shows the histogram of movement onset (the first detected wheel movement that leads to the response) relative to stimulus onset. The peak performance of the difference decoder at frame 3 (200ms after stimulus onset) is after about 90% of responses have already been initiated, but fewer than 10% of responses have been completed (Figure 5.2c), so for most trials this is during the action execution. Therefore it seems that the combination of the stimulus and action information is best predicted by the difference model around the critical time where the stimulus is seen and the choice is made; but after the choice is reported, the decoders that can capture steady-state activity are more accurate.

**Figure 5.2.** Stimulus decoding accuracy for different models aligned to stimulus onset. (a) Comparison of different decoding models. Each model is a logistic regression predicting the side of the stimulus for all trials in one session. For the three models using information from two frames as input, the x-axis position is the second of the two frames, so all models are aligned to the last frame they have access to. The lines are the mean cross-validated decoding accuracy across 52 sessions for 6 mice, with shaded standard deviation across sessions. All models perform above chance level (black line, shuffled stimulus side labels) immediately following stimulus onset. Black dotted line indicates animal performance. (b) Reaction time histogram, showing the number of trials (across all mice, all sessions) in which the mice initiated their movement in that time bin, bins are aligned to imaging frames. (c) Same as (b) but now showing the response time relative to stimulus onset, where each frame-aligned bin indicates the fraction of trials in which a response has been triggered, i.e. the wheel movement has crossed the threshold.
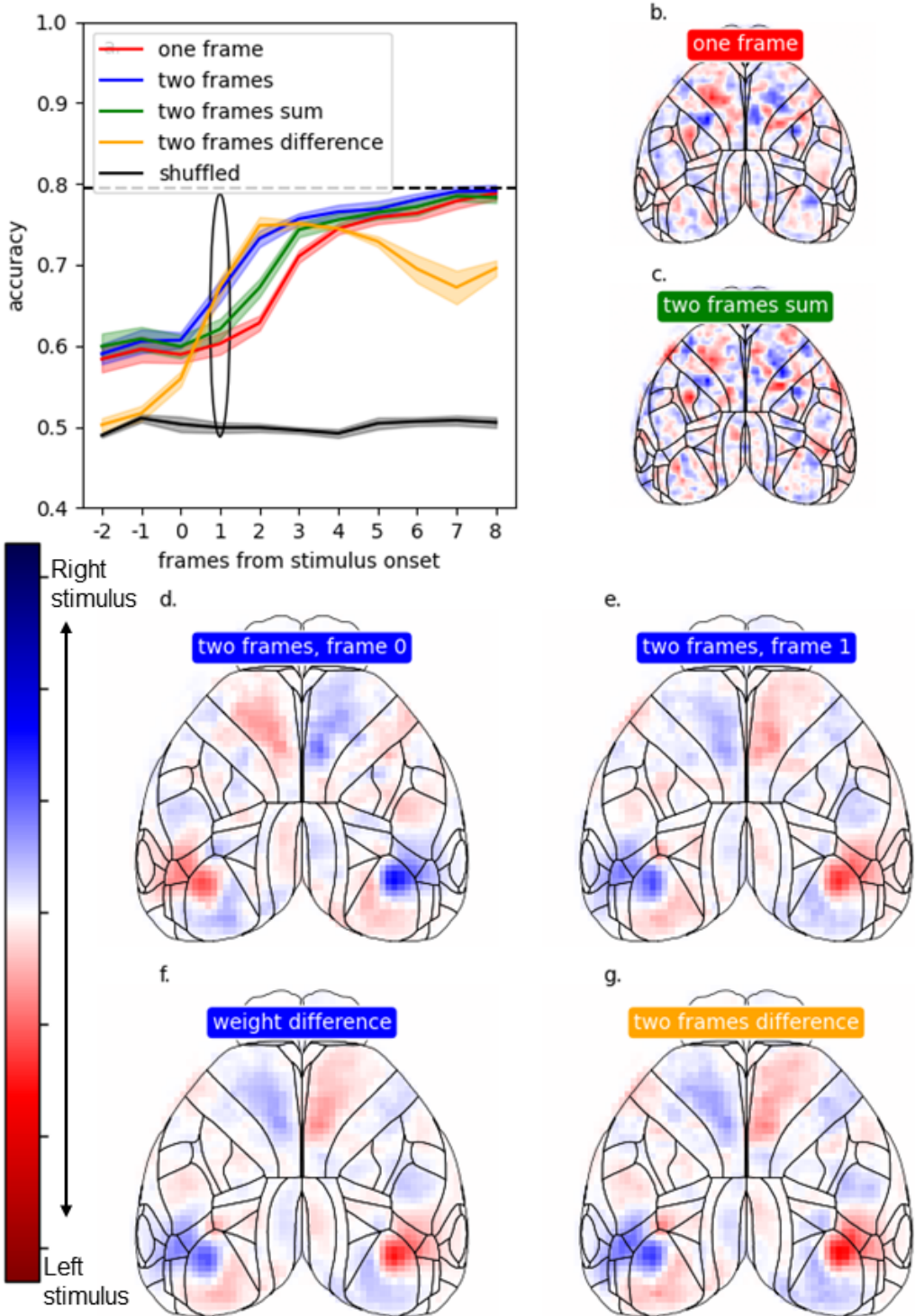
**5.5 Decoding stimulus side near stimulus onset is most accurate with a time derivative**

The main reason I used a logistic regression as opposed to a non-linear decoding method, was to have interpretable weights from the decoding. So I next wanted to visualize the weights for the different decoders to try to find what features in the data they learned, yielding some information about how the stimulus is represented across different time points in this task. To investigate the differences between the weights in the models at these different time points, I took the weights of the different models, and visualized them projected onto a map of the mouse dorsal cortex. Focusing first on the frame immediately after stimulus onset, in the decoding accuracy, the two frame and the difference models have the strongest performance, while the sum and the single frame models perform nearly the same as before stimulus onset (Figure 5.3a). When examining the weights on the two frames used by the two frame model, the strongest weights are localized to visual cortex (Figure 5.3d, e); moreover, they are localized in the expected receptive field for the stimuli used in this task (lower nasal visual field, so anterior lateral visual cortex, (Zhuang et al., 2017)). Surprisingly, the strong weights observed in visual cortex have opposite signs on the two different frames of the decoder. However, if the difference is taken between the weights on these two frames (Figure 5.3f), the pattern is nearly identical to the two frame difference model (Figure 5.3g). This shows that when given the flexibility of how to linearly combine the activity across two frames, the model learns to take the difference through time. This is strong evidence that the most informative form of the information in the widefield imaging data at the time of stimulus onset is its change over time. Also notably, these strong decoding weights in visual cortex are indicative of contralateral stimuli, with weights in the right visual cortex promoting the decoder choosing a left stimulus.
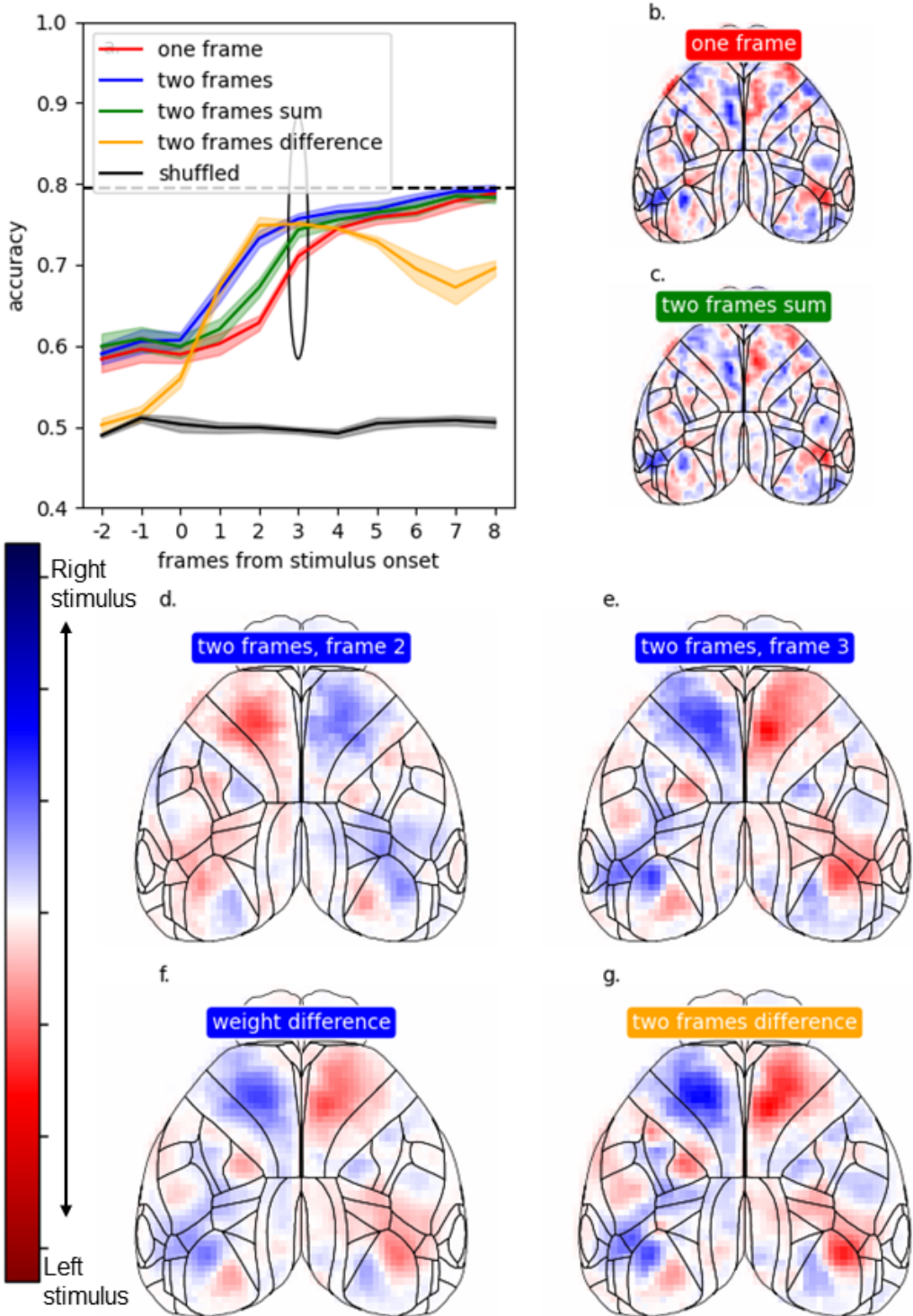
Next I focus on the third frame (200ms after stimulus onset), where the difference model is the most accurate (Figure 5.4a), and when most responses have been initiated but not yet completed (Figure 5.3 b,c). The one frame and sum models (Figures 5.4b and c) both perform above their prestimulus baseline at this time point, and appear to have strong weights for contralateral stimuli in the anterior visual cortex, the receptive field for our stimuli. However, there also seems to be strong weights distributed throughout the cortex, and these weights are for both contralateral and ipsilateral stimuli.

Comparing these weights to those of the best performing model (difference model, Figure 5.4g), the main similarities are the contralateral representation of the stimulus in anterior visual and in medial secondary motor cortex. The main features of the two best models that are missing or reduced in the one frame and sum models, are the larger extent of the contralateral representations and strong weights in M2 (Figure 5.4 f, g). Again, it appears the two frame model learns the same representation as the difference model, showing that this is the best way to combine activity across time to decode stimulus.
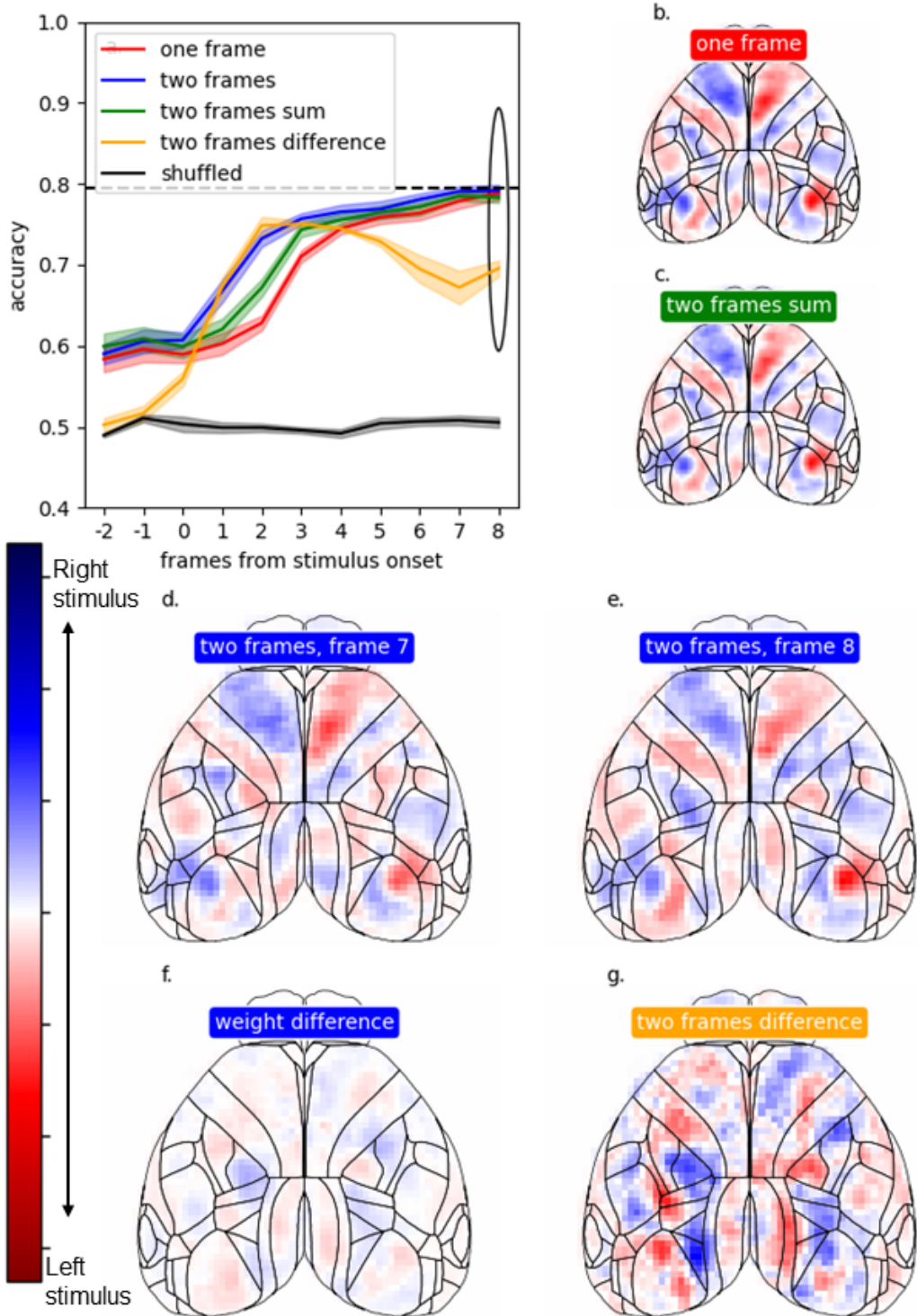
Finally, when comparing the performance of the different models well after the stimulus onset (~566 ms after stimulus onset, frame 8), the one frame model performs as well as the two frame model and better than the difference model, indicating that the change in activity across time does not seem to add any information about the stimulus at this late time point after a majority of the responses have already been made (Figure 5.5a). Furthermore, the weights in visual and motor cortex on the two frames of the two frame model are no longer opposite in sign, indicating that it has learned to combine activity through time in a way other than taking the difference (Figure 5.5 d, e).

**Figure 5.3**. Model decoding weights at frame 1. (a) Same as in Figure 5.2, except shading indicates s.e.m; the performance of the displayed frames is circled. (b) Decoding weights of the one frame model on frame 1, blue indicates that high activity in those pixels promotes the decoder predicting a right stimulus, red predicts left stimuli. (c) Weights for the two frame sum model. (d) Weights on frame 0 of the two frame model, this model has double the parameters and so is the combination of the weights shown in (d) and (e). (e) Weights on frame 1 for the two frame model. (f) The difference between the weights on frame 1 and frame 0 of the two frame model. (g) Weights of the two frame difference model.

**Figure 5.4**. Model decoding weights at frame 3. (a) Same as in Figure 5.4, the performance of the displayed frames is circled. (b) Decoding weights of the one frame model on frame 3, blue indicates that high activity in those pixels promotes the decoder predicting a right stimulus, red predicts left stimuli. (c) Weights for the two frame sum model. (d) Weights on frame 2 of the two frame model, this model has double the parameters and so is the combination of the weights shown in (d) and (e). (e) Weights on frame 3 for the two frame model. (f) The difference between the weights on frame 3 and frame 2 of the two frame model. (g) Weights of the two frame difference model.
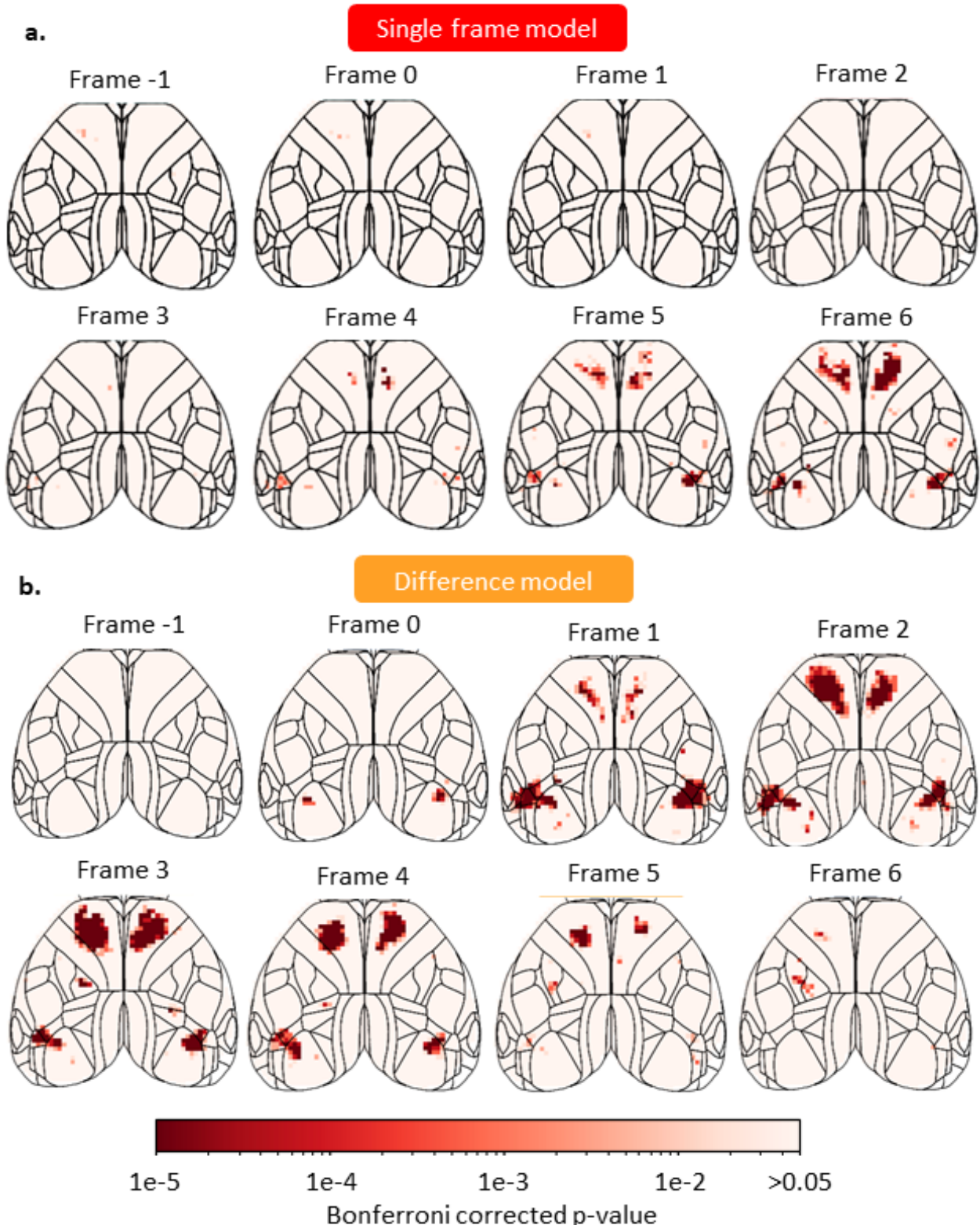
**Figure 5.5**. Model decoding weights at frame 8. (a) Same as in Figure 5.4, the performance of the displayed frames is circled. (b) Decoding weights of the one frame model on frame 8, blue indicates that high activity in those pixels promotes the decoder predicting a right stimulus, red predicts left stimuli. (c) Weights for the two frame sum model. (d) Weights on frame 7 of the two frame model, this model has double the parameters and so is the combination of the weights shown in (d) and (e). (e) Weights on frame 8 for the two frame model. (f) The difference between the weights on frame 8 and frame 7 of the two frame model. (g) Weights of the two frame difference model.

**5.6 Decoding weight signs for stimulus decoders are consistent in visual and motor cortex**

Though the mean weights for different decoders training on different sessions for each mouse appear to have similar weight distributions, I next wanted to test if the same locations consistently had weights that predicted the same stimulus side across sessions and mice. To answer this question, I trained the four decoding models as detailed above, then asked whether the sign of the weights of a given pixel was consistent across the decoders for all sessions and all mice. To do this, I took the decoding weights, one weight per session (n = 52), of a given pixel, binarized the weights such that they were either predicting right or left stimuli, and conducted a binomial test against the null hypothesis that the pixel's weight was randomly assigned to left or right stimuli. I did this for each pixel, again creating a map on the dorsal cortex, but this time the value for each pixel was the p-value with the Bonferroni correction for the number of pixels for the weights from a given model.
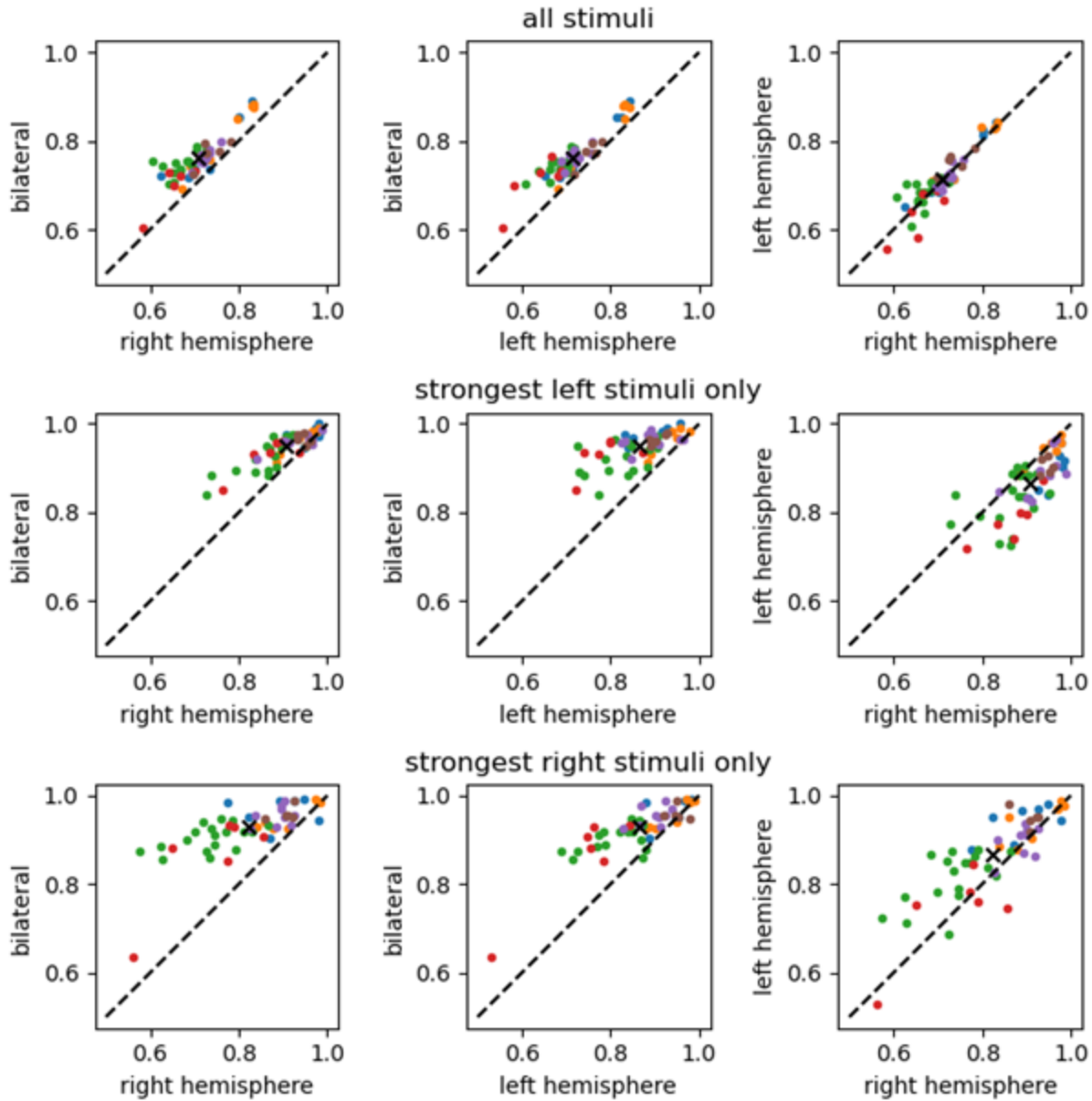
From this, I see that the decoding weights after stimulus onset are consistently predicting the same stimulus first in the visual cortex, then increasingly in M2, and finally in the limb primary somatosensory cortex (Figure 5.6b). The weights are more consistent across subjects in the difference model when that model performs best, in frames 1-4 relative to stimulus onset (Figure 5.6b), then the weights of the other models like the single frame model become more consistent as decoders trained on that activity become more accurate (Figure 5.6a).

**Figure 5.6**. Maps of significantly consistent decoding weights for two models through time. Bonferroni corrected p-value of the sign of decoding weights calculated using a binomial test across 52 sessions from six mice for the one frame model (a) and the difference model (b). Red color indicates the weights at that pixel consistently predicts a single stimulus side across sessions.

**5.7 Activity from both hemispheres is required for strong decoding performance**
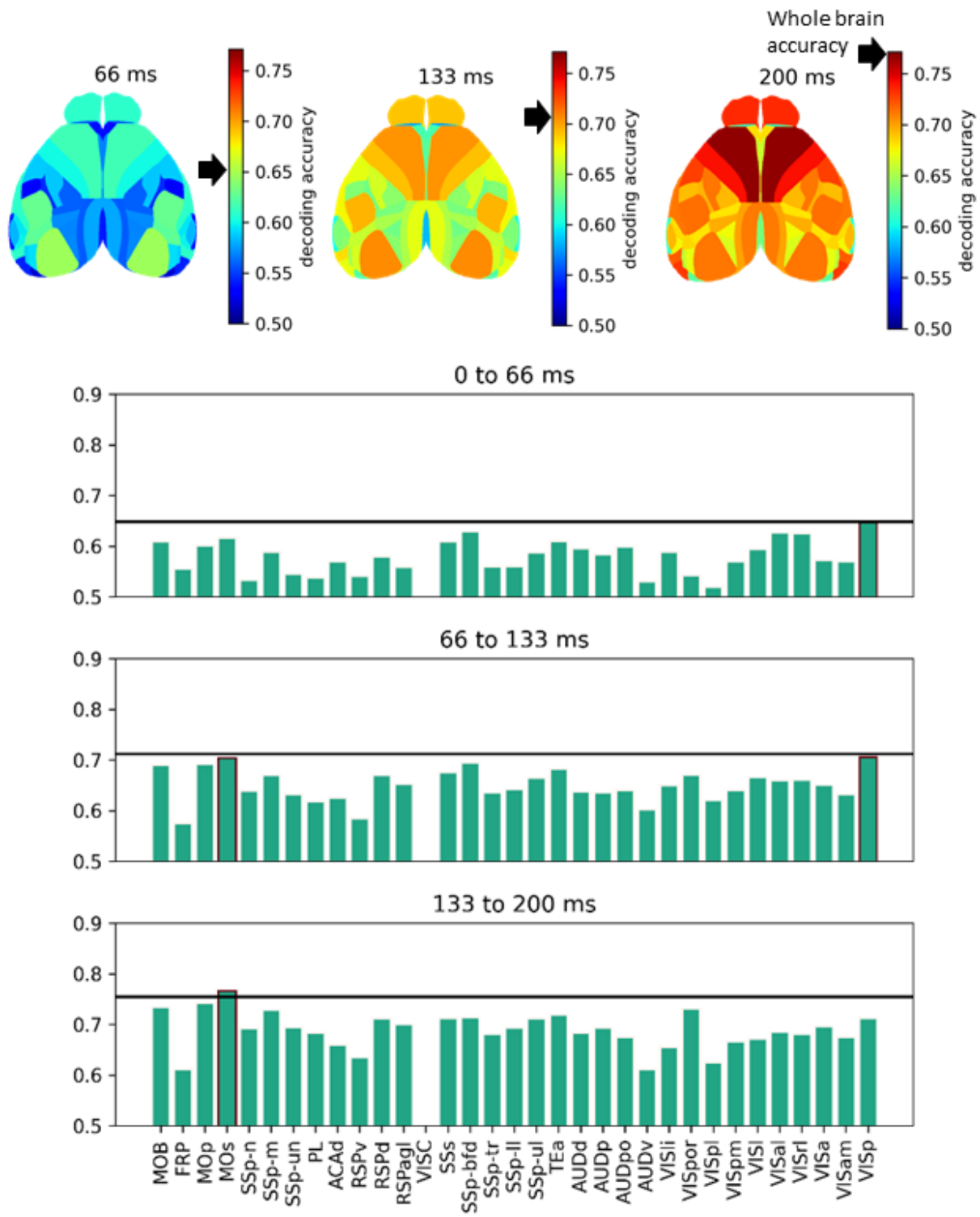
One finding from investigating the stimulus decoding models is that models with strong decoding performance always had weights of opposite signs on opposite hemispheres for the areas most heavily involved in decoding, especially visual cortex and M2. This could indicate that either each hemisphere is required for predicting only if a contralateral stimulus is present, or that both hemispheres are used in decoding all stimuli, and the difference is taken between those two hemispheres. To test which of these was true, we attempted decoding using only pixels from one hemisphere, or from both hemispheres, to directly compare which gave a better prediction accuracy. Bilateral decoding is consistently more accurate than decoding with just one hemisphere (Figure 5.7, first two columns). This is true even when comparing only trials with the strongest stimuli (100% contrast) contralateral to the single hemisphere, where the stimulus is unambiguous (Figure 5.7, bottom two rows). As expected, there is also an increase in accuracy for decoding high contrast contralateral stimuli when comparing accuracy for just the right versus just the left hemisphere, but  on average the hemispheres perform equivalently when comparing performance on all contrasts (Figure 5.7, third column). Because there is increased decoding accuracy for bilateral decoding over unilateral decoding, even when only comparing the strongest stimuli on the contralateral hemisphere, this indicates that the difference between the hemispheres is more informative than the representation of contralateral stimuli alone. Because the hemisphere comparison is more informative, this also suggests that the mice may use a behavioral strategy of comparing the information gathered by the two hemispheres.

**Figure 5.7.** Bilateral decoding accuracy is better than unilateral decoding accuracy. Scatter plots of accuracy for decoding stimulus side from both hemispheres versus right hemisphere (left column) both versus left hemisphere (middle column) or right hemisphere versus left hemisphere (right column). First row is decoding accuracy for all stimuli, middle row for only the 100% contrast left stimuli, bottom row for only the 100% contrast right stimuli. Each dot is for one session, each color is for one animal. Decoder used here is the difference model trained on the difference of frames 3 and 2 after stimulus onset.

**5.8 Task information is localized to V1 and M2 but broadcast broadly**

Up to this point I have only shown decoding the stimulus location from activity across the whole dorsal cortex. However, decades of neuroscience research has pointed to the localization of specific neural information to specific cortical regions. In contrast, some recent work using widefield imaging has indicated that some neural signals are actually widely distributed across the whole cortex (Musall et al., 2019). To see where along this localized-distributed spectrum the stimulus information in this task lies, we performed logistic regression decoding of stimulus location as previously described using the two frame model seen in Figure 5.3a with frames ranging from immediately following stimulus onset, (66ms) to 3 frames after (200ms). In comparison to the decoding we previously performed with all pixels from the dorsal cortex, we now performed this decoding only using activity from one dorsal cortical area (bilaterally) alone. This analysis revealed that just after stimulus onset, V1 performed at the accuracy of the whole cortex ($p > 0.05$, bonferroni corrected t-test), and all other areas performed below this level (Figure 5.8 a,d). One frame forward, V1 and M2 both perform as accurately as decoding with the whole cortex ($p > 0.05$, bonferroni corrected, Figure 5.8 b,e), and at the peak performance of the whole brain decoder using two frames, using M2 alone performs at the same level as the whole cortex ($p > 0.05$, bonferroni corrected, Figure 5.8 c,f). Though individual areas do perform as well as the whole cortex at decoding the stimulus side, there is also indication that information is distributed, as each cortical area performs above chance at decoding the stimulus side ($p < 0.05$, bonferroni corrected), and most not far below the best area.
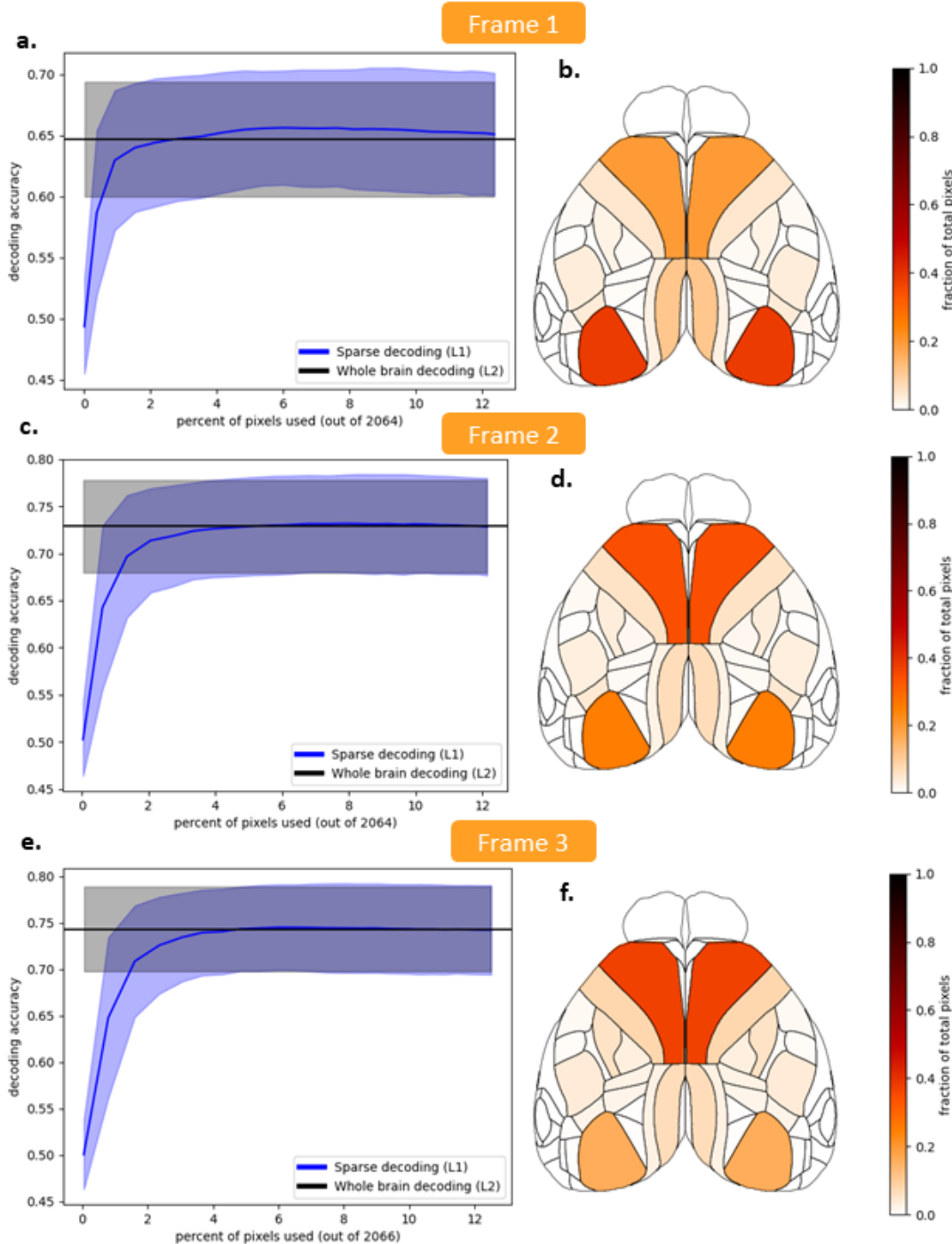
**Figure 5.8.** Stimulus decoding accuracy of individual cortical areas using the difference model. (top) Maps of decoding accuracy for each cortical area where the color indicates the decoding accuracy for that area on that frame relative to stimulus onset. Whole brain decoding accuracy for that time is indicated by the black arrow on the colormap. (bottom) Same data as top, represented as a bar plot. Bars outlined in red indicate that area is not statistically different from whole brain decoding (p > 0.05, bonferroni corrected for n=34 areas). All areas have significantly above chance decoding at that same level.

**5.9 Sparse decoders perform as well as decoding from all cortical pixels**

To further investigate the extent to which information is localized or distributed, I compared the decoding performance from using the entire cortex against just choosing select pixels that encode relevant information. I hypothesized that there existed a very sparse set of pixels that were able to yield performance at the same level as using all pixels from the whole cortex, and that these sparsely chosen pixels would mostly come from the areas with the strongest predictive power for stimulus identity. This seems plausible as widefield imaging data is relatively low dimensional, with a majority of the variance being captured by just a few components in PCA. This is mainly due to the high correlation of activity across the whole dorsal cortex (Shimaoka et al., 2019).

To test how many pixels are required for accurate decoding of the stimulus side, I first performed an L2 regularized decoding of the stimulus side using the difference model described above for frames 1, 2, and 3 for whole cortex decoding. I then repeated the same decoding, except this time used an L1 regularization with a range of levels of regularization. I then obtained the number of pixels used by decoders (number of non-zero parameters) with each level of regularization, as well as the accuracy of each of the decoders, and plotted the accuracy against the number of pixels used to obtain that accuracy.
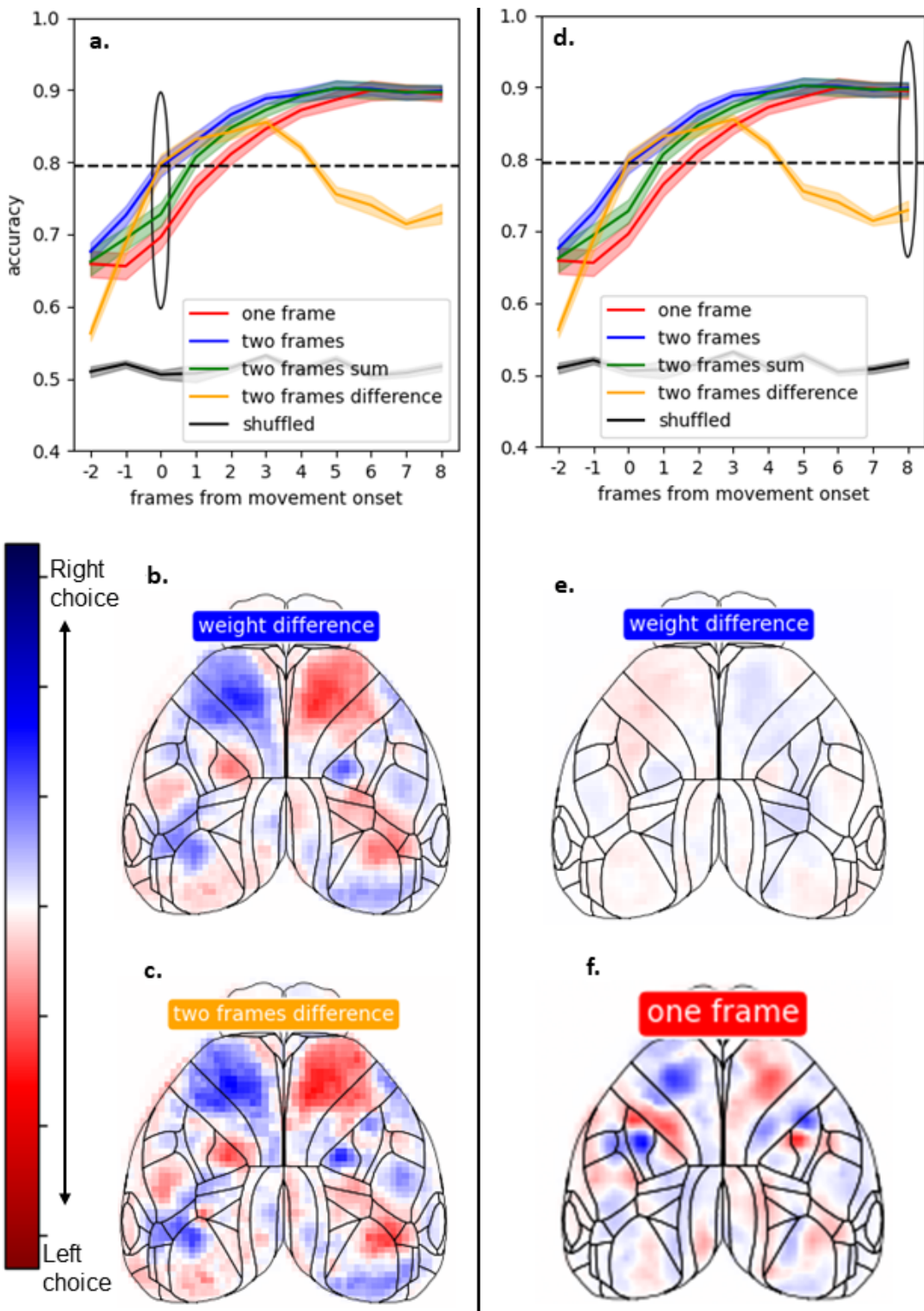
Using this analysis, I can obtain strong decoding performance with a very small percentage of the total available pixels (Figure 5.9 a, c, e). With only about 2-4% of the total pixels across the dorsal cortex, I can obtain a similar accuracy to decoding using all pixels in the dorsal cortex. This is an even sparser representation than was seen in Figure 5.8, as V1 contains ~9% and M2 ~13% of cortical pixels. To see which areas pixels are chosen from most often in the L1 decoding, for each session I took the decoder that used the fewest number of parameters that had prediction accuracy greater than or equal to the model using all pixels with the L2 decoder. I then mapped what fraction of the total decoding pixels used on that frame with the L1 decoder were in each cortical area. These results largely agreed with those in Figure 5.8, as initially most pixels come from V1 and secondarily from M2 (Figure 5.9b). After that, progressively more pixels are chosen from M2.

**Figure 5.9.** Sparse decoding performs as well as whole brain decoding with few pixels. (a) Stimulus decoding accuracy using an L1 regularization to sparsely choose pixels for decoding 1 frame following stimulus onset, different levels of regularization were used to decode with different numbers of pixels. Blue line is the mean decoding accuracy of the stimulus with this sparse representation plotted against the percent of pixels used for decoding. Black line is the mean accuracy with an L2 regularized decoding that uses all cortical pixels as used in previous figures. Shaded regions are the standard deviation across decoding for 52 sessions. (b) Map with color indicating the fraction of total pixels located in a given cortical area used by the first L1 decoder with accuracy greater than or equal to whole brain decoding. (c, e) Same as (a) for frames 2 and 3 after stimulus onset. (d, e) Same as (b) for frames 2 and 3.

**5.10 Logistic regression to decode action**

Finally, though predictions of the stimulus side should be highly correlated with the action, I wanted to assess how well I could decode the mouse's action, and to compare the weights of this decoding to those of stimulus decoding. To perform action decoding, I ran the four model comparison analysis presented in section 5.4, with the only differences being that the frames were now aligned to the onset of the wheel movement, and the model was now predicting the action of the mouse as opposed to the stimulus side. In comparison, the decoding of the action from the whole cortex was much more accurate than decoding of the stimulus side, especially after movement onset (Figure 5.10 a,d). This is to be expected, as the mouse should have full knowledge of its own choice before it is made, and certainly after it is made. Theoretically if we have enough data to fit the model, and the cortex contains a complete, linear representation of choice, the decoding should be 100% accurate. On the last frame just before the movement is initiated, when the decision is about to be made (frame 0, Figure 5.10a), the best performing models, like for the stimulus, are the difference and the two frame models. Again we see that the two frame model is learning to take the difference between the two frames in V1 and M2, but additionally it seems as if the time derivative is informative in the hind paw somatosensory region (Figure 5.10 d-g). After movement onset, where the decoders peak in their accuracy, the two frame model no longer is calculating the time derivative (Figure 5.10e), and instead the most informative weights, as seen in the one frame model, are in M2, M1, but most strongly in the forepaw somatosensory area (Figure 5.10f). It seems at this time point after a vast majority of the responses have been triggered the visual cortex no longer contributes to decoding of the action.

**Figure 5.10.** Action decoding is similar to stimulus, with higher accuracy and stronger decoding weights in somato-motor cortex. (a,d) Decoding model comparison as in Figure 5.3, except predicting the stimulus side and aligned to motor onset with focus on frame 0 (a) and frame 8 (d) relative to movement onset. (b) Decoding weight difference for the two frame model for frames 0 and -1. (c) Decoding weights for the difference model for frame 0. (e) same as (b) but for frame 8. (f) Decoding weights for the one frame model at frame 8.

**5.11 Discussion**

      With widefield whole dorsal cortex calcium imaging in the IBL task, I have shown that the best linear decoder for the stimulus or action around decision time takes the time derivative of the calcium activity, and also the difference between the two hemispheres in V1 and M2. Initially after stimulus onset, V1 is the most consistently and strongly predictive of the stimulus side, and all of the information that the cortex has access to is in V1. Following this, as the stimulus information becomes binarized into a choice and motor output, M2 becomes more predictive of the stimulus, containing all the information that the cortex has access to. This localization of information is further emphasized by seeing that a sparse decoder predominantly chooses pixels from V1 and M2, and can predict the stimulus side with as few as 2% of the total pixels in the cortex. However at the same time, the stimulus and action information is widely distributed, as activity in nearly all cortical regions had significant decoding of the stimulus side throughout the decision process.

      One initially surprising finding from these decoding results was that the best whole brain decoder around stimulus or action onset takes a time derivative. It is unclear, however, if this is reflective of the actual best way to predict the stimulus from the cortical neural activity or if this is only true when looking at population-level calcium signals. Calcium fluorescence from Gcamp6s already represents an integration of neural excitation (Pnevmatikakis et al., 2016), therefore taking a time derivative of this signal could be reconstructing a more realistic representation of the population spiking activity. Additionally, this time derivative could simply be acting as some sort of baseline correction. By subtracting off the activity of a previous frame, slower scale global fluctuations unrelated to the task would be removed, potentially leaving a more relevant signal. This is not always true, however, as the difference model is at chance accuracy before the stimulus onset, and worse than a single frame model after the decision has been made, which at least indicates that this time derivative is not artifactually always the best model. This also points to the possibility that performing such a baseline correction could obscure important neural information. The question of if this strong performance with the time derivative arises from population activity or from calcium imaging however, can likely be addressed with other IBL

datasets. The IBL neuropixels recordings can be used at population level to determine if the time difference is informative, and the upcoming mesoscope single cell calcium imaging could be used to determine if this is only a reflection of using calcium signals.

To my knowledge, it is a novel finding that there is an improvement in decoding task information from population activity in a lateralized task such as this when comparing activity across hemispheres as opposed to only using information from one hemisphere. It is unsurprising that this is the case, if this is considered in the framework of signal detection theory, from which two alternative forced-choice tasks arise (Fred Rieke et al., 1999; Green and Swets, 1966). In SDT the optimal decoding of a stimulus requires comparing a signal distribution to the noise distribution. In a lateralized task such as this, the signal distribution can be thought of as the activity in contralateral cortical areas, and the noise as ongoing activity unrelated to the stimulus in ipsilateral areas. Given this, it is unsurprising that there is stronger performance, even on the easiest trials, when comparing activity across the hemispheres, and this result can be seen as a validation of this model. In addition to this, it has been reported that homologous cortical areas on opposite hemispheres have largely shared resting state, task-independent neural variability (Shimaoka et al., 2019). Subtracting such shared variance would further enhance the signal-to-noise ratio of cortical information, improving decoding performance.

The results of decoding from single areas in the cortex are at once reassuring and surprising. It is reassuring to see that the areas with the most task-relevant information here are in V1 where the visual information is believed to enter the cortical network, and in M2, often associated with decision-making functions. It is surprising however, that all brain areas have some information about the task, as they all have above-chance decoding of the stimulus side. Previous work has shown that some signals are available across all of cortex, particularly the presence or preparation of movement (Musall et al., 2019; Steinmetz et al., 2019; Zatka-Haas et al., 2021), but this information was not previously seen to be predictive of stimulus or choice. This widespread presence of task information indicates that this information is broadcast widely across the cortex, but that when received by the most task-relevant areas, the signal is more reliable and information-rich.

If interpreted in the light of information routing in the cortex, it seems clear that this result is inconsistent with the small-world, shortest-path model for information routing, where information is directly passed along the shortest route from one area to the next (Avena-Koenigsberger et al., 2019; Hu et al., 2011; Kleinberg, 2000). On the other end of the routing spectrum, one can think of information simply diffusing across a network depending on the strength of the connectivity between nodes (Masuda et al., 2017). However, more efficient routing seems to be possible using a middle ground where information is selectively sent to areas with high node connectivity, which then can distribute that information to other nodes that are more sparsely connected (Avena-Koenigsberger et al., 2019; van den Heuvel et al., 2012). This model would be consistent with the data presented here, where it seems that some highly connected node is distributing task information across the cortex. This however highlights the other half of the routing problem, that information not only needs to be sent, but must also be received by the appropriate areas. The data presented here is consistent with a hypothesis that there is another, potentially independent process from the sending of information that allows it to be amplified in the areas that require this information (in this task visual cortex and M2), such as attention (Noudoost and Moore, 2011), or an expectation or prior belief of what will happen in the future (Doya et al., 2006).

The inhibition results presented in Chapter 3 are consistent with the model that all cortical areas have information about the stimulus side, but only V1 and M2 make use of that information. Choice biasing and reaction time modulation were restricted to inhibition of targets in the visual and motor cortices not, for example, in the paw somatosensory cortex. This further indicates that the information present outside of the areas with the strongest predictive power have some sort of redundant task information, or some information correlated with the stimulus, that is not causal for the behavior.

# 6     Decoding the bayesian prior from widefield imaging

Contribution note: The work in the following chapter was conceived of, and planned by myself and Tony Zador. I performed all of the experiments and built required hardware for these experiments. Analysis was done in collaboration with Tony Zador and Alex Pouget.

## 6.1 Introduction

Decision-making critically includes combining current sensory evidence with past experience to create a motor output. In the application of Bayes' Theorem to perception, this past experience is known as a prior. There is strong evidence that the brain acts as a bayesian machine, combining current evidence with past experience to create a posterior according to Bayes' theorem (Beck et al., 2008; Dayan et al., 1995; Doya et al., 2006; Kersten et al., 2004; Knill and Pouget, 2004; Körding and Wolpert, 2004; Moreno-Bote et al., 2011). Such integration of prior knowledge and current information allows for increased efficiency and accuracy, especially in the case of noisy sensory information from a population of noisy neurons (Beck et al., 2008; Dayan et al., 1995; Ma et al., 2006). This is clear in the behavior of mice performing the IBL task, as there is a larger biasing of the behavior towards the more likely stimulus side for ambiguous stimuli than for clear stimuli (The International Brain Laboratory et al., 2021). Such a behavioral shift as seen in the IBL behavior could be seen in two different frameworks, each with different predictions of what the neural representation should be.

One model which could explain this behavioral biasing is the predictive coding model of cortex (Rao and Ballard, 1999). Predictive coding states that the cortex represents stimuli by constantly predicting what it thinks will happen, and then signaling the mismatch (prediction error) between the prediction and the actual stimulus (Kok and de Lange, 2015). There is strong evidence for this model that single cells in sensory cortex can encode both prediction and prediction error (Bastos et al., 2012), and that blood oxygen level dependent (BOLD) signals in human V1 are consistent with several predictions of this model (Aitken et al., 2020; Kok et al., 2013; Kok and de Lange, 2015). This model applied to the IBL task would predict that before stimulus onset, a prediction of the most likely stimulus should be present in visual cortex, causing an increase in neural activity in contralateral visual cortex when compared to activity predicting the less likely stimulus. After stimulus onset, predictive coding says there should be a

lesser amount of activity for the expected stimulus than the surprising stimulus, as the surprising stimulus should elicit a large prediction error signal. This model also implies that the predictions are sent from higher order areas down to the primary sensory cortex, where the prediction and prediction error should be most strongly represented.

Another cognitive model that could explain the behavioral impact of the biased blocks on IBL mice is the gain-modulation hypothesis of spatial visual attention (Desimone and Duncan, 1995; Fazekas and Nanay, 2021; Maunsell and Treue, 2006; Reynolds and Heeger, 2009; Williford and Maunsell, 2006). This model claims that the population response to stimuli is modulated by attention by increasing the activity for stimuli in the field of attention, decreasing the activity for stimuli in the competing suppressive field, and performing a divisive normalization of the attended by the suppressed fields. This theory predicts that there should be a larger increase in activity for the expected, (attended) stimulus location after the stimulus onset, but does not explicitly make a prediction about the activity before stimulus onset. This model uses divisive normalization as the proposed mechanism, which could be from feed-forward, feed-back, or local connections, and so could be found in any cortical area, but is predicted to exist at all levels of processing, and to accumulate as the signal ascends the hierarchy (Reynolds and Heeger, 2009).

Given these two possible models for the improvement of behavioral performance due to expectation, how and where this representation of the prior knowledge is present in the cortex remains unclear. Here I use the biased blocks in the IBL visual decision-making task to find which cortical areas in the mice represent a bayesian stimulus prior, and how they represent it. I find that the same areas that encode the stimulus, V1 and M2, have a strong representation of the stimulus prior, along with the paw and trunk somatosensory cortices. The prior representation in V1 and M2 seems to be a surprising neural basis, which involves a selective depression of the areas that respond to the expected stimulus before the stimulus onset, and an enhancement in activity in these same areas following stimulus onset. The representation in the somatosensory cortex likely is a reflection of the altered body positioning that is correlated with the prior.

**6.2 Materials and methods**

All experimental materials and methods were the same as in chapter 5 as this is a new analysis of the same dataset.

*Identification of V1 and M2 activity hotspots*

To identify the hotspots of activity in V1 and M2, the mean response 3 frames after the onset of a 100% contrast stimulus contralateral to a given hemisphere was visualized. From this, I manually selected the pixels corresponding to the highest response in each of V1 and M2, which are approximately indicated in Figure 6.1 with circles. These are only approximations as each animal had a hotspot selected separately. These differences between animals in hotspots are believed to be from differences in headplate positioning, resulting in a different retinotopic area of visual cortex being activated for the same stimulus in different mice.

*Peri-stimulus time histograms (PSTHs)*

PSTHs for each identified hotspot were created by first taking the mean of the df/f activity within the hotspot across all trials for either the left or right block, for 20 frames before through 20 frames after stimulus onset (total of 2.66s). This mean of all pixels in each hotspot for each animal for each session was taken as a single sample. There were 80% more trials of stimuli of one side than the other in each block, so the trials were downsampled such that there were an equal number of positive as negative signed contrasts, ie in each plot there are the same number of trials for 100% contrast stimuli on the right side as 100% contrast on the left side, for each contrast. A t-test was then performed on each of the 40 time points in this PSTH, comparing the activity of trials where the block was contralateral to the hemisphere of the hotspot to the activity on trials where the block was ipsilateral to the hemisphere of the hotspot. Therefore the test pooled left V1 right block, and right V1 left block, to compare against the activity of left V1 left block and right V1 right block. To plot the PSTH, the mean was taken across each block-hemisphere pair for all sub-sampled trials.

*Logistic regression to decode block side on zero contrast trials*

Decoding of task variables was performed using logistic regression as implemented in scikit-learn (Pedregosa et al., 2011); the equation can be found in the methods section of Chapter 5. The input to the logistic regression was stimulus-aligned df/f of shape $n_{trials}$ by $n_{pixels}$, and was z-scored pixel wise separately for train and test data, with all non-brain pixels set to 0. Additionally all trials where no response was made were always dropped from analysis. The models were trained to predict the block identity. An l2 penalty was used as regularization, the amount of regularization used was determined using 5-fold cross-validation with the built-in function $LogisticRegressionCV$ with regularization values in the range of 0.02 to 5. The "class-weight" argument was set to "balanced," this automatically adjusts weights of the decoder inversely proportional to the class frequencies, which allows the model to be trained with uneven class frequencies while maintaining a chance prediction level of 0.5 instead of the frequency of the most abundant class. Training was performed using z-scored df/f from trials of all contrasts except for the zero contrast trials, and reported results are for the held-out zero-contrast trials, whose neural activity is z-scored separately from the training data. To limit noise from animal-to-animal and day-to-day variability, a separate model was trained for each recording session and each frame relative to stimulus onset.

*Pseudosession null distribution*

To generate a more stringent and accurate null distribution for blocks other than fully shuffled block identity, the pseudosession method was used (Harris, 2021). The problem with using a shuffled block identity as the null distribution, is that the block identity is a variable that changes relatively slowly through time (20-100 trials). This could yield nonsense correlations, or correlations between other slowly drifting signals that are present in neural recordings and behavioral sessions. To control for this, a null distribution is generated by making 1000 "pseudosessions" or new sessions of the same length as the true sessions, with block identities for each trial assigned using the same parameters as were used to generate the blocks in the true session. Decoding performance on these pseudosessions provides a more realistic

null distribution of the decoding of the block. Comparing the decoding accuracy on test data to the accuracy on each of these pseudosessions yields a p-value equal to the proportion of pseudosessions that outperform decoding on the true session. With an alpha value of 0.05, if the decoding on the true session is above the 95th percentile of the pseudosessions, it is considered above chance decoding accuracy.

*Sparse decoding to find the most informative pixels*

To determine the location of the most informative pixels for decoding, I used a logistic regression decoder as detailed above, except using an L1 regularization as opposed to L2. L1 regularization forces sparsity on weights, driving many weights to be 0, and only selecting the most informative features (Ng, 2004). To perform this decoding I trained a separate decoder for each session, and for L1 regularization coefficients from the set [0.02, 0.05, 0.1, 0.25, 0.5, 1, 1.5, 2, 5, 10]. For each decoder I then determined the number of non-zero coefficients, or the number of pixels used by that decoder, and which cortical areas those non-zero coefficients came from. To visualize the fraction of pixels that were chosen from each cortical area, for each session I took the first decoder that performed at or above the accuracy of an L2 decoder for that same session with the same 5-fold cross-validation splits, and located which cortical area the pixels were in. I then summed up all of the pixels in a given area from the selected decoder for each session, and normalized this by the total number of pixels used by all selected decoders to obtain the fraction of decoding pixels in an area. For the plots normalizing the number of pixels by the size of a cortical area, I used the same pixels from the selected decoders, but this time took the mean number of pixels located in each area across sessions. I then divided this by the number of pixels each cortical area contained, to get the fraction of pixels in an area that were used by that decoder.


**6.3 Mouse prior has opposite representation before and after stimulus onset**
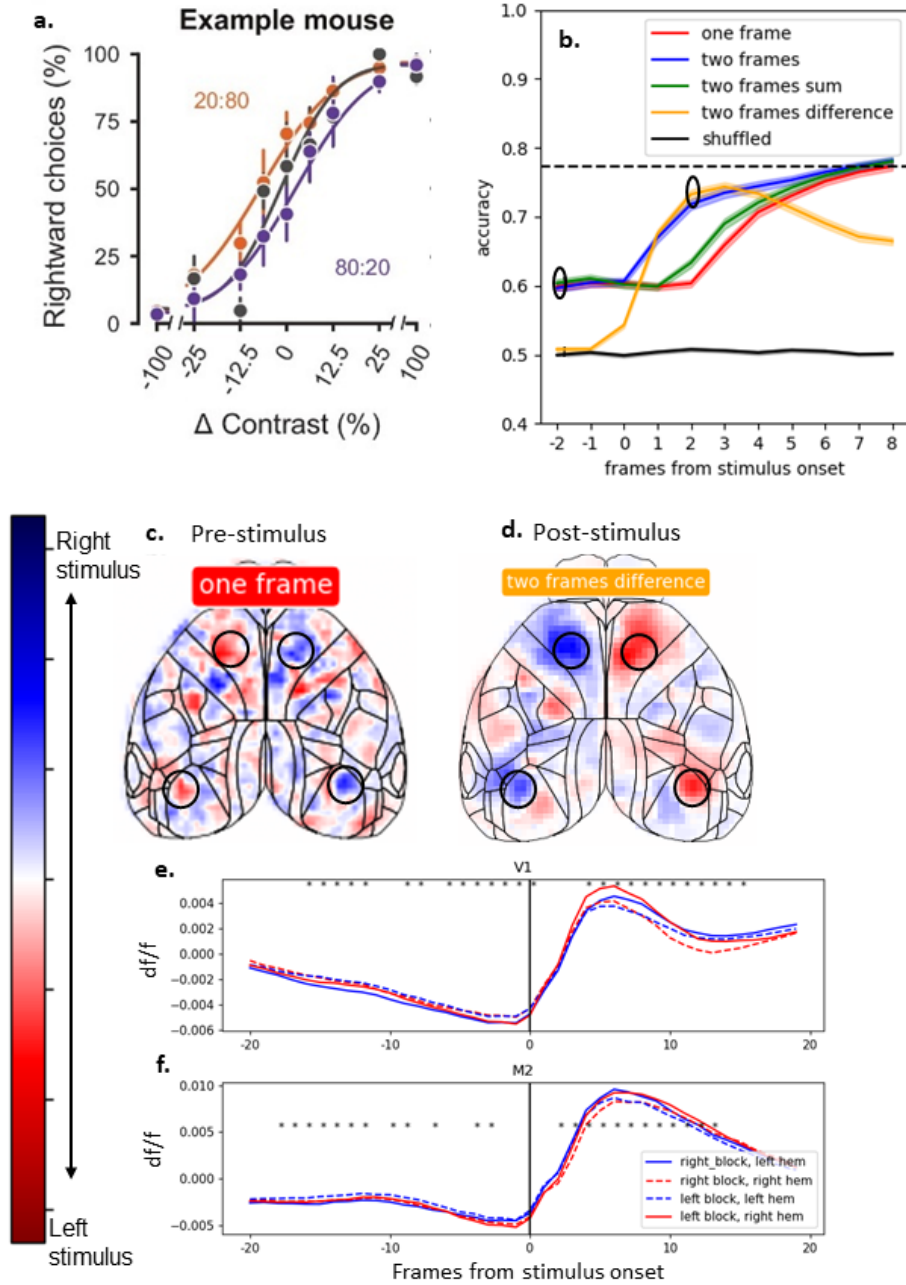
Though animals are constantly using prior information to guide their decisions, to experimentally manipulate the prior, the IBL task contains blocks of trials where the stimulus prior varies. While the mice are performing their visual decision-making task, the probability that the stimulus will come from a given side varies in blocks of 20-100 trials long where the stimulus is on one side of the screen for 80% of trials,

and on the other side for the remaining 20% of trials (see Chapter 1 for details). These are referred to as biased blocks or the stimulus prior. It is clear that the mice learn to use this information to guide their behavior, as when you plot separate psychometric curves for the different block identities, there is a vertical shift between the two curves (Figure 6.1a). Additionally, when mice are introduced to this block prior, their strategy shifts to weigh trial history more in their decision-making process than before the introduction of the block prior (The International Brain Laboratory et al., 2021). The information about this biasing also seems to be present in the neural activity from the widefield imaging before the onset of the stimulus, as there is above chance decoding of the stimulus identity before any stimulus appears on the screen (Figure 6.1b).

To investigate what cortical neural patterns this stimulus prior decoding uses, I visualized the mean decoding weights of a model that has strong stimulus decoding before the stimulus onset (the one frame model at frame -2, mean weights across 52 sessions, Figure 6.1c), and compared those to a model with strong stimulus decoding accuracy after the stimulus onset (the difference model from Chapter 5, at frame +2, Figure 6.1d). Surprisingly, the weights in areas previously identified as important for task-related events, V1 and M2, had the opposite sign between pre-stimulus and post-stimulus decoding. The weights of the post-stimulus decoder are as expected, showing a contralateral representation, with stronger weights in the blue direction indicating a right stimulus and located mostly in the left hemisphere. However the opposite seems to be true in the pre-stimulus decoding weights. This inverted representation could mean one of two things: an ipsilateral representation of stimulus where higher activity in the prestimulus period in V1 or M2 hotspots increases the likelihood of an ipsilateral choice, or this could be representative of increased suppression, where there is stronger suppression of contralateral stimuli before the stimulus onset, that is reversed to stronger activation after stimulus onset.

To determine which of these two possibilities is true, I plotted PSTHs for the mean activity of each of 4 identified hotspots, one in each hemisphere for V1 and M2. Critically, to ensure that the signals in this PSTH are not simply reflective of the higher frequency of a given stimulus due to the induced stimulus prior, the trials were sub-sampled such that there were the same number of contrasts for stimuli

on each side for each block condition. From these PSTHs, it can clearly be seen that there is general suppression of activity in both V1 and M2 leading up to stimulus onset (Figure 6.1e, f). In fact across the whole dorsal cortex there seems to be general suppression of activity before the onset of the stimulus (data not shown), this is likely due to a combination of the minimum of 200ms in which the mouse must hold the wheel still to initiate a new trial, and the fact that the baseline fluorescence was calculated across the whole session, so this period of stillness is likely the nadir of activity and thus fluorescence. Within this general suppression of activity however, there seems to be a small but significant difference between the level of suppression in the hotspots contralateral to a high stimulus prior versus ipsilateral to a high stimulus prior. It seems the inverted weights of the pre-stimulus decoder relative to the post-stimulus decoder are making use of an increased suppression before the stimulus onset of the hemisphere contralateral to the expected upcoming stimulus (Figure 6.1 e,f). This is statistically significant ($p < 0.05$, t-test) for many prestimulus time points before stimulus onset, particularly for the V1 hotspot, and to a lesser extent in the M2 hotspot. Interestingly, even though these PSTHs are for the same contrasts for the two different blocks, there is also a statistically significant increase in post-stimulus activity for contralateral blocks compared to ipsilateral blocks (Figure 6.1 e,f). It seems there is a two-fold representation of the prior, an increased suppression of the hemisphere contralateral to the expected side of stimulus onset, followed by an increased activation of that same hemisphere after stimulus onset.
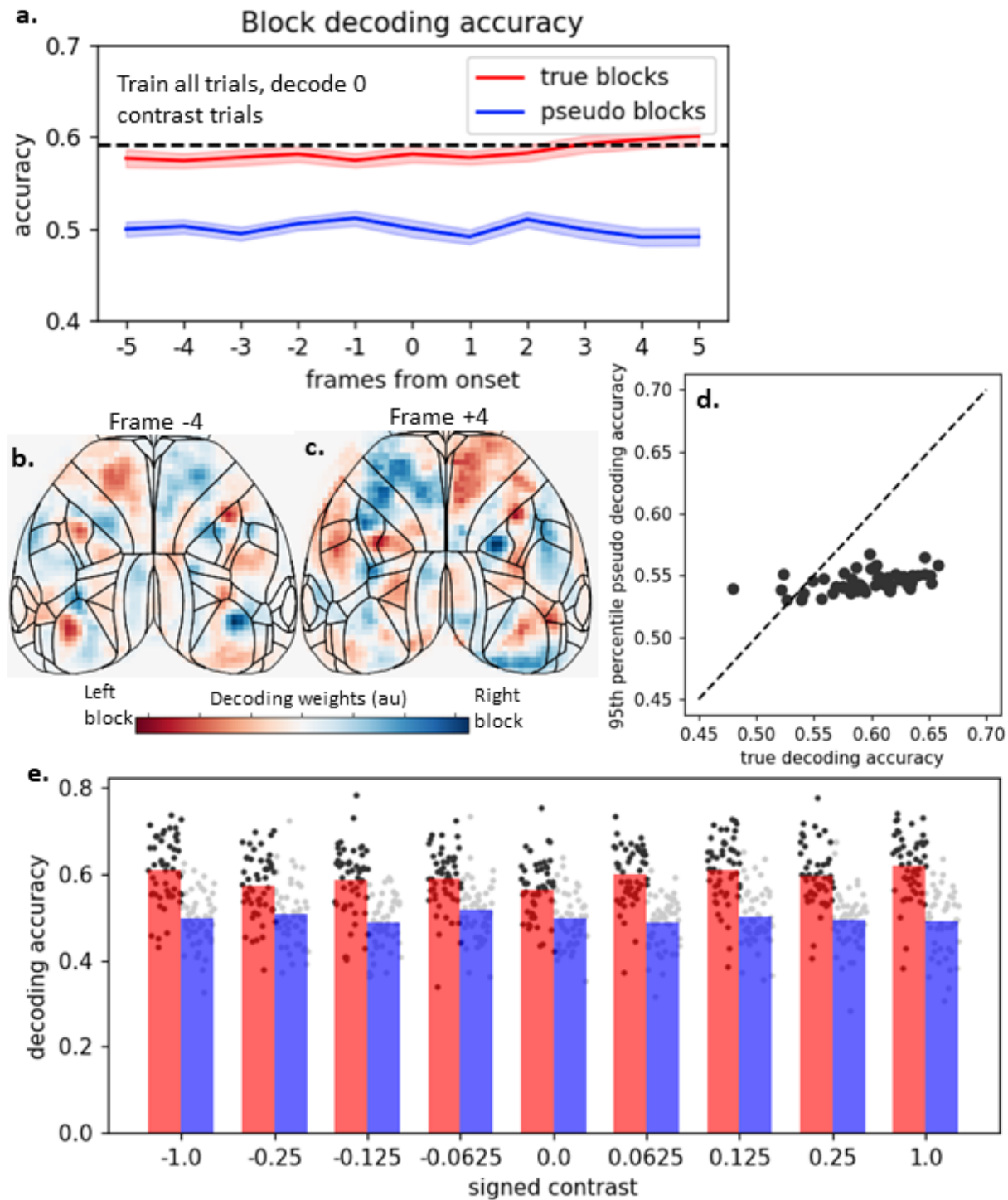
**Figure 6.1.** Mouse prior is represented as a prestimulus inhibition, and post stimulus excitation of stimulus encoding areas contralateral to the induced prior. (a) Example session of mouse biasing due to the block structure, indicating that the mice use the stimulus prior to influence their behavior. (b) Decoding of the stimulus identity as seen in Chapter 5, showing above chance prestimulus decoding of the stimulus identity, that increases post-stimulus. (c) Mean weights from prestimulus decoding of stimulus for the time point and model circled in (b). (d) mean weights for the best post-stimulus decoder, circled in (b). Circles in c and d indicate the approximate location of pixels used for the PSTHs in e and f. (e and f) PSTHs for V1 (e) and M2 (f) hotspots, solid lines are for hemispheres contralateral to block, dashed for ipsilateral to block, red lines for right hemisphere, and blue for left hemisphere. Asterisks indicate a significant difference for that time point between contralateral and ipsilateral cortex (solid versus dashed lines) at the $p < 0.05$ significance level with a t-test. Trials are sub-sampled so that there are the same number of trials containing each contrast for the left and right block.

This bi-directional modulation of activity as a result of the prior was a surprising finding that required confirmation in several ways. The findings shown above were seen by combining the activity across all contrasts, but of particular interest are the zero contrast trials, in which no stimulus appears on the screen, but the mouse must still report a decision. We would expect that if we were truly able to decode the block using these weights, we would be able to decode the block side before and after the stimulus onset for all trials, even with no stimulus appearing on the screen in the post-stimulus period. The surprising prediction that this makes for zero contrast trials is that despite there being no change to the visual environment before and after stimulus onset, weights in V1 and M2 of a given sign predict opposite representations of the prior before and after stimulus onset. To test if this is true, we first trained a decoder using one frame of stimulus aligned activity as its input, to predict the block side for a range of frames before and after the stimulus onset, in the same manner as described in Chapter 5. The only difference is that all zero contrast trials were held out as the final test data on which to evaluate the model, and the model was trained to predict the block side, not the stimulus side. Using this analysis, we see first that we can predict the side of the block before and after stimulus onset for zero contrast trials (Figure 6.2a). We see the same flip in weights between pre and post-stimulus activity for this block decoding as was observed for stimulus side decoding (Figure 6.2b, c). Therefore, these same weights, despite their opposite sign pre and post stimulus and no change to the visual environment, can predict the block side of the zero contrast trials above chance (Figure 6.2a).

One issue with decoding a variable that varies slowly through time, is that in any given experiment there are many confounding variables that also vary at similar time scales, such as the animal's satiety and arousal, or the potential bleaching of the calcium indicator or warming of the brain from the imaging light. To better control for these time-varying confounding variables, a null distribution other than purely random is required, as the true chance level is above 0.5; so I compared the decoding of block identity to decoding pseudo blocks (Harris, 2021). Pseudo blocks are blocks generated using the same parameters as were used to generate the true blocks that the animal actually experienced, but that the mouse never actually saw. By comparing decoding accuracy on the true blocks to the 95th percentile

decoding accuracy of 1000 pseudo blocks, we can determine that all but 4 sessions have above chance

block prediction at the 95% confidence level (Figure 6.2d).
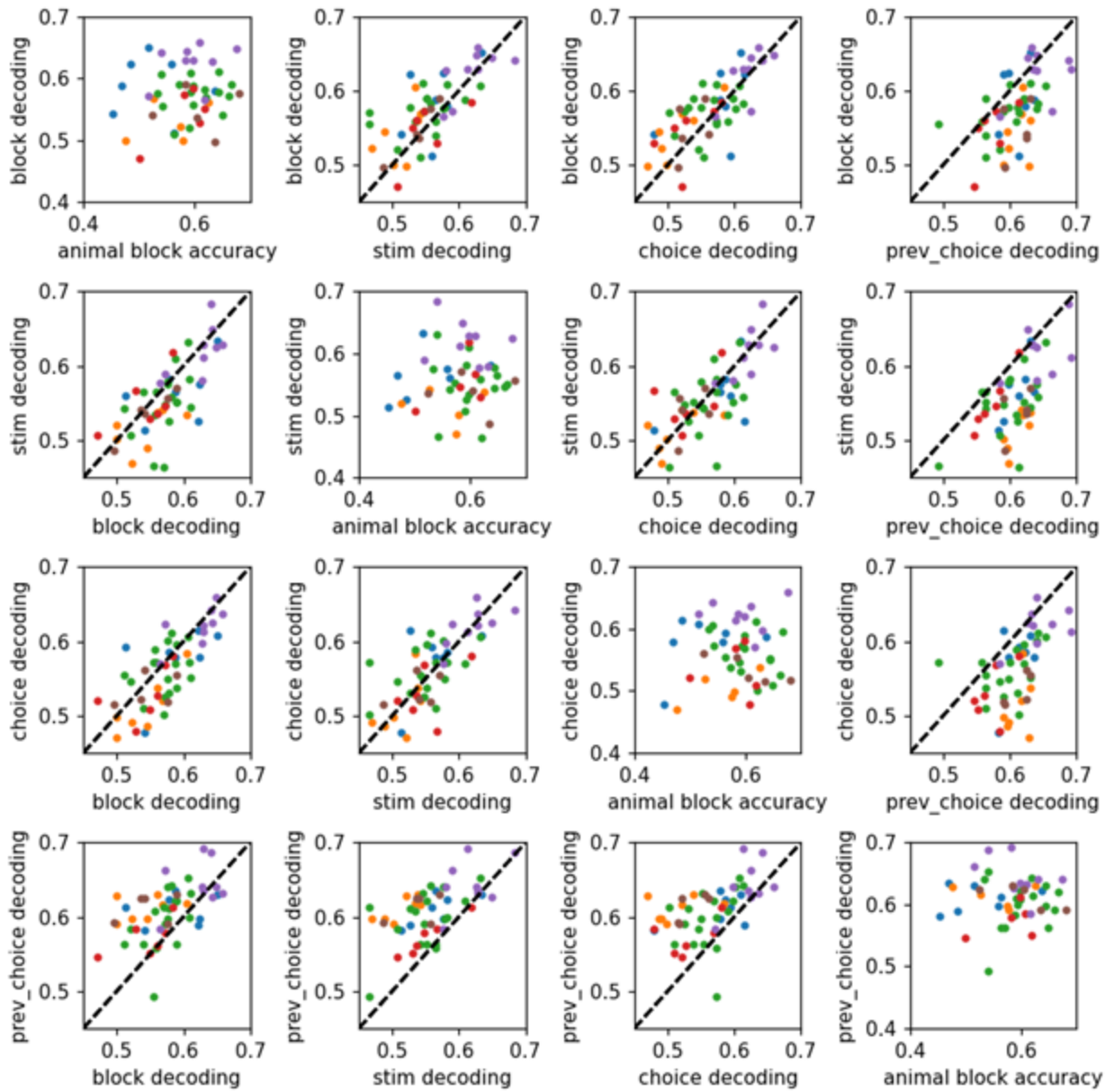
As a final sanity check to ensure the decoding of the prior before the onset of the stimulus is not

simply due to some mis-alignment of trials or other error, I made sure that there was no

contrast-dependence to the accuracy of block decoding before the onset of the stimulus. If there was some

error that led to stimulus information leaking into the data used by the decoder, we would expect stronger

decoding accuracy for higher contrast stimuli. To test this I trained a logistic regression model to predict

the block side using a single frame, 4 frames before the onset of the stimulus, using all contrasts and

5-fold cross validation such that a prediction was generated for each trial. I then tested the accuracy of

decoding the block on held out test data, and saw that there was no appreciable difference in decoding

accuracy between the different contrasts (Figure 6.2e). I furthermore compared the decoding at each

contrast level to the decoding of stimuli generated by pseudo-blocks, which showed on average that each

stimulus had above chance decoding strength.

**Figure 6.2.** Decoding of the block is not stimulus dependent. (a) Test performance of block decoding zero contrast trials before and after stimulus onset from a single imaging frame, red across sessions mean ± s.e.m. for decoding accuracy of the actual block identity from activity on zero contrast trials, blue mean ± s.e.m. for decoding the pseudo block control. (b) Mean decoding weights for the trial four frames before stimulus onset, with higher blue weights meaning higher activity there predicts a right block. (c) Same as (b) but for 4 frames after stimulus onset. (d) True block decoding versus 95th percentile pseudo block decoding, each dot is mean decoding for one session. (e) Decoding accuracy broken down by contrast for cross-validated block decoding trained and tested on all contrasts, red for true, blue for pseudo blocks.

## 6.4 Block prior decoding is influenced by choice history
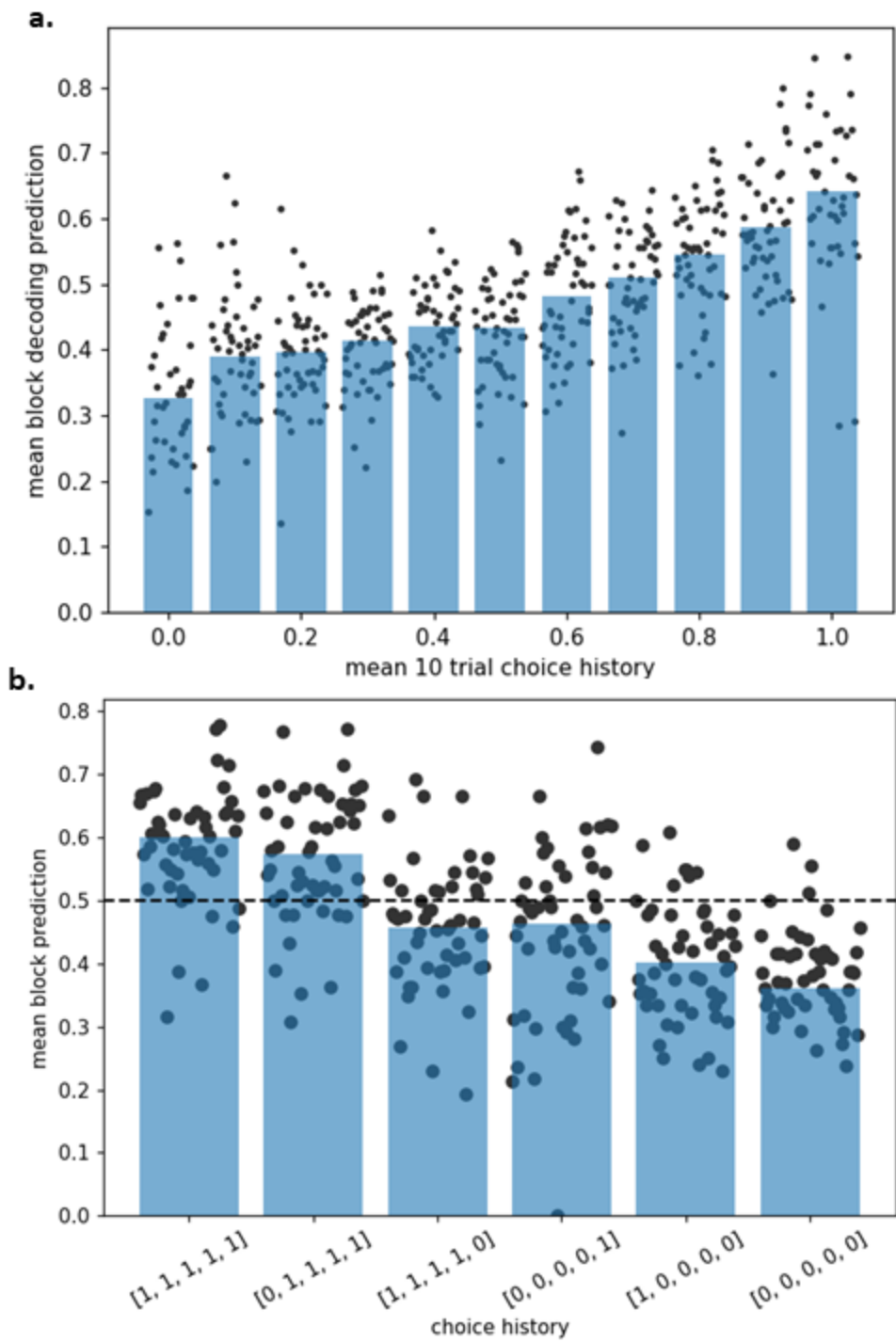
Above I have demonstrated that both the stimulus side, and the block identity can be decoded above chance before the onset of the stimulus. It is clear to see how these two variables are strongly correlated, as the block identity predicts the stimulus side with 80% accuracy. However, it is possible that the prestimulus decoding is more accurate for some task variable other than the upcoming stimulus side or block identity. To investigate this, I trained several decoders on a single frame of activity 2 frames before the stimulus onset, a separate decoder to predict each of: the block side, the upcoming stimulus side, the upcoming choice, and the previous choice. I then did a direct comparison of the decoding accuracy for each of these variables for each session. I also compared the decoding accuracy for each of these variables against the mouse's behavioral accuracy on zero contrast trials, a proxy for the strength of the animal's internal estimate of the prior. Disappointingly, I found no correlation between the animal's performance on blocks, and the prestimulus decoding of any of these variables (Figure 6.3, diagonal plots). It does seem however, that consistently the strongest prestimulus decoding is not for the block identity, but for the previous choice of the animal (Figure 6.3, bottom row).

**Figure 6.3.** Previous choice is the most easily decoded variable before stimulus onset. Four by four grid comparing the decoding accuracy of the block side, the stimulus of the upcoming trial, the choice of the upcoming trial, or the choice on the last trial. Diagonal is each of those variables versus the performance of the animal on zero contrast trials, a proxy for the strength of their internal prior representation. Each dot is a single session and each color is for a single animal, black dashed line is the line of equality.

This raised the question of if the prestimulus decoding of the prior is simply a reflection of the mouse's previous choice. This would be a possible explanation as some remaining trace of activity predictive of the previous trial would also be predictive of the block, as choices towards one side happen more frequently during blocks of that same side. Therefore, I next tested if the prior decoding could be explained by the previous choice alone, or if the prestimulus decoding of block side is representing something more like the true stimulus prior, which should be an integration of more than one previous trial. To test this, I took the decoding results from a decoder trained to predict the block prior from prestimulus activity, and then plotted the mean block side prediction for trials of a given sequence of choice histories. If the block decoding really is only a reflection of the previous trial, then block predictions should only be impacted by the last choice of the animal. However, if trial history further than one trial back impacts block decoding, it is more likely that this is truly decoding of some internal prior that takes the history of several trials into account.

Indeed, trial history later than the previous trial impacts block decoding. When plotting the mean choice of the past 10 trials, there is a progessive change in the block prediction as the fraction of previous choices gets further from 0.5 (Figure 6.4a). Furthermore, a single trial of choice towards one side does not completely revert the influence of the four preceding choices (Figure 6.4b). Additionally, a single choice can alter the block prediction as far as 4 trials back, such that block prediction of side 1 is lower for a trial history [0, 1, 1, 1, 1], than the choice history [1, 1, 1, 1, 1] (Figure 6.4b). This indicates the decoding of the block side is more representative of a version of stimulus prior that is integrated across at least 5 trials than simply the previous choice.
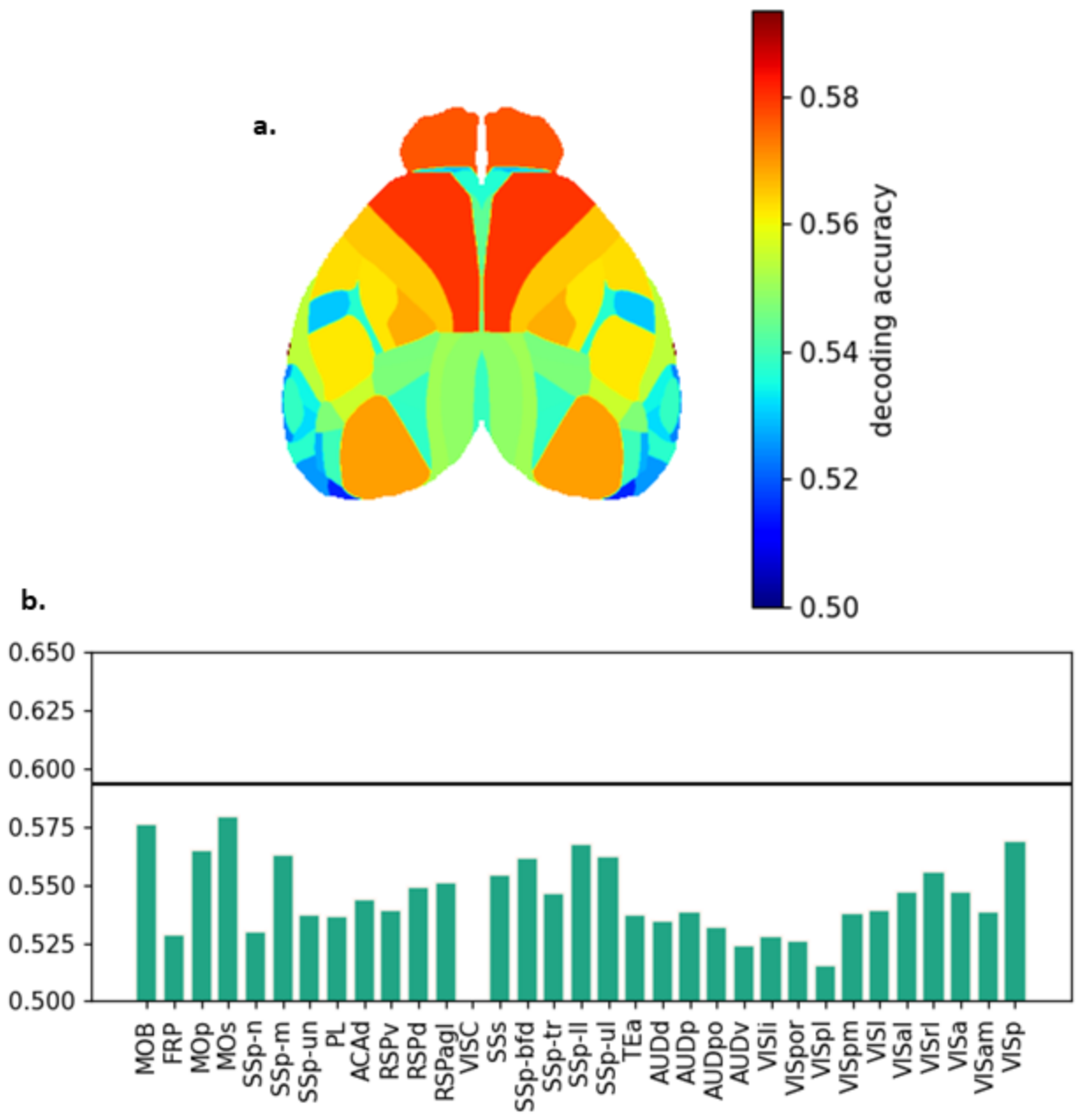
**Figure 6.4.** Trial choice history influences block prediction. (a) Block decoder prediction on trials with different trial choice histories. Block prediction of 0 indicates all predictions of block side 0, trial history of zero indicates all of the last 10 trials had choice 0. Dots are the mean of prediction for all trials matching the given trial history for a single session, bar is the mean of all trials matching that trial history across all mice and sessions. (b) Same as (a) except instead of a mean choice history, bars and dots are for specific trial histories where the last trial in the sequence is the trial before the block prediction is made.

**6.5 Stimulus prior decoding is distributed across cortical areas**

Now convinced that this prestimulus decoding of the block side is representative of the stimulus prior of the mice, we looked at which areas of the cortex contribute most to the representation of this information. With the whole brain decoding, I had shown strong decoding weights in V1 and M2, but I additionally wanted to see if either of these areas could decode the prior with the same accuracy as the whole cortex, or if the prior information is more distributed across the cortex than stimulus information. I also wanted to investigate if these two areas carried the most information for decoding the prior, or if any other area potentially contributed more to prior decoding.

To do this, I trained a separate decoder for each cortical area (bilaterally) on a single frame of activity for four separate frames before stimulus onset, and took the average decoding accuracy across those four frames. I then compared the decoding accuracy of each area to that of the whole dorsal cortex (also average across those four frames), to determine if any single area could match the predictive power of the whole cortex. The area with the highest, most consistent predictive power was M2, but many areas could consistently predict the prior, including V1, M1, olfactory bulb, and much of somatosensory cortex (Figure 6.5 a,b). However, unlike with stimulus decoding, no single area at any of these time points provided the same decoding accuracy as when the whole dorsal cortex was used ($p > 0.05$, bonferroni corrected t-test of each area versus whole brain decoding, Figure 6.5b).
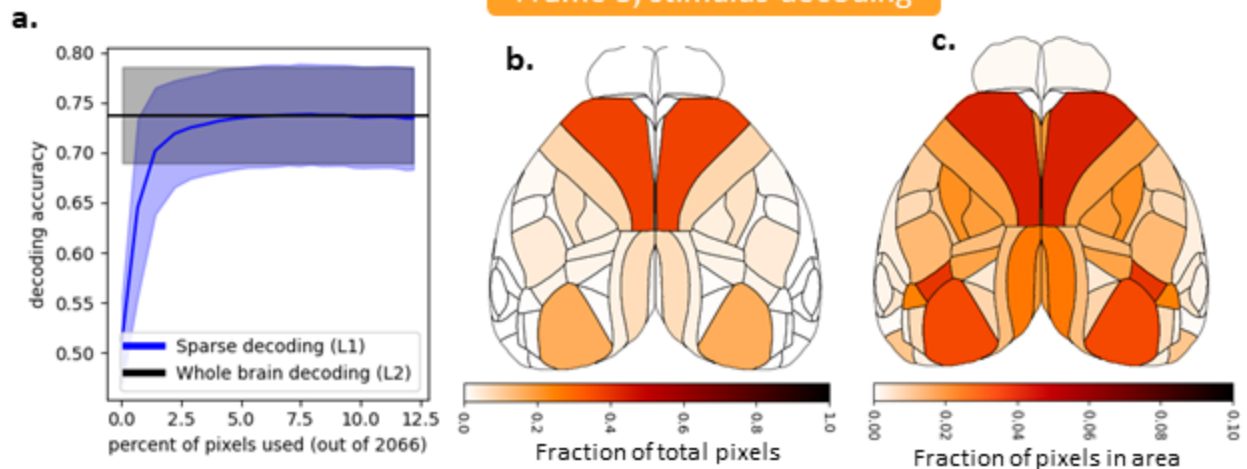
**Figure 6.5.** Prestimulus prior decoding is distributed across cortex, but strongest in motor cortex. (a) Decoding accuracy map of how well individual cortical areas can decode the prior using a single frame of imaging averaged across four pre-stimulus frames, colorbar maximum indicates whole brain accuracy level. (b) same data as in (a) but represented as a bar graph.
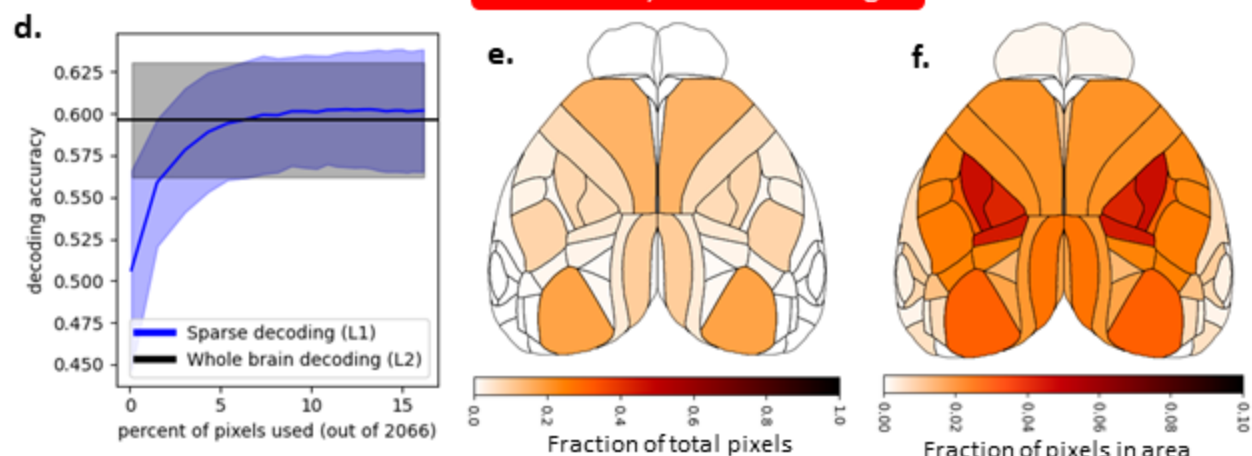
**6.6 Sparse decoding of the block identity disproportionately chooses pixels from V1 and S1**

To further explore the extent to which the information for the block identity is localized or distributed, I used a sparse L1 regularized logistic regression model to train a decoder to predict block side before the stimulus onset, to see from which cortical areas a sparse decoder chose pixels. I directly compared this to decoding of the stimulus side after stimulus onset, to determine the extent to which the most informative pixels were localized to a small set of areas or distributed across cortex for the decoding of the two different variables. To decode either the stimulus side or the block prior with L1 to the same level of accuracy as using the whole cortex (L2), took roughly the same number of pixels (Figure 6.6 a,d). When viewing which cortical regions the L1 decoder most used, it seemed both the stimulus decoder and block decoder relied most heavily on pixels chosen from V1 and M2 (Figure 6.6 b,e). However, there seems to be a correlation between the size of an area, and where pixels are chosen from, with more pixels chosen from larger areas. To control for the number of possible pixels that could be chosen in an area, I normalized the mean number of pixels across sessions chosen from an area by the number of possible pixels in an area. This showed a stark difference between the stimulus decoder and block decoder, where the stimulus decoder showed a strong over-representation of pixels in M2, V1, and anterior lateral visual cortex, but block decoding had the strongest over-representation in the paw and body trunk S1 with a slight over-representation in V1, but generally seemed to choose pixels from across the whole dorsal cortex (Figure 6.6 c,f). Though the sparse decoding of the stimulus side relies heavily on pixels in V1 and M2, it seems the decoding of the block is much more distributed, as the most informative pixels are much less concentrated, but it seems there is some concentration of pixels in V1 and paw and body trunk S1.

**Figure 6.6.** Sparse block decoding chooses pixels from across the cortex, with the strongest over-representation in S1 and V1. (a) Sparse L1 decoding of stimulus after stimulus onset using various numbers of pixels compared to using all pixels with an L1 decoder. (b) The fraction of all the decoding pixels located in each area out of all the pixels used for the L1 decoder of each session that reaches L2 performance with the fewest number of pixels. (c) Similar to (b) but now the area color corresponds to the across-sessions mean number of pixels in an area, normalized by the total number of pixels in an area. (d-f) Same as (a-c) but for prestimulus block decoding.

**6.7 Discussion**

Here I demonstrated that I am able to decode estimates of the stimulus prior in the mouse brain. Surprisingly, the representation of this prior seems to have an opposite sign before and after the onset of the stimulus, even for zero contrast trials when no stimulus appears on the screen. This representation is such that there is an increased suppression of the receptive field in V1 and M2 for the expected stimulus location before stimulus onset, and an increased activation of the same areas after the stimulus onset. I have shown that this decoding is most likely of the stimulus prior as the prestimulus decoding is not contrast dependent and the decoding prediction is stronger for trial histories with more choices towards a given side, and this effect is not fully reversed by a single choice to the other side. Furthermore, it seems that the representation of the prior is not isolated to this V1 and M2 suppression prestimulus, as there is strong prior decoding across the cortex, and a sparse prior decoder chooses pixels disproportionately from paw and body trunk somatosensory cortex.

This bidirectional modulation of V1 and M2 activity by the prior was unexpected, though it seems clear that this would improve behavioral performance. The increased suppression of stimulus responsive areas contralateral to the expected upcoming stimulus would decrease the noise in that area, and increasing the response after stimulus onset would increase the signal, therefore resulting in an increased signal to noise ratio, and a steeper psychometric curve, corresponding to an increase in descrimination sensitivity (Gold and Ding, 2013). Though there may be an increase in sensitivity for the in-block than out-of-block contrasts, the most noticeable effect of the blocks on behavior are an increase in bias, or the vertical shift of the psychometric curve. Another source of cortical information on the bias is the primary somatosensory cortex, most significantly the front paw, hind paw, and body trunk S1.

One possibility is that the ability to decode the prior from these cortical areas, indicates an underlying change in body position depending on the prior, such that, for instance, the mouse is leaning more towards the expected stimulus side. Such a physical embodiment of the animal's prior choices would clearly be a successful strategy for updating the prior, and would free up memory as it would only require updating once after each trial, as opposed to storing a representation of several previous trials

(Wilson and Golonka, 2013). Such an embodied representation of the prior would also likely manifest as a motor bias towards choices of one side, which would produce a bias in the psychometric curve (Gold and Ding, 2013). Interestingly there is preliminary unpublished work from an IBL member that indicates the paw and body position can vary predictably with the block structure in the IBL task (Schartner, 2021). Future work could use the videos recorded of the mice during these sessions to determine if the body and paw positioning of these mice do vary significantly with the block structure, and if this correlates with our ability to decode the block side from neural activity.

Other ongoing work describing the behavior in the IBL task seems to indicate that the best behavioral model of the animal's internal representation of the prior is an exponential smoothing over the past 5-7 actions (Charles Findling & Alexandre Pouget). There are several results from the above data that are consistent with this model. The first is that the variable that can most easily be decoded from the pre-stimulus activity is the previous choice, which would have the strongest weight in this model. Secondly, when conditioning on previous choices, the block decoding accuracy depends on more than just the choice on the previous trial, but instead choices have an effect at least 4 trials in the past, indicating that the prior I decode from neural activity does correlate with choice history. Therefore, the results presented here are consistent with the current understanding of the internal representation of the mouse stimulus prior in the IBL task.

Though a large body of work in the predictive coding field has shown the influence of a bayesian prior and stimulus expectation in primary visual cortex in humans (Aitken et al., 2020; Kok et al., 2017, 2013, 2012; Pajani et al., 2015; Samaha et al., 2018), such a result has never been seen in mice. Surprisingly however, the findings presented here are opposite those seen in the human fMRI literature. In human V1, there appears to be an increased prestimulus activation for expected stimuli relative to unexpected stimuli, and a lower post-stimulus activation for expected stimuli (Kok et al., 2012). In the data presented here, there is lower V1 activation prestimulus for expected stimuli and higher V1 activation post stimulus for expected stimuli. This difference could be due to a decoupling between the neurovasculature and the neural activity, especially for the prestimulus results as unevoked BOLD signal

often has very weak correlation with actual neural activity (Drew, 2019). Alternatively, the difference could be a layer or cell-type specific difference, as BOLD signals originate in deep layers of cortex and are predominantly driven by activity of inhibitory neurons (Drew, 2019), whereas widefield imaging signals reflect mostly activity from the dorsal most layers (Cardin et al., 2020; Ren and Komiyama, 2021), and the calcium indicator in these experiments is restricted to excitatory neurons. Hopefully this discrepancy can be resolved soon with the IBL brainwide map recordings, as these will provide single-cell and population level activity across the cortex in the IBL task.

While the results presented here seem at odds with the predictive coding hypothesis, they also are not fully explained by the leading model of selective spatial attention, divisive normalization (Reynolds and Heeger, 2009). Divisive normalization does predict that there will be a larger stimulus-driven activation for stimuli in the attended location as opposed to the unattended, which matches the results here. However, it also predicts that the strongest effects of attention/expectation would be in the higher visual cortical areas, whereas they were mostly restricted to V1 here. Furthermore, the normalization model seems to predict that before stimulus onset, there would be a predictive activation in the receptive field of the expected stimulus, but we saw a selective decrease in activity. Finally the main effect of normalization is an increase in signal to noise ratio, which causes an increase in the slope of the psychometric curve, whereas the main behavioral effect of the blocks is a biasing of the psychometric curve.

There is no known model that predicts the modulation of activity in visual cortex presented here, which certainly makes this a novel finding. However, this should be taken with caution as it is a novel, unpredicted finding and was only seen with correlative techniques. This will be on much more solid footing if confirmed with other modalities, such as the IBL neuropixels recordings, or the upcoming IBL mesoscope recordings. Additionally, a causal manipulation could be performed by using targeted inhibition of the receptive field of an upcoming stimulus in the prestimulus period to see if this causes an increase in performance after the stimulus onset.

# 7 Simultaneous mesoscale imaging and inhibition of mouse dorsal cortex

<u>Contribution note:</u> The work in the following chapter was conceived of, planned by, and analyzed by myself and Tony Zador. I performed all of the experiments and built required hardware for these experiments.

## 7.1 Introduction

Having shown both mesoscale inactivation across the dorsal cortex and mesoscale functional imaging across the dorsal cortex, the next logical step was to combine them so that we could monitor the online changes in neural activity that result from the inactivation. As the surgical prep, and much of the optical apparatus is the same for both of these techniques, only moderate alterations were required to combine these two techniques simultaneously. Additionally, although mesoscale activity manipulation with optogenetics are commonplace in neuroscience (Deisseroth, 2015), rarely is the result of that manipulation monitored in more than one brain area distal to the manipulation target. There are likely to be effects of manipulation distal to the target given that the brain is a highly interconnected network (Wolff and Ölveczky, 2018). Combining these two techniques allows tracking of the network-wide effects of optogenetic or other perturbations. One possible explanation for the results from previous chapters and work in the Olveczky and Bruno labs (Hong et al., 2018; Kawai et al., 2015; Otchy et al., 2015) showing differences between chronic and acute manipulation, is that the acute inactivation of an area causes disruptions of other areas in a connected network, whose activity is less affected by chronic changes in activity. The goal of this experiment, though not yet achieved, was to determine if there were global effects of local perturbation and how chronic and acute manipulations differ in their network effects.

In this chapter, I will demonstrate the potential of using Scanning Optogenetics with Widefield Imaging (SOWI) for mesoscale imaging and inactivation. I will demonstrate consistent local effects of inactivation, as well as some distal effects. Furthermore I will show some unresolved issues and artifacts associated with this technique and propose some solutions or options for reducing their impact on the data.

### 7.2 Materials and methods

*Transgenic mice*

The four mice used in this study were the same widefield imaging mice used in the two previous chapters, with the addition of another transgene. They were heterozygous for each Camk2a-tTA (JAX strain 007004), and tetO-GCaMP6s (JAX strain 024742) such that they expressed GCaMP6s in most cortical excitatory neurons (Wekselblatt et al., 2016). In addition to these two transgenes that allow imaging of dorsal cortical neurons, they were also crossed to a VGAT-ires-cre (Jackson labs, 028862) line to allow the viral targeting of inhibitory interneurons with a cre-dependent ChrimsonR virus.

*Viral injections*

The ChrimsonR virus AAV9-PHP.eB.hSyn.Flex.rc[ChrimsonRtdTomato].WPRE.bGH (Addgene62723, (Klapoetke et al., 2014), produced by the Penn Vector core) was delivered by retro-orbital injection (Yardeni et al., 2011). The injection deliverable was 100ul prepared in sterile saline containing 1e12 virus particles and 2% Evans Blue dye (Sigma) to visualize if the injection was successful or not. To perform the injection, mice with an existing clear-skull cap implant were anesthetized with 2% inhaled isofluorane until deeply sedated, then the 100ul solution was injected into the retro-orbital vein with a 1ul insulin syringe. If the injection was successful, the mouse would appear blue from the dye. After 3 weeks of incubation, the cortex was inspected under a fluorescence microscope; if red fluorescence was present, then there had been successful expression of the opsin in the cortex.

*Combined imaging and inhibition*

To perform the simultaneous imaging and inhibition experiment, I kept as much of the imaging hardware and protocol the same as possible as described in Chapter 5, and added the inhibition to that. To excite the ChrimsonR opsin, I added a 635nm wavelength laser, whose beam was collected in a 50um diameter optical patch cable, and collimated with a thorlabs collimator. This collimated beam was then directed onto the two mirrors of a thorlabs two mirror galvonometer. The galvovometer was controlled using an NI-DAQ and custom MATLAB software as described in Chapter 3. All of the different

excitation wavelengths for the experiment were directed to the same optical path, between the two lenses of an infinite conjugate lens pair where they were reflected by a narrow band-pass dichroic that reflects most visible wavelengths except for a narrow band in the green spectrum (Chroma, ZT530/55dcbp-UF1), allowing for the gcamp emission to pass through to the PCO Edge 5.5 camera.

The 635nm wavelength laser used for optogenetic inactivation was focused to a point of 400um diameter at the cortical surface, with a maximum power of 3.2 $mW/mm^2$. Laser stimulation was performed with a 40hz sine wave. To attempt to reduce the visually evoked response to the inactivation laser, two red LEDs (Sparkfun, 08862) were placed about 3mm from each eye.

*Alteration to widefield imaging pre-processing*

One alteration was made to the pre-processing of the widefield calcium imaging data. For all previous experiments, the baseline fluorescence was calculated by taking the mean fluorescence across the full length of the session. To ensure that reductions of activity from baseline were seen as negative df/f in these experiments, the baseline was instead calculated by taking the mean of the 10 frames preceding the onset of the laser. This way imaging frames where inhibition is occurring are not included in the baseline activity.
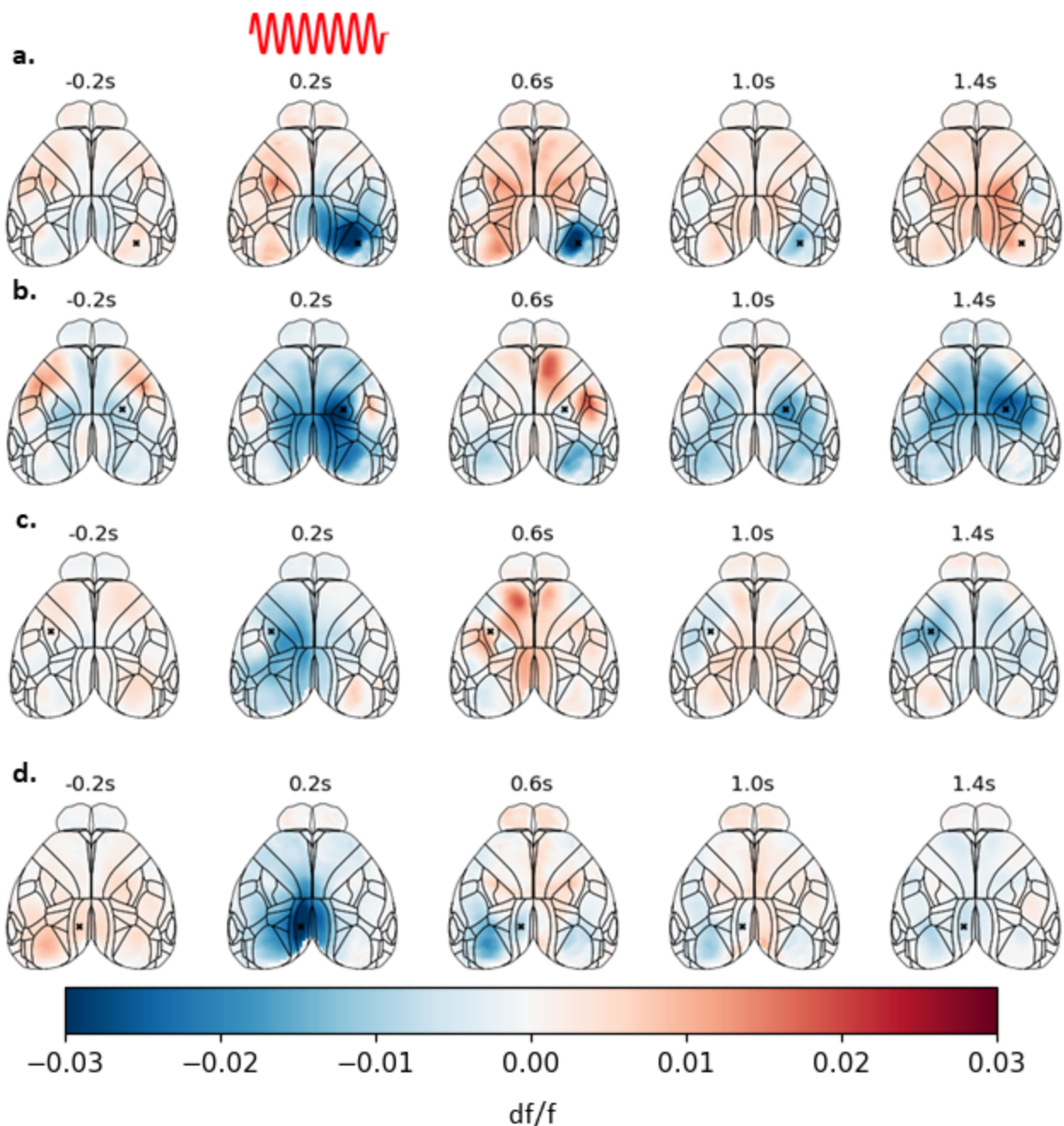
**7.3 Inactivation of dorsal cortex seen in wide field calcium imaging**

To first confirm that there is indeed inhibition of cortical activity with inhibitory SOWI, I visualized the mean activity across the cortex during inhibition of several different targets on the cortical surface. I first focused on unilateral inhibition where the laser was on for 200ms. Figure 7.1 displays the mean activity for several time points before and after laser onset. These examples were chosen to display some of the features of this inhibition, including that there can be long-lasting effects of inactivation that last for hundreds of milliseconds after the laser offset (Figure 7.1 a,d). Another is that there can be strong effects distal to the site of inhibition, as the inactivation of paw somatosensory areas can result in activation of ipsilateral M2 (Figure 7.1 b,c). Despite these unintended effects, it is clear that the desired
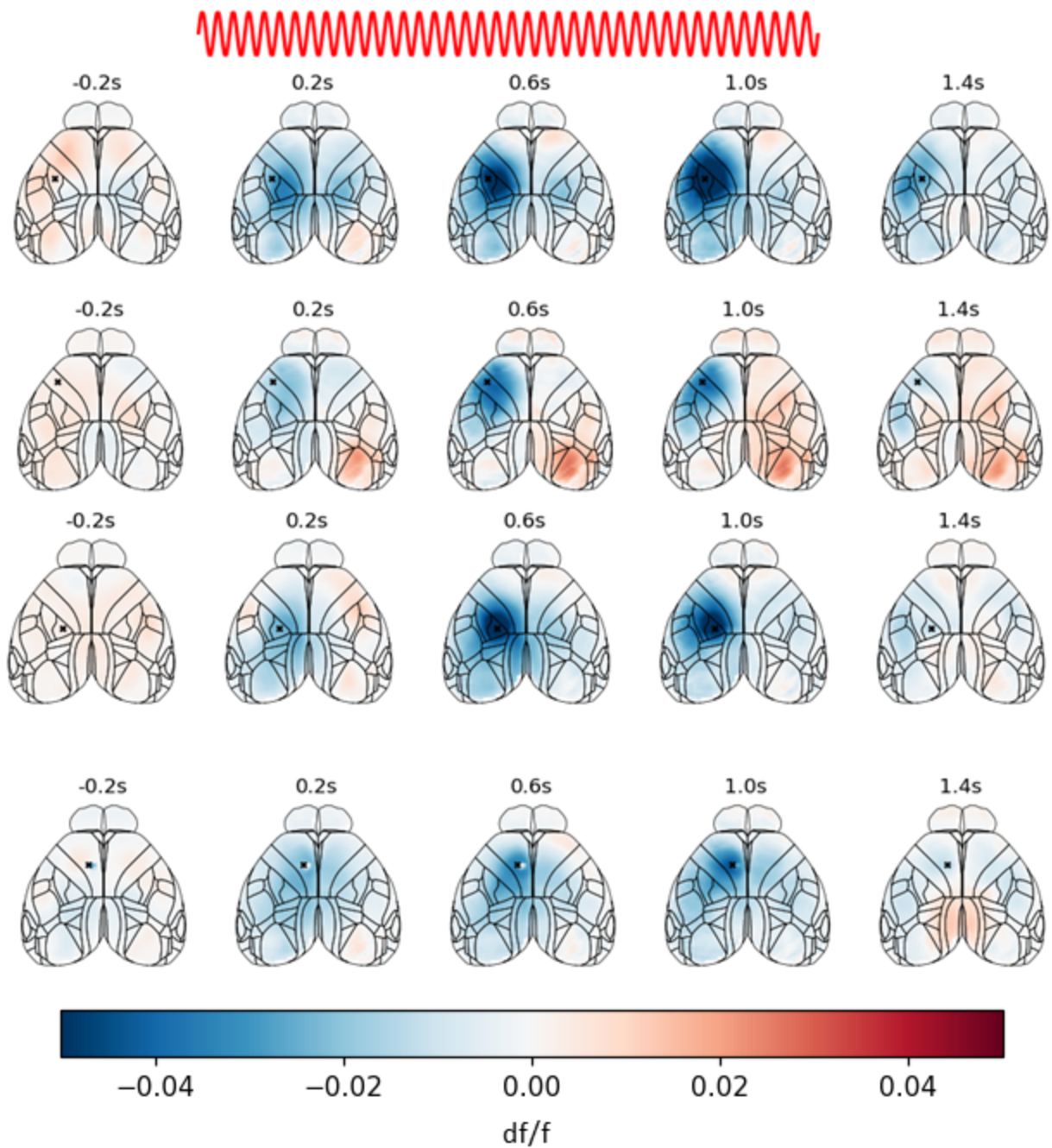
target has a strong decrease in activity following the laser stimulation, and then recovers to its normal activity following this.

When using a longer length of inactivation, a different example mouse shows increasing spread of the reduction of activity throughout the length of inactivation (Figure 7.2). It appears as if this prolonged inactivation decreases the activity across the whole dorsal cortex, except in cases where the largest artifact in this data is present, the visual detection of the inhibition light. Despite attempts to mask the presence of the red LED, there was a consistent, strong activation of visual cortex, stronger for inactivation coordinates more proximal to the eyes (Figure 7.2 a-d), and also present in mice with no virus injected (data not shown and Nick Steinmetz, personal communication).
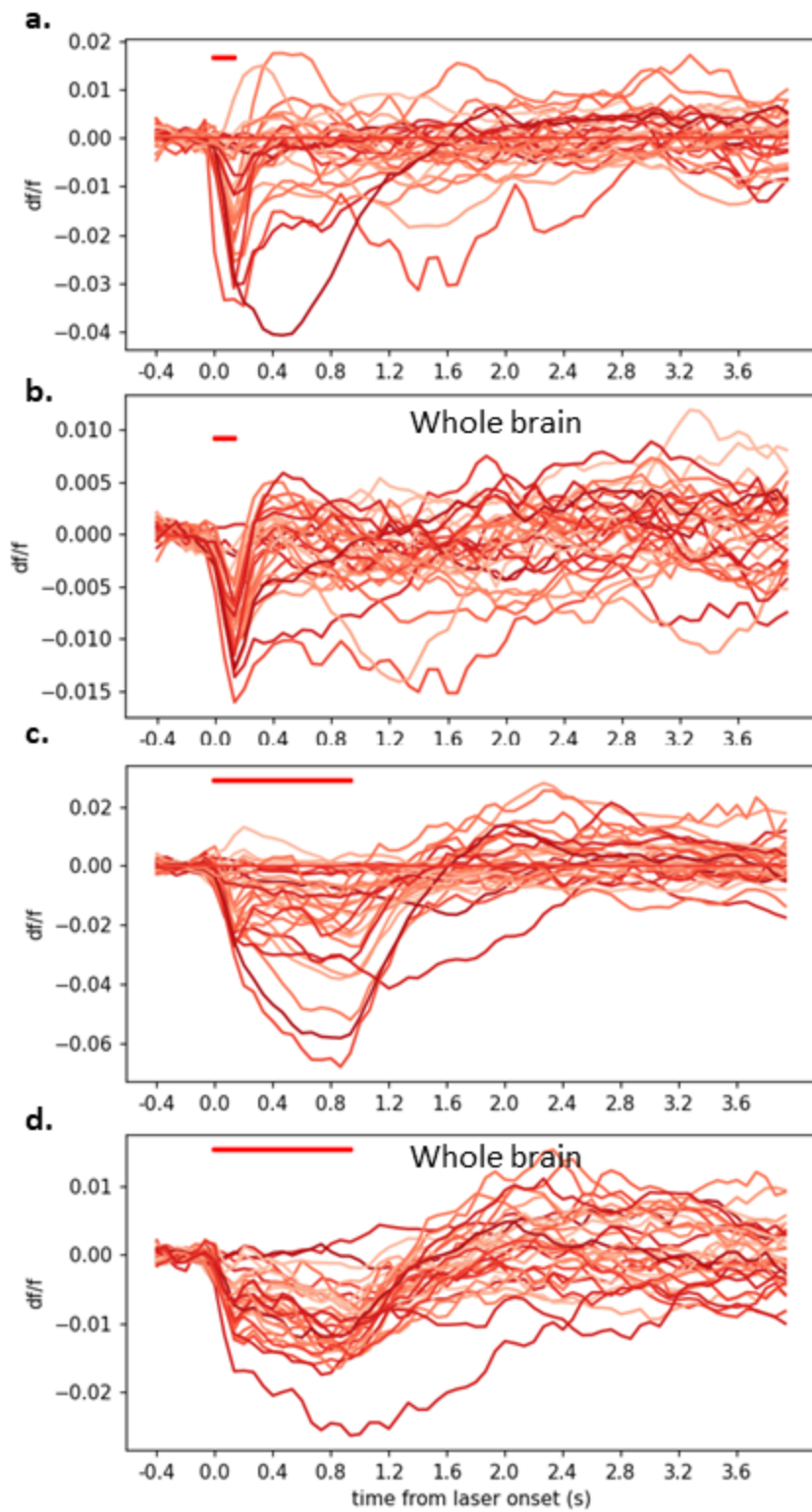
When inhibiting an individual area, one possible global change to the cortical network would be an increase in activity in a different area in response to the decrease in activity at the inhibition location, such that the overall cortical activity remains constant. This network balance seems to not be true, as with either brief, or long inactivation, the activity of the whole cortex is nearly always reduced by the inactivation (Figure 7.3 b,d). Surprisingly, rebound activation (Guo et al., 2014; Li et al., 2019) was not consistently present following laser offset, either at the locus of inhibition (Figure 7.3 a,c) or across the whole cortex (Figure 7.3 b,d) for either long or short inactivation. There seemed to be some rebound activation for some inhibition areas, and sustained suppression for others, but more repetitions and statistical analyses would be needed to conclude if any of these are significant deviations from expected ongoing activity.

**Figure 7.1.** Whole dorsal cortical effects of spatially restricted cortical inhibition. Four time traces of the mean effect of 200ms activation of inhibitory neurons with ChrimsonR for trials over 3 days for one mouse. Sinuosoidal laser was delivered from time 0 to .2s, the .2s frame shown here is the last frame in which the laser was on. Black X indicates the intended target of the inhibition.
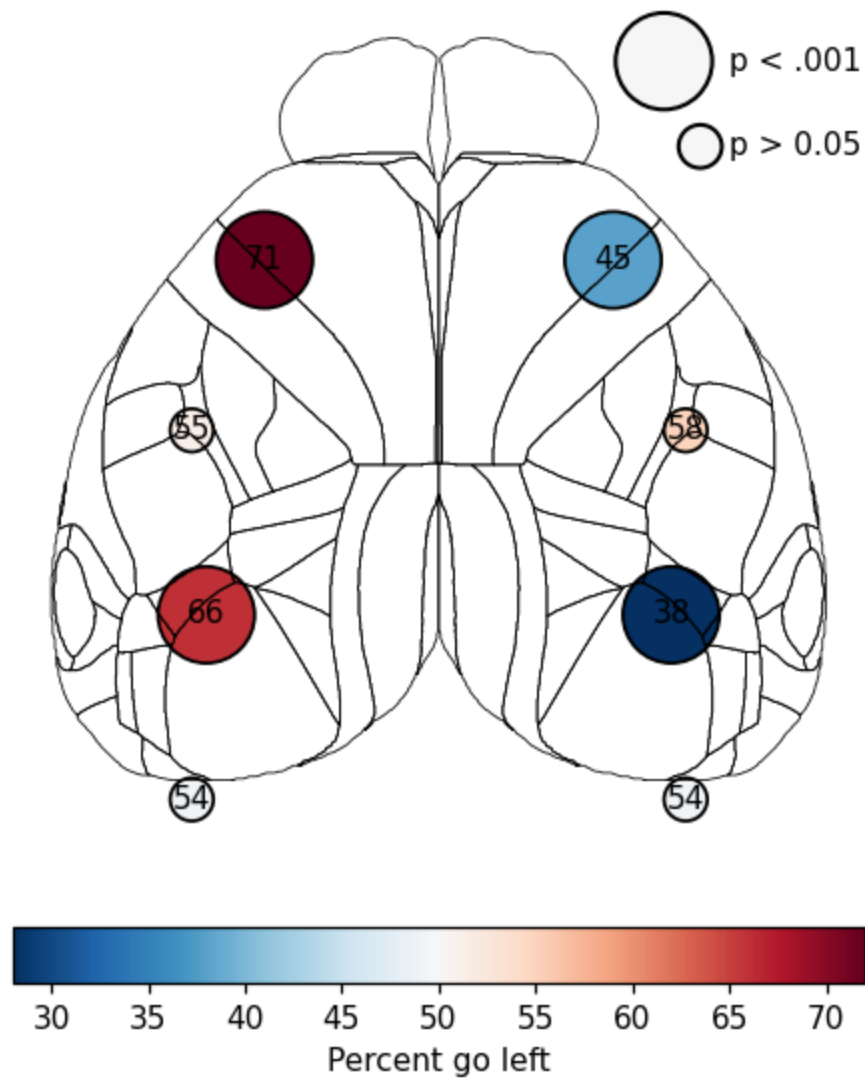
**Figure 7.2.** Whole dorsal cortical effects of spatially restricted cortical inhibition. Four time traces of the mean effect of 200ms activation of inhibitory neurons with ChrimsonR for trials over 3 days for one mouse. Sinuosoidal laser was delivered from time 0 to 1s, the 1s frame shown here is the last frame in which the laser was on. Black X indicates the intended target of the inhibition.

**Figure 7.3.** Fluorescence traces for inactivation of each targeted location. Each line indicates the df/f for a single inhibition location, mean across trials for one animal. Red bar indicates the time in which the laser was on. (a,c) Mean df/f for the pixels within a radius of 2 pixels from the inhibition target. (b,d) Mean df/f across all cortical pixels for each inactivation of each target.

**7.4 Inactivation of dorsal cortex causes behavioral deficits**

I next wanted to confirm that the same behavioral effects that were seen in the inactivation scan in Chapter 3 could be recapitulated with inhibitory SOWI using ChrimsonR systemic viral delivery. To do this I performed a similar inactivation scan, as before, this time focusing on only six targets, one in each hemisphere of the visual cortex, the motor cortex, and the somatosensory cortex. From the previous results, I expected to see significant ipsilateral biasing when motor or visual cortex were inactivated, but not somatosensory cortex. This result was exactly as expected, showing decreased contralateral, and increased ipsilateral choices for inhibition of motor or visual cortex, but not somatosensory cortex (Figure 7.4).

**Figure 7.4.** Inactivation during widefield imaging with systemic viral delivery of ChrimsonR virus recapitulates previous scan results. Similar to figures Chapter 3, each dot represents a single laser location, the size of the dot signifies the level of bonferroni corrected significance from a chi-squared test comparing the left and right choices made at a given inhibition spot versus those made when the laser is directed to the two control spots off the cortical surface. The color and number within the circle indicates the percent left choices made when the laser is directed to that spot. Data are for 3 sessions for each of 4 mice, for a total of 5386 control trials and an average of 521 inhibition trials per non-control spot.

**7.5 Discussion**

In this chapter I have demonstrated a proof-of-principle for simultaneous scanning optogenetics with widefield imaging, SOWI. To my knowledge this is the first report of such an experiment, though I am aware of one other group pursuing a similar experiment (Nick Steinmetz, personal communication). I have demonstrated that there are consistent local decreases in widefield calcium activity in response to focal inhibition of cortical targets. I have shown that some inhibition sites have unexpected effects distal of the original inhibition, such as the activation of M2 following inhibition of paw somatosensory cortex. Importantly however, there are also some issues to be resolved in using this technique, with the largest impediment to applications being the activation of visual cortex by the optogenetic laser.

To use SOWI to answer many questions about network dynamics and truly causal functional connectivity, it requires that the experiment alters neural activity in only the desired location due to activation of an opsin. However, in the current state, the significant visual response to the optogenetic stimulation adds significant doubt to any conclusions about affects distal to the site of laser stimulation. This response to red light was surprising given the dogma that mice cannot see red light (Rocha et al., 2016). This is so ingrained that many mouse facilities use a red light during the night stages of mouse rearing, though it is clear that the mice here can see 635nm light, and a recent report shows that rats have strong visual descrimination up to 729nm (Nikbakht and Diamond, 2021). Currently the only technique I tried to limit this activation was to mask the laser onset with LEDs which were always on during the experiment, but this clearly failed. The extent of this visual activation could be decreased by ensuring a high expression of the opsin, which would allow a decreased laser intensity for the same level of neural suppression or activation. The best alternative however, would be to use an optogenetic channel activated by a wavelength that will not activate a visual response in V1, such as infrared or potentially another method of activating neurons such as sonogenetics (Duque et al., 2022).

If this issue is solved though, there seems to be many critical scientific questions that could be addressed with SOWI. It could be addressed if there is any way in which to make optogenetic

manipulations an on-neural-manifold manipulation, or at least to reduce the off-manifold effects of manipulation (Jazayeri and Afraz, 2017). In a similar vein, optogenetic manipulations could be tailored to try to reproduce activity patterns previously recorded that lead to specific behavioral effects. This could be used to causally test the role of correlational relationships such as those established in Chapters 5 & 6. In a similar transition from correlational to causal research, if SOWI is used for activation instead of suppression, one could create a truly causal map of functional connectivity, which has almost exclusively been performed using correlation, though one recent experiment has demonstrated the usefulness of causally mapping networks (Sans-Dublanc et al., 2021).

Already even with the areas in this dataset where inactivation did not elicit visual responses, one aspect of the manipulations presented here seems very unnatural. Typically activity in widefield imaging is very highly correlated across the midline, such that activity in one area on one hemisphere is very highly correlated with its homologous area in the other hemisphere (Shimaoka et al., 2019). However, even just from the example inactivations shown in this chapter it is clear that most unilateral inactivations do not cause a strong inactivation in the homologous area on the other hemisphere, and even sometimes activate the other hemisphere. This is a clear example that optogenetics can easily lead to unnatural patterns of neural activity that may not be biologically plausible, and could cause behavioral disruption in trivial or uninteresting ways (Jazayeri and Afraz, 2017).

# General Discussion and Perspectives

The overarching goal of this work was to contribute to knowledge of how the brain solves the IBL visual decision-making task. Though we by no means have a complete understanding of how the brain performs this task, I have made important contributions towards this goal. I have helped create and collect data for a standardized visual decision-making task that introduced reproducible mouse behavior to the neuroscience community and will underlie many IBL goals. I have recorded single neuron activity from across the entire brain, contributing thousands of neurons towards the IBL dataset that will help not only create models of how the whole brain performs decision-making behavior, but has also produced standardized methodology and equipment for the community, and will produce the first electrophysiological atlas of the mouse brain. I have used causal manipulations to determine that V1 and M2 are critical nodes for performing this behavior, and that they play different roles in the decision-making process. Altering activity in V1 seems to affect only the accumulation of evidence whereas inactivation of M2 appears to bias the starting point of a drift-diffusion process. I have found correlational evidence that indicates that not only are these two areas the most informative in cortex for solving the simple decision-making problem, but that they also, along with somatosensory cortex, underlie the representation of the bayesian stimulus prior. And finally, I have reported preliminary results from a technique that could be used to ask many basic questions about how neural manipulations affect the whole cortical network and to make neural manipulations as realistic and informative as possible.

## 1        Contributions to and perspectives on the IBL

In essence, all of the findings in this thesis can be seen as contributions to the IBL, as all experiments were performed in the standardized IBL task. Therefore any insight from my experiments can be directly interpreted in light of any of the many other experiments in the IBL task. My direct contributions towards the development of and data collection in the IBL task, as well as my neuropixels

recordings, were pedestrian requirements that all experimental IBL members needed to perform. The unique contributions I have made to the IBL are potentially even more beneficial to the collaboration, and will hopefully influence models and future experiments, and shape how the collaboration proceeds to address outstanding questions. Specifically, I hope to convey to the IBL that correlates of behavioral events are widespread across the cortex, and likely the brain. However in the cortex at least, it seems only V1 and M2 have causal roles in the task. The role of V1 however is still in question if it is truly causal, as its chronic removal does not impair task performance. Another key takeaway from my findings for the IBL is that the prior seems to be relatively distributed across cortical regions, but does have a strong basis in V1, M2, and somatosensory cortex. The stimulus prior information present in the somatosensory cortex is likely a reflection of differences in the body positioning of mice for different priors, a form of embodied cognition (Wilson and Golonka, 2013). In a preliminary analysis of some video data in the IBL task, many sessions do seem to show significant correlations between whisking and paw position with the stimulus probability (Schartner, 2021). The video data is available for many of my sessions, and it would be exciting to see if there was a correlation between prior decoding accuracy from prestimulus somatosensory cortex and prior decoding accuracy from the prestimulus video data.

One of the most exciting conclusions from my work is that the representation of the stimulus prior in V1 and M2 is in opposite directions before and after the stimulus onset, with a suppression of the hemisphere for the expected stimulus before, and an increased excitation after the stimulus onset. This representation was completely unexpected. It would be very reassuring to see this finding repeated using the neuropixels dataset, and this work is in progress by other IBL members. It is also notable that this is a relatively weak signal at the population level, so it is possible that there are only a few neurons performing this computation in each of these areas. Because it is such a weak signal however, it is possible it could be amplified by restricting the imaging to specific cell types, either that are located in specific layers or of a functional subtype. This my also help to determine the origin of this signal, if it is more likely to be feedback from higher cortical areas as predicted by predictive coding, or feed-forward or local connections.

My widefield imaging in the IBL task additionally is a contribution to the IBL because there are current plans for other IBL members to perform the same imaging throughout learning of the task. The findings I present here will provide a starting point for analyses of the learned representations in widefield imaging. Furthermore, my findings will hopefully be reproduced by other researchers in the IBL, and there will be an increase in the number of animals and sessions that could be used to perform the same analyses, potentially clarifying some issues that suffer from low sample size, such as decoding using only zero contrast trials and cross-animal comparisons of potential strategy differences. This could be key if the representation of the prior is at all based on the embodied mechanism proposed above, as each animal would likely have an idiosyncratic embodiment of the prior (Kawai et al., 2015).

Overall my relationship with the IBL has been tumultuous. After initial excitement and promise, I was very discouraged for the first several years of my membership. There were many issues with deploying code before it was ready, pressure to perform experiments before the whole pipeline was available, and frustration with overcomplication of seemingly simple procedures. For several years I thought that the many hours put into meetings and producing data I would likely never analyze myself were wasted time. I believe now that these were unavoidable growing pains in the unique, bottom-up meso-scale collaboration that the IBL has undertaken. My recent collation of my data into this thesis and collaborations with other IBL members have shown me the promise of doing science at this scale. The underlying data infrastructure of the IBL and the standardized task, have proven to be extremely important for my work and likely for the impact my work will have on the field of neuroscience. It is invaluable to be able to easily and directly compare the results of different experiments, which has only ever been truly possible within individual labs using the same task. Too often there are small changes to tasks that make the results between studies incomparable. Though there are still some researchers doing this within the IBL (and I was tempted to as well), there are many researchers also directly working on the main IBL task, which I now see is the key to the success of our collaboration. Hopefully the IBL will continue to thoroughly explore this task with many different experimental approaches, leading to a much

richer picture of the neural implementation of decision-making. We may have even reached critical mass such that other labs outside of the IBL will begin to contribute to this body of research.

I now strongly believe that large collaborations are the future of science, as it seems is increasingly the realization of much of the scientific community ("Exploring the Future of International Large-Scale Science," n.d.; "Research collaborations bring big rewards," 2021; Malhotra et al., 2021). I do not believe, however, that the IBL has performed up to its full potential, and have a few suggestions based on my experience within the organization. The first is that the researchers performing experiments towards the IBL platform projects, such as the brainwide electrophysiology map, often feel undervalued and that they are being pulled in different directions by needing to contribute to this larger project, as well as to have their own personal project to complete. I believe a better model, which it seems the IBL may naturally be moving towards, is to have subgroups working together on large-to-medium size projects, where individual researchers can maintain more ownership over it than a collaboration-wide project. For example, the diversification of the IBL into using widefield imaging, mesoscale imaging, and fiber photometry, are all spearheaded by smaller groups rather than all members of the IBL contributing to them as was the case for the brainwide map. This way each member has more stake in the deliverable, there are more approaches towards the same goal, and researchers can work on different projects within the collaboration. I think the one critical resource that will keep the IBL together is the data infrastructure. This has been invaluable, especially for the direct comparison of results from diverse experiments. If there is one thing they should be spending money on, it is the software development team. As long as this data infrastructure remains strong, I believe the IBL can synergistically contribute more to neuroscience research than its member labs can alone.

## 2      Brainwide activity, but localized effects of inactivation

At first glance it may seem contradictory that there is widespread information about the choice and stimulus, with activity from each area able to predict the stimulus side, yet only a restricted set of areas are affected by the inactivation. However the limited effect of inactivation has been documented

previously in other visually guided tasks (Pinto et al., 2019; Zatka-Haas et al., 2021), and seems to indicate that though information about stimulus and choice are broadcast across the cortex, only a few areas actually use this information. One possible hypothesis for such widespread stimulus activity is that the animals used in this and similar experiments are highly overtrained, and learn stereotypical coordinated movements that can engage the whole body (Kawai et al., 2015). Under this hypothesis, activity across the dorsal cortex would be required for performance of the task, because it would require somatosensory feedback and motor commands for the whole somato-motor cortex. The inactivation results I show here argue against this hypothesis, if all of these areas were required for task performance, then their inactivation would impair the behavior, yet the impairments are restricted to V1 and M2. Therefore, it appears that this widely broadcast information is a redundant representation of the activity in the areas that actively influence behavior.

If not whole body coordination, then why is information about the stimulus found across the whole cortex? One possibility is that this widespread information is only present with this widefield imaging modality. The signal from widefield transcranial imaging such as this is comprised of a combination of spiking activity of local layer 1 and 2/3 neurons (Ren and Komiyama, 2021; Yizhar et al., 2011) as well as a strong contribution from the layer 1 neuropil which is made up mostly of layer 5 and layer 2/3 dendrites (Muralidhar et al., 2014) but also has a non-negligible contribution from axons projecting to that area (Ren and Komiyama, 2021). It is possible that this broadcast stimulus information is present in the neuropil, but not reflected in the spiking data. Evidence argues against this though, as despite these various contributions to the widefield signal, it is representative of local multiunit activity (Makino et al., 2017). This point will hopefully be easy to address soon though, as calcium indicators restricted to the cell body become available (Cardin et al., 2020). In any case, the representation of the stimulus and choice across the cortex from spiking data is another question that the IBL will help to address with the brainwide activity map.

A more interesting hypothesis for this general broadcasting of information, with localization of the concentration of this information, is that this is a solution to the routing problem of information in the

cortex (Olshausen et al., 1993). The routing problem states that there must be a mechanism that sends information between areas in the brain that maximizes some combination of energy efficiency, information fidelity, speed of transit, and robustness to perturbation (Avena-Koenigsberger et al., 2019; Laughlin and Sejnowski, 2003). The data from this thesis support a model for information routing in the cortex where the information is globally broadcast from sub-cortex and locally gain-modulated in areas that have a prior expectation for incoming information, giving the required target a more sharply tuned version of the signal. This model clearly provides a strong robustness to perturbation, as the information is present throughout the cortex, and the chronic removal of one required node (V1) does not lead to catastrophic failure. It also provides strong signal fidelity as it includes gain modulation of the information in particular nodes, and rapid transit as only a single broadcasting step is required. Where it clearly suffers is in efficiency, as sending information across the whole cortex would require far more energy than to a targeted location. It is possible that this is a strategy particular to smaller brains where the energy cost would be more limited, or in highly over-trained tasks where there are very strong expectations of the environment. Still this seems to be a novel solution to the routing problem that has yet to be computationally explored.

This dichotomy of global activity but local causal effects was only observable through the combination of correlational recordings and causal manipulations. This combination not only allowed us to determine which areas are most useful for solving the task, they both provide different lines of evidence towards what role the different areas are playing in the decision-making process. Separately, each experiment only gives a hint at these different roles, but taken together, we get a clearer picture of the different aspects of decision-making that V1 and M2 contribute. From the widefield imaging we see that initially, V1 is the most informative of the stimulus or choice, but shortly after, M2 becomes more informative. Combined with the inhibition results showing that V1 inactivations cause slowing of the diffusion process, and M2 inactivations cause a shift in the starting point of the diffusion process, there is stronger evidence that V1 performs perception of the stimulus, and M2 calculates or represents the decision variable.

From the combination of the results in this thesis, my model of how the mouse cortex is solving the task is as follows. The prior belief of the stimulus location from the previous choices before the onset of the stimulus results in a suppression of baseline activity for the expected stimulus location in V1 and M2. It is simultaneously embodied in the mouse's body position as it prepares to make the expected choice. After the go cue indicating the stimulus onset, there is an increase in activity in V1; however it is weighted such that there is a larger increase for the hemisphere contralateral to blocks, and there is a larger increase for the hemisphere contralateral to the actual stimulus. This is then spread throughout the cortex, with the strongest representation in M2, which binarizes the stimulus representation as from the left or right side, and results in a decision being reported. Correlates of this action are also widespread, including feeding back to V1. Of course there is also subcortical involvement in this process, especially likely in the actual motor production and the updating of the stimulus prior based on an integration of previous choices.

## 3        Acute versus chronic manipulations

It is somewhat troubling that acute inhibition of the visual cortex provides consistent behavioral disruption if done either bilaterally or unilaterally, but chronic removal of V1 activity does not impair visual decision making in the IBL task. The silver lining to this however, is that it is clear that V1 at least is connected to areas in the brain that do affect decision making. Monitoring the activity in other putative areas that could be driving visual behavior during V1 inhibition may help solve the question of if V1 is simply an upstream area where activity disruption here trivially disrupts activity in the true task node. One prime candidate is the superior colliculus, which mediates many innate visual behaviors, and show activity change when cortically blind humans relearn visual tasks (Das et al., 2014). And additionally thalamic areas seem to change their activity in cortically blind primates (Kinoshita et al., 2019) and show strong visual activity in mice (Steinmetz et al., 2019). A combination of similar experiments as performed here, recording, and manipulating activity both chronically and acutely would elucidate which of these areas are truly underlying visual decision making in mice, and if any of them are completely redundant

with each other. Also interesting would be to compare the reaction times of the mice with V1 lesions to that of intact mice and V1 inhibited mice. Because V1 appears to accumulate evidence in this task, if there is an alteration in the RT of mice without V1, that would provide evidence that V1 is normally the locus of stimulus information accumulation. However no difference in the RT profile would be uninformative for the role of V1 in the intact brain.

A natural question given the lack of chronic necessity of visual cortex seen in these experiments is do the inhibition and decoding results even matter given that the mice can perform this task in the absence of V1? Given that V1 both causally influences behavior, and is correlated with behavior, seems that activity here is at least informative of the behavior, even if it is only a redundant representation of some other brain area. Additionally, as mentioned above, even if V1 is not truly involved in the default neural solution for this task and only has a permissive role, its identification as having a causal influence can be used to find which other areas are required both chronically and acutely to solve the task. Therefore these results do further our understanding of how the brain solves a visual decision-making task, though they pose more questions as well.

Another key finding in this thesis is that the visual cortex contains a representation of the stimulus prior both before and after stimulus onset. The aspirations and optogenetic inhibitions I performed were all using only the basic visual descrimination task of the IBL, and therefore I did not assess the switching of the prior in blocks of trials. It is possible the V1 is essential for this higher level function, and that either acute or chronic manipulation would reduce the extent to which the animals use the stimulus prior. Another future direction could be to perform a similar inhibition scan, but this time only during the ITI to see if removal of cortical activity in any area disrupts the use of the stimulus prior. From the decoding results, it seems possible that inhibition of V1, M2 or somatosensory cortex would reduce use of the prior, but given that it is such a distributed signal, it is also possible that this information is very redundant, and inhibition of any one cortical area would not alter the prior.

Another future direction for determining the differences in the effects of acute and chronic inactivation would be to perform widefield imaging during both. One question for example, is what effect

159

do these different manipulations have on task activity in M2? Does acute inactivation disrupt it and chronic inactivation leave its activity intact? Or perhaps aspiration of V1 drives all decision-making activity to subcortical areas so that there is no longer any task representation in the cortex. Widefield imaging has been used to describe significant widespread alterations in neural functional connectivity following a stroke (Cramer et al., 2019), and changes in the progression and correlation of activity following inhibition of M2 (Makino et al., 2017), so there are likely to be significant differences in cortical activity following the loss of visual cortex. However because performance is unaltered after this lesion, it would not be entirely surprising if the cortex was not required at all for the performance of this task, though such a finding would likely disturb many systems neuroscientists.

## 4       The promise and future of these high throughput techniques

It is important to note that the main techniques used in this thesis, widefield whole dorsal cortex imaging and inactivation scans across the dorsal cortex, are relatively low cost, high throughput experiments and they have many potential future applications. The most difficult aspect to working with widefield imaging data is the preprocessing of the data, but now there is a simple, freely available standard preprocessing pipeline available (Couto et al., 2021), there is a very low barrier to entry in using this technique. Here I have only focused on imaging all excitatory neural populations, but already this has been extended to characterize the contributions of different cell types to behavioral processes (Musall et al., 2021), and could even be used to monitor the release of different neurotransmitters across the cortical surface (Cardin et al., 2020). Because of the unique spatial scale, low cost, and chronic implementation, widefield imaging is growing in popularity and will continue to produce many novel scientific findings (Cardin et al., 2020; Ren and Komiyama, 2021).

One application of widefield imaging that has not yet been reported is its use to monitor the acute alterations to neural circuits during optogenetic inhibition with SOWI. To my knowledge only one study has been published demonstrating cortex wide effects of an acute neural manipulation, where inactivation of motor cortex with muscimol was shown to disrupt task related correlation of activity of the cortex in

trained mice (Makino et al., 2017). However this was done in a single cortical area, without much temporal or spatial precision. Optogenetics is a more frequently used neural manipulation that allows better spatial and temporal resolution (Li et al., 2019), and with SOWI, these cortex wide effects could be thoroughly explored. Enumerating imaging and inhibition or activation of different cell types with this setup alone could provide a wealth of novel information on the basic dynamics that underlie cortical function. One specific example of such an experiment would be to compare the global effects of inhibition of a set of cortical areas to the effects of exciting those same areas to see if optogenetic activation and inactivation are truly opposites or if they have different effects on the cortical network.

Besides simply using SOWI to manipulate ongoing resting state activity, there are many permutations of investigating the effect of optogenetic inhibition on behavior, and determining if there are neural correlates to that behavioral alteration. One example would be to do a time series of brief inactivations of V1 or M2 in the IBL task while performing widefield imaging. Determining if inhibition in different time bins relative to task events causes both different behavioral effects and different distal neural effects could be an informative tool for assessing the transfer of information between nodes in this task. Another more practical use for this combination would simply be to monitor the effects of any inhibition that you perform, so that you can tailor the power, size, and length of laser stimulation to increase the precision of your neural manipulation. Innumerable future experiments could be performed with SOWI, and several more rigs to use it in our lab could be constructed at minimal cost. I hope that someone is able to take over these experiments and leverage this technique to answer any of these many questions.

# References

Abbott, L.F., Angelaki, D.E., Carandini, M., Churchland, A.K., Dan, Y., Dayan, P., Deneve, S., Fiete, I., Ganguli, S., Harris, K.D., Häusser, M., Hofer, S., Latham, P.E., Mainen, Z.F., Mrsic-Flogel, T., Paninski, L., Pillow, J.W., Pouget, A., Svoboda, K., Witten, I.B., Zador, A.M., 2017. An International Laboratory for Systems and Computational Neuroscience. Neuron 96, 1213–1218. https://doi.org/10.1016/j.neuron.2017.12.013

Aitken, F., Turner, G., Kok, P., 2020. Prior Expectations of Motion Direction Modulate Early Sensory Processing. J. Neurosci. 40, 6389–6397. https://doi.org/10.1523/JNEUROSCI.0537-20.2020

Ajina, S., Pollard, M., Bridge, H., 2020. The Superior Colliculus and Amygdala Support Evaluation of Face Trait in Blindsight. Front. Neurol. 11.

Allen, W.E., Kauvar, I.V., Chen, M.Z., Richman, E.B., Yang, S.J., Chan, K., Gradinaru, V., Deverman, B.E., Luo, L., Deisseroth, K., 2017. Global Representations of Goal-Directed Behavior in Distinct Cell Types of Mouse Neocortex. Neuron 94, 891-907.e6. https://doi.org/10.1016/j.neuron.2017.04.017

Angier, N., 1990. Great 15-Year Project To Decipher Genes Stirs Opposition. N. Y. Times.

Avena-Koenigsberger, A., Yan, X., Kolchinsky, A., Heuvel, M.P. van den, Hagmann, P., Sporns, O., 2019. A spectrum of routing strategies for brain networks. PLOS Comput. Biol. 15, e1006833. https://doi.org/10.1371/journal.pcbi.1006833

Baker, M., 2016. 1,500 scientists lift the lid on reproducibility. Nature 533, 452–454. https://doi.org/10.1038/533452a

Bastos, A.M., Usrey, W.M., Adams, R.A., Mangun, G.R., Fries, P., Friston, K.J., 2012. Canonical microcircuits for predictive coding. Neuron 76, 695–711. https://doi.org/10.1016/j.neuron.2012.10.038

Beck, J.M., Ma, W.J., Kiani, R., Hanks, T., Churchland, A.K., Roitman, J., Shadlen, M.N., Latham, P.E., Pouget, A., 2008. Probabilistic population codes for Bayesian decision making. Neuron 60, 1142–1152. https://doi.org/10.1016/j.neuron.2008.09.021

Botvinik-Nezer, R., Holzmeister, F., Camerer, C.F., Dreber, A., Huber, J., Johannesson, M., Kirchler, M., Iwanir, R., Mumford, J.A., Adcock, R.A., Avesani, P., Baczkowski, B.M., Bajracharya, A., Bakst, L., Ball, S., Barilari, M., Bault, N., Beaton, D., Beitner, J., Benoit, R.G., Berkers, R.M.W.J., Bhanji, J.P., Biswal, B.B., Bobadilla-Suarez, S., Bortolini, T., Bottenhorn, K.L., Bowring, A., Braem, S., Brooks, H.R., Brudner, E.G., Calderon, C.B., Camilleri, J.A., Castrellon, J.J., Cecchetti, L., Cieslik, E.C., Cole, Z.J., Collignon, O., Cox, R.W., Cunningham, W.A., Czoschke, S., Dadi, K., Davis, C.P., Luca, A.D., Delgado, M.R., Demetriou, L., Dennison, J.B., Di, X., Dickie, E.W., Dobryakova, E., Donnat, C.L., Dukart, J., Duncan, N.W., Durnez, J., Eed, A., Eickhoff, S.B., Erhart, A., Fontanesi, L., Fricke, G.M., Fu, S., Galván, A., Gau, R., Genon, S., Glatard, T., Glerean, E., Goeman, J.J., Golowin, S.A.E., González-García, C., Gorgolewski, K.J., Grady, C.L., Green, M.A., Guassi Moreira, J.F., Guest, O., Hakimi, S., Hamilton, J.P., Hancock, R., Handjaras, G., Harry, B.B., Hawco, C., Herholz, P., Herman, G., Heunis, S., Hoffstaedter, F., Hogeveen, J., Holmes, S., Hu, C.-P., Huettel, S.A., Hughes, M.E., Iacovella, V., Iordan, A.D., Isager, P.M., Isik, A.I., Jahn, A., Johnson, M.R., Johnstone, T., Joseph, M.J.E., Juliano, A.C., Kable, J.W., Kassinopoulos, M., Koba, C., Kong, X.-Z., Koscik, T.R., Kucukboyaci, N.E., Kuhl, B.A., Kupek, S., Laird, A.R., Lamm, C., Langner, R., Lauharatanahirun, N., Lee, H., Lee, S., Leemans, A., Leo, A., Lesage, E., Li, F., Li, M.Y.C., Lim, P.C., Lintz, E.N., Liphardt, S.W., Losecaat Vermeer, A.B., Love, B.C., Mack, M.L., Malpica, N., Marins, T., Maumet, C., McDonald, K., McGuire, J.T., Melero, H., Méndez Leal, A.S., Meyer, B., Meyer, K.N., Mihai, G., Mitsis, G.D., Moll, J., Nielson, D.M., Nilsonne, G., Notter, M.P., Olivetti, E., Onicas, A.I., Papale, P., Patil, K.R., Peelle, J.E., Pérez, A., Pischedda, D., Poline, J.-B., Prystauka, Y., Ray, S., Reuter-Lorenz, P.A., Reynolds, R.C., Ricciardi, E., Rieck, J.R., Rodriguez-Thompson, A.M., Romyn, A., Salo, T., Samanez-Larkin, G.R., Sanz-Morales, E., Schlichting, M.L., Schultz, D.H.,

Shen, Q., Sheridan, M.A., Silvers, J.A., Skagerlund, K., Smith, A., Smith, D.V., Sokol-Hessner, P., Steinkamp, S.R., Tashjian, S.M., Thirion, B., Thorp, J.N., Tinghög, G., Tisdall, L., Tompson, S.H., Toro-Serey, C., Torre Tresols, J.J., Tozzi, L., Truong, V., Turella, L., van 't Veer, A.E., Verguts, T., Vettel, J.M., Vijayarajah, S., Vo, K., Wall, M.B., Weeda, W.D., Weis, S., White, D.J., Wisniewski, D., Xifra-Porxas, A., Yearling, E.A., Yoon, S., Yuan, R., Yuen, K.S.L., Zhang, L., Zhang, X., Zosky, J.E., Nichols, T.E., Poldrack, R.A., Schonberg, T., 2020. Variability in the analysis of a single neuroimaging dataset by many teams. Nature 582, 84–88. https://doi.org/10.1038/s41586-020-2314-9

Brunton, B.W., Botvinick, M.M., Brody, C.D., 2013. Rats and Humans Can Optimally Accumulate Evidence for Decision-Making. Science 340, 95–98. https://doi.org/10.1126/science.1233912

Burgess, C.P., Lak, A., Steinmetz, N.A., Zatka-Haas, P., Bai Reddy, C., Jacobs, E.A.K., Linden, J.F., Paton, J.J., Ranson, A., Schröder, S., Soares, S., Wells, M.J., Wool, L.E., Harris, K.D., Carandini, M., 2017. High-Yield Methods for Accurate Two-Alternative Visual Psychophysics in Head-Fixed Mice. Cell Rep. 20, 2513–2524. https://doi.org/10.1016/j.celrep.2017.08.047

Busse, L., Ayaz, A., Dhruv, N.T., Katzner, S., Saleem, A.B., Schölvinck, M.L., Zaharia, A.D., Carandini, M., 2011. The Detection of Visual Contrast in the Behaving Mouse. J. Neurosci. 31, 11351–11361. https://doi.org/10.1523/JNEUROSCI.6689-10.2011

Button, K.S., Ioannidis, J.P.A., Mokrysz, C., Nosek, B.A., Flint, J., Robinson, E.S.J., Munafò, M.R., 2013. Power failure: why small sample size undermines the reliability of neuroscience. Nat. Rev. Neurosci. 14, 365–376. https://doi.org/10.1038/nrn3475

Cardin, J.A., Crair, M.C., Higley, M.J., 2020. Mesoscopic Imaging: Shining a Wide Light on Large-Scale Neural Dynamics. Neuron 108, 33–43. https://doi.org/10.1016/j.neuron.2020.09.031

Cassidy, A.S., Merolla, P., Arthur, J.V., Esser, S.K., Jackson, B., Alvarez-Icaza, R., Datta, P., Sawada, J., Wong, T.M., Feldman, V., Amir, A., Rubin, D.B.-D., Akopyan, F., McQuinn, E., Risk, W.P., Modha, D.S., 2013. Cognitive computing building block: A versatile and efficient digital neuron model for neurosynaptic cores, in: The 2013 International Joint Conference on Neural Networks (IJCNN). Presented at the The 2013 International Joint Conference on Neural Networks (IJCNN), pp. 1–10. https://doi.org/10.1109/IJCNN.2013.6707077

Chapuis, G., n.d. Craniotomy surgery protocol v0.1.1.

Chen, T.-W., Li, N., Daie, K., Svoboda, K., 2017. A Map of Anticipatory Activity in Mouse Motor Cortex. Neuron 94, 866-879.e4. https://doi.org/10.1016/j.neuron.2017.05.005

Couto, J., Musall, S., Sun, X.R., Khanal, A., Gluf, S., Saxena, S., Kinsella, I., Abe, T., Cunningham, J.P., Paninski, L., Churchland, A.K., 2021. Chronic, cortex-wide imaging of specific cell populations during behavior. Nat. Protoc. 16, 3241–3263. https://doi.org/10.1038/s41596-021-00527-z

Cramer, J.V., Gesierich, B., Roth, S., Dichgans, M., Düring, M., Liesz, A., 2019. In vivo widefield calcium imaging of the mouse cortex for analysis of network connectivity in health and brain disease. NeuroImage 199, 570–584. https://doi.org/10.1016/j.neuroimage.2019.06.014

Daie, K., Svoboda, K., Druckmann, S., 2021. Targeted photostimulation uncovers circuit motifs supporting short-term memory. Nat. Neurosci. 24, 259–265. https://doi.org/10.1038/s41593-020-00776-3

Das, A., Tadin, D., Huxlin, K.R., 2014. Beyond Blindsight: Properties of Visual Relearning in Cortically Blind Fields. J. Neurosci. 34, 11652–11664. https://doi.org/10.1523/JNEUROSCI.1076-14.2014

Dayan, P., Hinton, G.E., Neal, R.M., Zemel, R.S., 1995. The Helmholtz machine. Neural Comput. 7, 889–904. https://doi.org/10.1162/neco.1995.7.5.889

de Vries, S.E.J., Lecoq, J.A., Buice, M.A., Groblewski, P.A., Ocker, G.K., Oliver, M., Feng, D., Cain, N., Ledochowitsch, P., Millman, D., Roll, K., Garrett, M., Keenan, T., Kuan, L., Mihalas, S., Olsen, S., Thompson, C., Wakeman, W., Waters, J., Williams, D., Barber, C., Berbesque, N., Blanchard, B., Bowles, N., Caldejon, S.D., Casal, L., Cho, A., Cross, S., Dang, C., Dolbeare, T., Edwards, M., Galbraith, J., Gaudreault, N., Gilbert, T.L., Griffin, F., Hargrave, P., Howard, R., Huang, L., Jewell, S., Keller, N., Knoblich, U., Larkin, J.D., Larsen, R., Lau, C., Lee, E., Lee, F., Leon, A., Li, L., Long, F., Luviano, J., Mace, K., Nguyen, T., Perkins, J., Robertson, M., Seid, S.,

Shea-Brown, E., Shi, J., Sjoquist, N., Slaughterbeck, C., Sullivan, D., Valenza, R., White, C., Williford, A., Witten, D.M., Zhuang, J., Zeng, H., Farrell, C., Ng, L., Bernard, A., Phillips, J.W., Reid, R.C., Koch, C., 2020. A large-scale standardized physiological survey reveals functional organization of the mouse visual cortex. Nat. Neurosci. 23, 138–151. https://doi.org/10.1038/s41593-019-0550-9

deCharms, R.C., Zador, A., 2000. Neural Representation and the Cortical Code. Annu. Rev. Neurosci. 23, 613–647. https://doi.org/10.1146/annurev.neuro.23.1.613

Deisseroth, K., 2015. Optogenetics: 10 years of microbial opsins in neuroscience. Nat. Neurosci. 18, 1213–1225. https://doi.org/10.1038/nn.4091

Desimone, R., Duncan, J., 1995. Neural mechanisms of selective visual attention. Annu. Rev. Neurosci. 18, 193–222. https://doi.org/10.1146/annurev.ne.18.030195.001205

Developers, T., 2022. TensorFlow. Zenodo. https://doi.org/10.5281/zenodo.5949169

Doya, K., Ishii, S., Pouget, A., Rao, R.P.N. (Eds.), 2006. Bayesian Brain: Probabilistic Approaches to Neural Coding, Computational Neuroscience Series. MIT Press, Cambridge, MA, USA.

Drew, P.J., 2019. Vascular and neural basis of the BOLD signal. Curr. Opin. Neurobiol., Computational Neuroscience 58, 61–69. https://doi.org/10.1016/j.conb.2019.06.004

Duque, M., Lee-Kubli, C.A., Tufail, Y., Magaram, U., Patel, J., Chakraborty, A., Mendoza Lopez, J., Edsinger, E., Vasan, A., Shiao, R., Weiss, C., Friend, J., Chalasani, S.H., 2022. Sonogenetic control of mammalian cells using exogenous Transient Receptor Potential A1 channels. Nat. Commun. 13, 600. https://doi.org/10.1038/s41467-022-28205-y

Elliott, K.C., 2012. Epistemic and methodological iteration in scientific research. Stud. Hist. Philos. Sci. Part A, Structures and Strategies in Ancient Greek and Roman Technical Writing 43, 376–382. https://doi.org/10.1016/j.shpsa.2011.12.034

Elliott, K.C., Cheruvelil, K.S., Montgomery, G.M., Soranno, P.A., 2016. Conceptions of Good Science in Our Data-Rich World. Bioscience 66, 880–889. https://doi.org/10.1093/biosci/biw115

Emilien, G., Ponchon, M., Caldas, C., Isacson, O., Maloteaux, J.M., 2000. Impact of genomics on drug discovery and clinical medicine. QJM Mon. J. Assoc. Physicians 93, 391–423. https://doi.org/10.1093/qjmed/93.7.391

Erlich, J.C., Bialek, M., Brody, C.D., 2011. A Cortical Substrate for Memory-Guided Orienting in the Rat. Neuron 72, 330–343. https://doi.org/10.1016/j.neuron.2011.07.010

Errington, T.M., Denis, A., Perfito, N., Iorns, E., Nosek, B.A., 2021. Challenges for assessing replicability in preclinical cancer biology. eLife 10, e67995. https://doi.org/10.7554/eLife.67995

Exploring the Future of International Large-Scale Science [WWW Document], n.d. . Am. Acad. Arts Sci. URL https://www.amacad.org/events/large-scale-science (accessed 3.1.22).

Fazekas, P., Nanay, B., 2021. Attention Is Amplification, Not Selection. Br. J. Philos. Sci. 72, 299–324. https://doi.org/10.1093/bjps/axy065

Fechner, G.T., 1860. Elemente der psychophysik. Breitkopf und Hartel, Leipzig.

Finkelstein, A., Fontolan, L., Economo, M.N., Li, N., Romani, S., Svoboda, K., 2021. Attractor dynamics gate cortical information flow during decision-making. Nat. Neurosci. 24, 843–850. https://doi.org/10.1038/s41593-021-00840-6

Fred Rieke, David Warland, Rob de Ruyter Van Stevenick, William Bialek, 1999. Spikes: exploring the neural code. MIT press.

Frégnac, Y., Laurent, G., 2014. Neuroscience: Where is the brain in the Human Brain Project? Nature 513, 27–29. https://doi.org/10.1038/513027a

Gao, Z., Davis, C., Thomas, A.M., Economo, M.N., Abrego, A.M., Svoboda, K., De Zeeuw, C.I., Li, N., 2018. A cortico-cerebellar loop for motor planning. Nature 563, 113–116. https://doi.org/10.1038/s41586-018-0633-x

Gibbs, R.A., 2020. The Human Genome Project changed everything. Nat. Rev. Genet. 21, 575–576. https://doi.org/10.1038/s41576-020-0275-3

Glaser, J.I., Benjamin, A.S., Chowdhury, R.H., Perich, M.G., Miller, L.E., Kording, K.P., 2020. Machine Learning for Neural Decoding. eNeuro 7. https://doi.org/10.1523/ENEURO.0506-19.2020

Glickfeld, L.L., Histed, M.H., Maunsell, J.H.R., 2013. Mouse Primary Visual Cortex Is Used to Detect Both Orientation and Contrast Changes. J. Neurosci. 33, 19416–19422. https://doi.org/10.1523/JNEUROSCI.3560-13.2013

Gold, J.I., Ding, L., 2013. How mechanisms of perceptual decision-making affect the psychometric function. Prog. Neurobiol., Conversion of Sensory Signals into Perceptions, Memories and Decisions 103, 98–114. https://doi.org/10.1016/j.pneurobio.2012.05.008

Gold, J.I., Shadlen, M.N., 2002. Banburismus and the brain: decoding the relationship between sensory stimuli, decisions, and reward. Neuron 36, 299–308. https://doi.org/10.1016/s0896-6273(02)00971-6

Graham, D.J., 2014. Routing in the brain. Front. Comput. Neurosci. 8, 44. https://doi.org/10.3389/fncom.2014.00044

Green, D.M., Swets, J.A., 1966. Signal detection theory and psychophysics, Signal detection theory and psychophysics. John Wiley, Oxford, England.

Guo, Z.V., Li, N., Huber, D., Ophir, E., Gutnisky, D., Ting, J.T., Feng, G., Svoboda, K., 2014. Flow of cortical activity underlying a tactile decision in mice. Neuron 81, 179–194. https://doi.org/10.1016/j.neuron.2013.10.020

Hao, Y., Thomas, A.M., Li, N., 2021. Fully autonomous mouse behavioral and optogenetic experiments in home-cage. eLife 10, e66112. https://doi.org/10.7554/eLife.66112

Harris, K.D., 2021. Nonsense correlations in neuroscience. https://doi.org/10.1101/2020.11.29.402719

Heitz, R.P., 2014. The speed-accuracy tradeoff: history, physiology, methodology, and behavior. Front. Neurosci. 8.

Hennig, J.A., Golub, M.D., Lund, P.J., Sadtler, P.T., Oby, E.R., Quick, K.M., Ryu, S.I., Tyler-Kabara, E.C., Batista, A.P., Yu, B.M., Chase, S.M., 2018. Constraints on neural redundancy. eLife 7, e36774. https://doi.org/10.7554/eLife.36774

Hong, Y.K., Lacefield, C.O., Rodgers, C.C., Bruno, R.M., 2018. Sensation, movement and learning in the absence of barrel cortex. Nature 561, 542–546. https://doi.org/10.1038/s41586-018-0527-y

Hu, Y., Wang, Y., Li, D., Havlin, S., Di, Z., 2011. Possible origin of efficient navigation in small worlds. Phys. Rev. Lett. 106, 108701. https://doi.org/10.1103/PhysRevLett.106.108701

Huberman, A.D., Niell, C.M., 2011. What can mice tell us about how vision works? Trends Neurosci. 34, 464–473. https://doi.org/10.1016/j.tins.2011.07.002

Hunter, P., 2015. Simulating the human brain. EMBO Rep. 16, 685–688. https://doi.org/10.15252/embr.201540571

Huxlin, K.R., Martin, T., Kelly, K., Riley, M., Friedman, D.I., Burgin, W.S., Hayhoe, M., 2009. Perceptual Relearning of Complex Visual Motion after V1 Damage in Humans. J. Neurosci. 29, 3981–3991. https://doi.org/10.1523/JNEUROSCI.4882-08.2009

Inagaki, H.K., Fontolan, L., Romani, S., Svoboda, K., 2019. Discrete attractor dynamics underlies persistent activity in the frontal cortex. Nature 566, 212–217. https://doi.org/10.1038/s41586-019-0919-7

Isa, T., Yoshida, M., 2021. Neural Mechanism of Blindsight in a Macaque Model. Neuroscience 469, 138–161. https://doi.org/10.1016/j.neuroscience.2021.06.022

Jaramillo, S., Zador, A.M., 2014. Mice and rats achieve similar levels of performance in an adaptive decision-making task. Front. Syst. Neurosci. 8.

Jazayeri, M., Afraz, A., 2017. Navigating the Neural Space in Search of the Neural Code. Neuron 93, 1003–1014. https://doi.org/10.1016/j.neuron.2017.02.019

Jun, J.J., Steinmetz, N.A., Siegle, J.H., Denman, D.J., Bauza, M., Barbarits, B., Lee, A.K., Anastassiou, C.A., Andrei, A., Aydın, Ç., Barbic, M., Blanche, T.J., Bonin, V., Couto, J., Dutta, B., Gratiy, S.L., Gutnisky, D.A., Häusser, M., Karsh, B., Ledochowitsch, P., Lopez, C.M., Mitelut, C., Musa, S., Okun, M., Pachitariu, M., Putzeys, J., Rich, P.D., Rossant, C., Sun, W., Svoboda, K., Carandini, M., Harris, K.D., Koch, C., O'Keefe, J., Harris, T.D., 2017. Fully integrated silicon probes for high-density recording of neural activity. Nature 551, 232–236. https://doi.org/10.1038/nature24636

Kafkafi, N., Agassi, J., Chesler, E.J., Crabbe, J.C., Crusio, W.E., Eilam, D., Gerlai, R., Golani, I., Gomez-Marin, A., Heller, R., Iraqi, F., Jaljuli, I., Karp, N.A., Morgan, H., Nicholson, G., Pfaff, D.W., Richter, S.H., Stark, P.B., Stiedl, O., Stodden, V., Tarantino, L.M., Tucci, V., Valdar, W., Williams, R.W., Würbel, H., Benjamini, Y., 2018. Reproducibility and replicability of rodent phenotyping in preclinical studies. Neurosci. Biobehav. Rev. 87, 218–232. https://doi.org/10.1016/j.neubiorev.2018.01.003

Kawai, R., Markman, T., Poddar, R., Ko, R., Fantana, A.L., Dhawale, A.K., Kampff, A.R., Ölveczky, B.P., 2015. Motor Cortex Is Required for Learning but Not for Executing a Motor Skill. Neuron 86, 800–812. https://doi.org/10.1016/j.neuron.2015.03.024

Kell, D.B., Oliver, S.G., 2004. Here is the evidence, now what is the hypothesis? The complementary roles of inductive and hypothesis-driven science in the post-genomic era. BioEssays 26, 99–105. https://doi.org/10.1002/bies.10385

Kersten, D., Mamassian, P., Yuille, A., 2004. Object perception as Bayesian inference. Annu. Rev. Psychol. 55, 271–304. https://doi.org/10.1146/annurev.psych.55.090902.142005

Kinoshita, M., Kato, R., Isa, K., Kobayashi, Kenta, Kobayashi, Kazuto, Onoe, H., Isa, T., 2019. Dissecting the circuit for blindsight to reveal the critical role of pulvinar and superior colliculus. Nat. Commun. 10, 135. https://doi.org/10.1038/s41467-018-08058-0

Klapoetke, N.C., Murata, Y., Kim, S.S., Pulver, S.R., Birdsey-Benson, A., Cho, Y.K., Morimoto, T.K., Chuong, A.S., Carpenter, E.J., Tian, Z., Wang, J., Xie, Y., Yan, Z., Zhang, Y., Chow, B.Y., Surek, B., Melkonian, M., Jayaraman, V., Constantine-Paton, M., Wong, G.K.-S., Boyden, E.S., 2014. Independent optical excitation of distinct neural populations. Nat. Methods 11, 338–346. https://doi.org/10.1038/nmeth.2836

Kleinberg, null, 2000. Navigation in a small world. Nature 406, 845. https://doi.org/10.1038/35022643

Knill, D.C., Pouget, A., 2004. The Bayesian brain: the role of uncertainty in neural coding and computation. Trends Neurosci. 27, 712–719. https://doi.org/10.1016/j.tins.2004.10.007

Kok, P., Brouwer, G.J., Gerven, M.A.J. van, Lange, F.P. de, 2013. Prior Expectations Bias Sensory Representations in Visual Cortex. J. Neurosci. 33, 16275–16284. https://doi.org/10.1523/JNEUROSCI.0742-13.2013

Kok, P., de Lange, F.P., 2015. Predictive Coding in Sensory Cortex, in: Forstmann, B.U., Wagenmakers, E.-J. (Eds.), An Introduction to Model-Based Cognitive Neuroscience. Springer, New York, NY, pp. 221–244. https://doi.org/10.1007/978-1-4939-2236-9_11

Kok, P., Jehee, J.F.M., de Lange, F.P., 2012. Less Is More: Expectation Sharpens Representations in the Primary Visual Cortex. Neuron 75, 265–270. https://doi.org/10.1016/j.neuron.2012.04.034

Kok, P., Mostert, P., Lange, F.P. de, 2017. Prior expectations induce prestimulus sensory templates. Proc. Natl. Acad. Sci. U. S. A. 114, 10473–10478. https://doi.org/10.1073/pnas.1705652114

Körding, K.P., Wolpert, D.M., 2004. Bayesian integration in sensorimotor learning. Nature 427, 244–247. https://doi.org/10.1038/nature02169

Laughlin, S.B., Sejnowski, T.J., 2003. Communication in neuronal networks. Science 301, 1870–1874. https://doi.org/10.1126/science.1089662

Lazer, D., Kennedy, R., King, G., Vespignani, A., 2014. The Parable of Google Flu: Traps in Big Data Analysis. Science 343, 1203–1205. https://doi.org/10.1126/science.1248506

Lester, H., Arridge, S.R., 1999. A survey of hierarchical non-linear medical image registration. Pattern Recognit. 32, 129–149. https://doi.org/10.1016/S0031-3203(98)00095-8

Li, N., Chen, S., Guo, Z.V., Chen, H., Huo, Y., Inagaki, H.K., Chen, G., Davis, C., Hansel, D., Guo, C., Svoboda, K., 2019. Spatiotemporal constraints on optogenetic inactivation in cortical circuits. eLife 8, e48622. https://doi.org/10.7554/eLife.48622

Li, N., Chen, T.-W., Guo, Z.V., Gerfen, C.R., Svoboda, K., 2015. A motor cortex circuit for motor planning and movement. Nature 519, 51–56. https://doi.org/10.1038/nature14178

Li, N., Daie, K., Svoboda, K., Druckmann, S., 2016. Robust neuronal dynamics in premotor cortex during motor planning. Nature 532, 459–464. https://doi.org/10.1038/nature17643

Li, X., Ai, L., Giavasis, S., Jin, H., Feczko, E., Xu, T., Clucas, J., Franco, A., Sólon Heinsfeld, A.,

Adebimpe, A., Vogelstein, J.T., Yan, C.-G., Esteban, O., Poldrack, R.A., Craddock, C., Fair, D., Satterthwaite, T., Kiar, G., Milham, M.P., 2021. Moving Beyond Processing and Analysis-Related Variation in Neuroscience (preprint). Neuroscience. https://doi.org/10.1101/2021.12.01.470790

Liu, L.D., Chen, S., Hou, H., West, S.J., Faulkner, M., Laboratory, T.I.B., Economo, M.N., Li, N., Svoboda, K., 2021. Accurate Localization of Linear Probe Electrode Arrays across Multiple Brains. eNeuro 8. https://doi.org/10.1523/ENEURO.0241-21.2021

Lopes, G., Bonacchi, N., Frazão, J., Neto, J.P., Atallah, B.V., Soares, S., Moreira, L., Matias, S., Itskov, P.M., Correia, P.A., Medina, R.E., Calcaterra, L., Dreosti, E., Paton, J.J., Kampff, A.R., 2015. Bonsai: an event-based framework for processing and controlling data streams. Front. Neuroinformatics 9.

Lopes, G., Farrell, K., Horrocks, E.A., Lee, C.-Y., Morimoto, M.M., Muzzu, T., Papanikolaou, A., Rodrigues, F.R., Wheatcroft, T., Zucca, S., Solomon, S.G., Saleem, A.B., 2021. Creating and controlling visual environments using BonVision. eLife 10, e65541. https://doi.org/10.7554/eLife.65541

Ma, W.J., Beck, J.M., Latham, P.E., Pouget, A., 2006. Bayesian inference with probabilistic population codes. Nat. Neurosci. 9, 1432–1438. https://doi.org/10.1038/nn1790

Mainen, Z.F., Häusser, M., Pouget, A., 2016. A better way to crack the brain. Nature 539, 159–161. https://doi.org/10.1038/539159a

Makino, H., Ren, C., Liu, H., Kim, A.N., Kondapaneni, N., Liu, X., Kuzum, D., Komiyama, T., 2017. Transformation of Cortex-wide Emergent Properties during Motor Learning. Neuron 94, 880-890.e8. https://doi.org/10.1016/j.neuron.2017.04.015

Malhotra, A., Majchrzak, A., Lyytinen, K., 2021. Socio-Technical Affordances for Large-Scale Collaborations: Introduction to a Virtual Special Issue. Organ. Sci. 32, 1371–1390. https://doi.org/10.1287/orsc.2021.1457

Masuda, N., Porter, M.A., Lambiotte, R., 2017. Random walks and diffusion on networks. Phys. Rep., Random walks and diffusion on networks 716–717, 1–58. https://doi.org/10.1016/j.physrep.2017.07.007

Maunsell, J.H.R., Treue, S., 2006. Feature-based attention in visual cortex. Trends Neurosci. 29, 317–322. https://doi.org/10.1016/j.tins.2006.04.001

Mayford, M., Bach, M.E., Huang, Y.Y., Wang, L., Hawkins, R.D., Kandel, E.R., 1996. Control of memory formation through regulated expression of a CaMKII transgene. Science 274, 1678–1683. https://doi.org/10.1126/science.274.5293.1678

Mazzocchi, F., 2015. Could Big Data be the end of theory in science? EMBO Rep. 16, 1250–1255. https://doi.org/10.15252/embr.201541001

Meijer, G., Chapuis, G., Pan-Vazquez, A., Urai, A.E., Wilson, C.J., Socha, K., Noel, J.-P., Bonacchi, N., 2021. Appendix 1: IBL electrophysiological (Ephys Neuropixels) rig setup instructions: Hardware and Software v1.0.

Mišić, B., Sporns, O., McIntosh, A.R., 2014. Communication Efficiency and Congestion of Signal Traffic in Large-Scale Brain Networks. PLoS Comput. Biol. 10, e1003427. https://doi.org/10.1371/journal.pcbi.1003427

Moreno-Bote, R., Knill, D.C., Pouget, A., 2011. Bayesian sampling in visual perception. Proc. Natl. Acad. Sci. U. S. A. 108, 12491–12496. https://doi.org/10.1073/pnas.1101430108

Müller-Wille, S., Charmantier, I., 2012. Natural history and information overload: The case of Linnaeus. Stud. Hist. Philos. Biol. Biomed. Sci. 43, 4–15. https://doi.org/10.1016/j.shpsc.2011.10.021

Munafò, M.R., Davey Smith, G., 2018. Robust research needs many lines of evidence. Nature 553, 399–401. https://doi.org/10.1038/d41586-018-01023-3

Muralidhar, S., Wang, Y., Markram, H., 2014. Synaptic and cellular organization of layer 1 of the developing rat somatosensory cortex. Front. Neuroanat. 7.

Murphy, T.H., Michelson, N.J., Boyd, J.D., Fong, T., Bolanos, L.A., Bierbrauer, D., Siu, T., Balbi, M., Bolanos, F., Vanni, M., LeDue, J.M., 2020. Automated task training and longitudinal monitoring of mouse mesoscale cortical circuits using home cages. eLife 9, e55964.

https://doi.org/10.7554/eLife.55964

Musall, S., Kaufman, M.T., Juavinett, A.L., Gluf, S., Churchland, A.K., 2019. Single-trial neural dynamics are dominated by richly varied movements. Nat. Neurosci. 22, 1677–1686. https://doi.org/10.1038/s41593-019-0502-4

Musall, S., Sun, X.R., Mohan, H., An, X., Gluf, S., Drewes, R., Osten, P., Churchland, A.K., 2021. Pyramidal cell types drive functionally distinct cortical activity patterns during decision-making (preprint). Neuroscience. https://doi.org/10.1101/2021.09.27.461599

Najafi, F., Churchland, A.K., 2018. Perceptual Decision-making: a field in the midst of a transformation. Neuron 100, 453–462. https://doi.org/10.1016/j.neuron.2018.10.017

Najafi, F., Elsayed, G.F., Cao, R., Pnevmatikakis, E., Latham, P.E., Cunningham, J.P., Churchland, A.K., 2020. Excitatory and Inhibitory Subnetworks Are Equally Selective during Decision-Making and Emerge Simultaneously during Learning. Neuron 105, 165-179.e8. https://doi.org/10.1016/j.neuron.2019.09.045

Newsome, W.T., Britten, K.H., Movshon, J.A., 1989. Neuronal correlates of a perceptual decision. Nature 341, 52–54. https://doi.org/10.1038/341052a0

Newsome, W.T., Paré, E.B., 1988. A selective impairment of motion perception following lesions of the middle temporal visual area (MT). J. Neurosci. Off. J. Soc. Neurosci. 8, 2201–2211.

Ng, A.Y., 2004. Feature selection, $L_1$ vs. $L_2$ regularization, and rotational invariance, in: Proceedings of the Twenty-First International Conference on Machine Learning, ICML '04. Association for Computing Machinery, New York, NY, USA, p. 78. https://doi.org/10.1145/1015330.1015435

Nikbakht, N., Diamond, M.E., 2021. Conserved visual capacity of rats under red light. eLife 10, e66429. https://doi.org/10.7554/eLife.66429

Noudoost, B., Moore, T., 2011. The role of neuromodulators in selective attention. Trends Cogn. Sci. 15, 585–591. https://doi.org/10.1016/j.tics.2011.10.006

Olshausen, B., Anderson, C., Van Essen, D., 1993. A neurobiological model of visual attention and invariant pattern recognition based on dynamic routing of information. J. Neurosci. 13, 4700–4719. https://doi.org/10.1523/JNEUROSCI.13-11-04700.1993

Otchy, T.M., Wolff, S.B.E., Rhee, J.Y., Pehlevan, C., Kawai, R., Kempf, A., Gobes, S.M.H., Ölveczky, B.P., 2015. Acute off-target effects of neural circuit manipulations. Nature 528, 358–363. https://doi.org/10.1038/nature16442

Pachitariu, M., Rossant, C., Steinmetz, N., Colonell, J., Winter, O., Bondy, A.G., kushbanga, Bhagat, J., Sosa, M., O'Shea, D., Nakamura, K.C., geffenlab, Saxena, R., Liddell, A., Guzman, J., Botros, P., bryzgalovdm, carsen-stringer, denman, daniel, Karamanlis, D., Beau, M., 2020. MouseLand/Kilosort2: 2.0 final. Zenodo. https://doi.org/10.5281/zenodo.4147288

Pajani, A., Kok, P., Kouider, S., Lange, F.P. de, 2015. Spontaneous Activity Patterns in Primary Visual Cortex Predispose to Visual Hallucinations. J. Neurosci. 35, 12947–12953. https://doi.org/10.1523/JNEUROSCI.1520-15.2015

Pancaldi, V., 2014. Biological noise to get a sense of direction: an analogy between chemotaxis and stress response. Front. Genet. 5.

Paszke, A., Gross, S., Massa, F., Lerer, A., Bradbury, J., Chanan, G., Killeen, T., Lin, Z., Gimelshein, N., Antiga, L., Desmaison, A., Köpf, A., Yang, E., DeVito, Z., Raison, M., Tejani, A., Chilamkurthy, S., Steiner, B., Fang, L., Bai, J., Chintala, S., 2019. PyTorch: An Imperative Style, High-Performance Deep Learning Library. ArXiv191201703 Cs Stat.

Pedregosa, F., Varoquaux, G., Gramfort, A., Michel, V., Thirion, B., Grisel, O., Blondel, M., Prettenhofer, P., Weiss, R., Dubourg, V., Vanderplas, J., Passos, A., Cournapeau, D., Brucher, M., Perrot, M., Duchesnay, É., 2011. Scikit-learn: Machine Learning in Python. J. Mach. Learn. Res. 12, 2825–2830.

Pinto, L., Rajan, K., DePasquale, B., Thiberge, S.Y., Tank, D.W., Brody, C.D., 2019. Task-Dependent Changes in the Large-Scale Dynamics and Necessity of Cortical Regions. Neuron 104, 810-824.e9. https://doi.org/10.1016/j.neuron.2019.08.025

Pnevmatikakis, E.A., Soudry, D., Gao, Y., Machado, T.A., Merel, J., Pfau, D., Reardon, T., Mu, Y.,

Lacefield, C., Yang, W., Ahrens, M., Bruno, R., Jessell, T.M., Peterka, D.S., Yuste, R., Paninski, L., 2016. Simultaneous Denoising, Deconvolution, and Demixing of Calcium Imaging Data. Neuron 89, 285–299. https://doi.org/10.1016/j.neuron.2015.11.037

Poddar, R., Kawai, R., Ölveczky, B.P., 2013. A Fully Automated High-Throughput Training System for Rodents. PLOS ONE 8, e83171. https://doi.org/10.1371/journal.pone.0083171

Poo, M., 2014. Whereto the mega brain projects? Natl. Sci. Rev. 1, 12–14. https://doi.org/10.1093/nsr/nwt019

Rangarajan, J.R., Vande Velde, G., van Gent, F., De Vloo, P., Dresselaers, T., Depypere, M., van Kuyck, K., Nuttin, B., Himmelreich, U., Maes, F., 2016. Image-based in vivo assessment of targeting accuracy of stereotactic brain surgery in experimental rodent models. Sci. Rep. 6, 38058. https://doi.org/10.1038/srep38058

Rao, R.P., Ballard, D.H., 1999. Predictive coding in the visual cortex: a functional interpretation of some extra-classical receptive-field effects. Nat. Neurosci. 2, 79–87. https://doi.org/10.1038/4580

Ratcliff, R., 1978. A theory of memory retrieval. Psychol. Rev. 85, 59–108. https://doi.org/10.1037/0033-295X.85.2.59

Ratcliff, R., McKoon, G., 2008. The Diffusion Decision Model: Theory and Data for Two-Choice Decision Tasks. Neural Comput. 20, 873–922. https://doi.org/10.1162/neco.2008.12-06-420

Ratcliff, R., Tuerlinckx, F., 2002. Estimating parameters of the diffusion model: Approaches to dealing with contaminant reaction times and parameter variability. Psychon. Bull. Rev. 9, 438–481. https://doi.org/10.3758/BF03196302

Ren, C., Komiyama, T., 2021. Characterizing Cortex-Wide Dynamics with Wide-Field Calcium Imaging. J. Neurosci. 41, 4160–4168. https://doi.org/10.1523/JNEUROSCI.3003-20.2021

Research collaborations bring big rewards: the world needs more, 2021. . Nature 594, 301–302. https://doi.org/10.1038/d41586-021-01581-z

Reynolds, J.H., Heeger, D.J., 2009. The normalization model of attention. Neuron 61, 168–185. https://doi.org/10.1016/j.neuron.2009.01.002

Rocha, F.A. de F., Gomes, B.D., Silveira, L.C. de L., Martins, S.L., Aguiar, R.G., Souza, J.M. de, Ventura, D.F., 2016. Spectral Sensitivity Measured with Electroretinogram Using a Constant Response Method. PLOS ONE 11, e0147318. https://doi.org/10.1371/journal.pone.0147318

Sahraie, A., Macleod, M.-J., Trevethan, C.T., Robson, S.E., Olson, J.A., Callaghan, P., Yip, B., 2010. Improved detection following Neuro-Eye Therapy in patients with post-geniculate brain damage. Exp. Brain Res. 206, 25–34. https://doi.org/10.1007/s00221-010-2395-z

Sahraie, A., Trevethan, C.T., MacLeod, M.J., Murray, A.D., Olson, J.A., Weiskrantz, L., 2006. Increased sensitivity after repeated stimulation of residual spatial channels in blindsight. Proc. Natl. Acad. Sci. U. S. A. 103, 14971–14976. https://doi.org/10.1073/pnas.0607073103

Samaha, J., Boutonnet, B., Postle, B.R., Lupyan, G., 2018. Effects of meaningfulness on perception: Alpha-band oscillations carry perceptual expectations and influence early visual responses. Sci. Rep. 8, 6606. https://doi.org/10.1038/s41598-018-25093-5

Sans-Dublanc, A., Chrzanowska, A., Reinhard, K., Lemmon, D., Nuttin, B., Lambert, T., Montaldo, G., Urban, A., Farrow, K., 2021. Optogenetic fUSI for brain-wide mapping of neural activity mediating collicular-dependent behaviors. Neuron 109, 1888-1905.e10. https://doi.org/10.1016/j.neuron.2021.04.008

Schartner, M., 2021. Motor correlates of cognitive variables in the international brain laboratory task.

Shadlen, M.N., Kiani, R., 2013. Decision Making as a Window on Cognition. Neuron 80, 791–806. https://doi.org/10.1016/j.neuron.2013.10.047

Shamash, P., Carandini, M., Harris, K.D., Steinmetz, N.A., 2018. A tool for analyzing electrode tracks from slice histology (preprint). Neuroscience. https://doi.org/10.1101/447995

Shannon, C., 1948. A mathematical theory of communication. Bell Syst. Tech. J. 27, 379–423.

Shenoy, K.V., Sahani, M., Churchland, M.M., 2013. Cortical Control of Arm Movements: A Dynamical Systems Perspective. Annu. Rev. Neurosci. 36, 337–359. https://doi.org/10.1146/annurev-neuro-062111-150509

Shimaoka, D., Steinmetz, N.A., Harris, K.D., Carandini, M., 2019. The impact of bilateral ongoing activity on evoked responses in mouse cortex. eLife 8, e43533. https://doi.org/10.7554/eLife.43533

Siegle, J.H., Jia, X., Durand, S., Gale, S., Bennett, C., Graddis, N., Heller, G., Ramirez, T.K., Choi, H., Luviano, J.A., Groblewski, P.A., Ahmed, R., Arkhipov, A., Bernard, A., Billeh, Y.N., Brown, D., Buice, M.A., Cain, N., Caldejon, S., Casal, L., Cho, A., Chvilicek, M., Cox, T.C., Dai, K., Denman, D.J., de Vries, S.E.J., Dietzman, R., Esposito, L., Farrell, C., Feng, D., Galbraith, J., Garrett, M., Gelfand, E.C., Hancock, N., Harris, J.A., Howard, R., Hu, B., Hytnen, R., Iyer, R., Jessett, E., Johnson, K., Kato, I., Kiggins, J., Lambert, S., Lecoq, J., Ledochowitsch, P., Lee, J.H., Leon, A., Li, Y., Liang, E., Long, F., Mace, K., Melchior, J., Millman, D., Mollenkopf, T., Nayan, C., Ng, L., Ngo, K., Nguyen, T., Nicovich, P.R., North, K., Ocker, G.K., Ollerenshaw, D., Oliver, M., Pachitariu, M., Perkins, J., Reding, M., Reid, D., Robertson, M., Ronellenfitch, K., Seid, S., Slaughterbeck, C., Stoecklin, M., Sullivan, D., Sutton, B., Swapp, J., Thompson, C., Turner, K., Wakeman, W., Whitesell, J.D., Williams, D., Williford, A., Young, R., Zeng, H., Naylor, S., Phillips, J.W., Reid, R.C., Mihalas, S., Olsen, S.R., Koch, C., 2021. Survey of spiking in the mouse visual system reveals functional hierarchy. Nature 592, 86–92. https://doi.org/10.1038/s41586-020-03171-x

Sorge, R.E., Martin, L.J., Isbester, K.A., Sotocinal, S.G., Rosen, S., Tuttle, A.H., Wieskopf, J.S., Acland, E.L., Dokova, A., Kadoura, B., Leger, P., Mapplebeck, J.C.S., McPhail, M., Delaney, A., Wigerblad, G., Schumann, A.P., Quinn, T., Frasnelli, J., Svensson, C.I., Sternberg, W.F., Mogil, J.S., 2014. Olfactory exposure to males, including men, causes stress and related analgesia in rodents. Nat. Methods 11, 629–632. https://doi.org/10.1038/nmeth.2935

Steinmetz, N.A., Cazettes, F., Chapuis, G., Urai, A.E., Pan-Vazquez, A., Meijer, G., Bonacchi, N., Winter, O., n.d. IBL protocol for electrophysiology recording using Neuropixels probe, v0.0.12.

Steinmetz, N.A., Koch, C., Harris, K.D., Carandini, M., 2018. Challenges and opportunities for large-scale electrophysiology with Neuropixels probes. Curr. Opin. Neurobiol. 50, 92–100. https://doi.org/10.1016/j.conb.2018.01.009

Steinmetz, N.A., Zatka-Haas, P., Carandini, M., Harris, K.D., 2019. Distributed coding of choice, action and engagement across the mouse brain. Nature 576, 266–273. https://doi.org/10.1038/s41586-019-1787-x

Steverson, K., Chung, H.-K., Zimmermann, J., Louie, K., Glimcher, P., 2019. Sensitivity of reaction time to the magnitude of rewards reveals the cost-structure of time. Sci. Rep. 9, 20053. https://doi.org/10.1038/s41598-019-56392-0

Stoerig, P., 2006. Chapter 12 Blindsight, conscious vision, and the role of primary visual cortex, in: Progress in Brain Research. Elsevier, pp. 217–234. https://doi.org/10.1016/S0079-6123(06)55012-5

The International Brain Laboratory, 2021. Behavior: Appendix 3: IBL protocol for setting up the behavioral training rig. https://doi.org/10.6084/m9.figshare.11634732.v6

The International Brain Laboratory, 2020a. Behavior: Appendix 1: IBL protocol for headbar implant surgery in mice. https://doi.org/10.6084/m9.figshare.11634726.v4

The International Brain Laboratory, 2020b. Behavior: Appendix 2: IBL protocol for mice training. https://doi.org/10.6084/m9.figshare.11634729.v3

The International Brain Laboratory, Aguillon-Rodriguez, V., Angelaki, D., Bayer, H., Bonacchi, N., Carandini, M., Cazettes, F., Chapuis, G., Churchland, A.K., Dan, Y., Dewitt, E., Faulkner, M., Forrest, H., Haetzel, L., Häusser, M., Hofer, S.B., Hu, F., Khanal, A., Krasniak, C., Laranjeira, I., Mainen, Z.F., Meijer, G., Miska, N.J., Mrsic-Flogel, T.D., Murakami, M., Noel, J.-P., Pan-Vazquez, A., Rossant, C., Sanders, J., Socha, K., Terry, R., Urai, A.E., Vergara, H., Wells, M., Wilson, C.J., Witten, I.B., Wool, L.E., Zador, A.M., 2021. Standardized and reproducible measurement of decision-making in mice. eLife 10, e63711. https://doi.org/10.7554/eLife.63711

The International Brain Laboratory, Bonacchi, N., Chapuis, G., Churchland, A., Harris, K.D., Hunter, M., Rossant, C., Sasaki, M., Shen, S., Steinmetz, N.A., Walker, E.Y., Winter, O., Wells, M., 2020.

Data architecture for a large-scale neuroscience collaboration. https://doi.org/10.1101/827873

Theil, S., 2015. Why the Human Brain Project Went Wrong&mdash;and How to Fix It [WWW Document]. Sci. Am. https://doi.org/10.1038/scientificamerican1015-36

Urai, A.E., Aguillon-Rodriguez, V., Laranjeira, I.C., Cazettes, F., Laboratory, T.I.B., Mainen, Z.F., Churchland, A.K., 2021. Citric Acid Water as an Alternative to Water Restriction for High-Yield Mouse Behavior. eNeuro 8. https://doi.org/10.1523/ENEURO.0230-20.2020

Vale-Martínez, A., Guillazo-Blanch, G., Aldavert-Vera, L., Segura-Torres, P., Martí-Nicolovius, M., 1999. Intracranial self-stimulation in the parafascicular nucleus of the rat. Brain Res. Bull. 48, 401–406. https://doi.org/10.1016/S0361-9230(99)00017-9

van den Heuvel, M.P., Kahn, R.S., Goñi, J., Sporns, O., 2012. High-cost, high-capacity backbone for global brain communication. Proc. Natl. Acad. Sci. U. S. A. 109, 11372–11377. https://doi.org/10.1073/pnas.1203593109

Virtanen, P., Gommers, R., Oliphant, T.E., Haberland, M., Reddy, T., Cournapeau, D., Burovski, E., Peterson, P., Weckesser, W., Bright, J., van der Walt, S.J., Brett, M., Wilson, J., Millman, K.J., Mayorov, N., Nelson, A.R.J., Jones, E., Kern, R., Larson, E., Carey, C.J., Polat, İ., Feng, Y., Moore, E.W., VanderPlas, J., Laxalde, D., Perktold, J., Cimrman, R., Henriksen, I., Quintero, E.A., Harris, C.R., Archibald, A.M., Ribeiro, A.H., Pedregosa, F., van Mulbregt, P., 2020. SciPy 1.0: fundamental algorithms for scientific computing in Python. Nat. Methods 17, 261–272. https://doi.org/10.1038/s41592-019-0686-2

Vong, L., Ye, C., Yang, Z., Choi, B., Chua, S., Lowell, B.B., 2011. Leptin action on GABAergic neurons prevents obesity and reduces inhibitory tone to POMC neurons. Neuron 71, 142–154. https://doi.org/10.1016/j.neuron.2011.05.028

Weiskrantz, L., Warrington, E.K., Sanders, M.D., Marshall, J., 1974. Visual capacity in the hemianopic field following a restricted occipital ablation. Brain J. Neurol. 97, 709–728. https://doi.org/10.1093/brain/97.1.709

Wekselblatt, J.B., Flister, E.D., Piscopo, D.M., Niell, C.M., 2016. Large-scale imaging of cortical dynamics during sensory perception and behavior. J. Neurophysiol. 115, 2852–2866. https://doi.org/10.1152/jn.01056.2015

Williford, T., Maunsell, J.H.R., 2006. Effects of spatial attention on contrast response functions in macaque area V4. J. Neurophysiol. 96, 40–54. https://doi.org/10.1152/jn.01207.2005

Wilson, A., Golonka, S., 2013. Embodied Cognition is Not What you Think it is. Front. Psychol. 4.

Wolff, S.B., Ölveczky, B.P., 2018. The promise and perils of causal circuit manipulations. Curr. Opin. Neurobiol., Neurobiology of Behavior 49, 84–94. https://doi.org/10.1016/j.conb.2018.01.004

Wool, L.E., 2020. Knowledge across networks: how to build a global neuroscience collaboration. Curr. Opin. Neurobiol., Whole-brain interactions between neural circuits 65, 100–107. https://doi.org/10.1016/j.conb.2020.10.020

Yardeni, T., Eckhaus, M., Morris, H.D., Huizing, M., Hoogstraten-Miller, S., 2011. Retro-orbital injections in mice. Lab Anim. 40, 155–160. https://doi.org/10.1038/laban0511-155

Yizhar, O., Fenno, L.E., Davidson, T.J., Mogri, M., Deisseroth, K., 2011. Optogenetics in neural systems. Neuron 71, 9–34. https://doi.org/10.1016/j.neuron.2011.06.004

Zatka-Haas, P., Steinmetz, N.A., Carandini, M., Harris, K.D., 2021. Sensory coding and the causal impact of mouse cortex in a visual decision. eLife 10, e63163. https://doi.org/10.7554/eLife.63163

Zhao, S., Ting, J.T., Atallah, H.E., Qiu, L., Tan, J., Gloss, B., Augustine, G.J., Deisseroth, K., Luo, M., Graybiel, A.M., Feng, G., 2011. Cell type–specific channelrhodopsin-2 transgenic mice for optogenetic dissection of neural circuitry function. Nat. Methods 8, 745–752. https://doi.org/10.1038/nmeth.1668

Zhuang, J., Ng, L., Williams, D., Valley, M., Li, Y., Garrett, M., Waters, J., 2017. An extended retinotopic map of mouse cortex. eLife 6, e18372. https://doi.org/10.7554/eLife.18372